Current Opinion in Solid State and Materials Science 27 (2023) 101108

Contents lists available at ScienceDirect

Current Opinion in Solid State & Materials Science

journal homepage: www.elsevier.com/locate/cossms

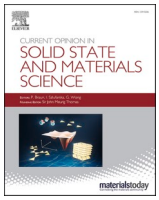

Recent advances in nanomechanical and *in situ* testing techniques: Towards extreme conditions

Daniel Kiener [a,*], Michael Wurmshuber [a,b], Markus Alfreider [a], Gerald J.K. Schaffar [a], Verena Maier-Kiener [a]

[a] Department Materials Science, Montanuniversität Leoben, Jahnstraße 12, 8700 Leoben, Austria
[b] Department of Materials Science & Engineering, Friedrich-Alexander-Universität Erlangen-Nürnberg, Martensstraße 5, 91058 Erlangen, Germany

ARTICLE INFO

Keywords:
Nanoindentation
Miniaturized mechanical testing
Fracture mechanics
Continuous stiffness measurement

ABSTRACT

Nanoindentation based techniques were significantly enhanced by continuous stiffness monitoring capabilities. In essence, this allowed to expand from point-wise discrete measurement of hardness and elastic modulus towards advanced plastic characterization routines, spanning the whole rate-dependent spectrum from steady state creep properties via quasi static flow curves to impact or brittle fracture. While representing a significant step forwards already, these techniques can tremendously benefit from additional or complementary input provided by *in situ* or *operando* experiments. In fact, by combining and merging these approaches, impressive advances were made towards well controlled nanomechanical investigations at various non-ambient conditions. Here we will discuss some novel experimental avenues facilitated by deliberate extreme environments, and also indicate how future improvements and enhancements will potentially provide previously unseen insights into fundamental material behavior at extreme conditions.

1. Introduction

Nanoindentation has become one of the most popular mechanical characterization techniques in materials sciences and beyond [1,2]. This is to a large extent due to the ease of use and high amount of automation of this technique. By today's standards, nanoindentations can be executed within less than a second and with lateral resolution challenging that of optical microscopy [3]. Another avenue of advancement to the technique was provided by the integration of continuous stiffness measurement (CSM) [4–6]. In conventional nanoindentation, only a single measurement of hardness and modulus was acquired at the end of the prescribed indentation depth. Using CSM these quantities can now be measured continuously during the whole indentation process, even including the unloading segment [7,8]. Building on this, measurement protocols were advanced to extend from a continuous evaluation of hardness and modulus to providing access to more complex characteristics such as strain rate sensitivity and creep properties [9]. By conducting these rate controlled experiments at varying temperatures, researchers also gain access to activation energies of the underlying rate controlling processes.

Another field of research where monitoring a sample stiffness is of ominous importance is the field of elastic–plastic fracture mechanics. Similar to the classical nanoindentation situation, by using continuous stiffness measurement a single experiment allows to monitor the specimen stiffness and deduce the current crack length therefrom in a continuous fashion [10]. Conventionally, this would require running multiple experiments with different initial crack lengths. In a sense, one can regard every sinusoidal unloading during the quasi-static loading as a partial unloading experiment, from which the current crack length is deduced. This can again be regarded in analogy to studying indentation depth dependent properties, achieved either by a single CSM indent or many conventional imprints to different depths [11–14].

Besides these rather obvious and established applications of CSM-enabled nanoindentation or micromechanical experiments, there is a number of emerging or conceivable methods to further enhance the field, which we attempt to address in this work.

In recent years significant advances were made in conducting such miniaturized indentation or deformation experiments *in situ* within scanning or transmission electron microscopes (SEM, TEM) [15–18]. First of all this provides advances with respect to local positioning and alignment [19], but enables also a rich parallel data stream of additional or complementary information to be gathered. In the field of micro-

* Corresponding author.
E-mail address: daniel.kiener@unileoben.ac.at (D. Kiener).

https://doi.org/10.1016/j.cossms.2023.101108
Received 7 June 2023; Received in revised form 20 September 2023; Accepted 21 September 2023

mechanics, this would relate for example to the identification of slip systems or the visual determination of the current crack length on the sample surface. When conceptually extending to more extreme conditions, the vacuum environment of electron microscopes certainly facilitates mitigating the oxidation challenges, but also rises issues with respect to potential material degradation in a dry vacuum environment. Moreover, the limited scanning speeds impose a certain temporal resolution on our imaging capabilities. With the increasing availability of direct electron detectors or other complementary fast measurement schemes such as acoustic emission [20], these limits will also be pushed in the future. This will allow well controlled *in situ* and *operando* conditions, providing previously inaccessible information at extreme conditions and enable scientists to address material characteristics over a wide range of physical properties and environmental conditions. In this work, we pick up and build upon where Durst & Maier [9] ended eight years ago, and attempt to highlight some of the recent advances in the field using continuous stiffness measurement approaches, in particular enhanced by *in situ* setups. We will also sketch potentially fruitful avenues for further evolution, as well as some remaining challenges that should be tackled by the community.

There are different ways to approach this, for example from developing the technology to application on material systems, or just in a chronological historical manner. We attempt to take a somewhat different path in following the complexity of the material behavior. Thus we will evolve from rather simple deformation to fracture, then regard *in situ* observations for enhanced fidelity, and finally address external stimuli such as temperature, radiation or chemical attack for more realistic material testing conditions.

With this strategy in mind, chapter 2 will concern developments in rate dependent material behavior, from measuring quasi-static flow curves by spherical nanoindentation to creep properties at low strain rates. Commonly, nanoindentation is regarded as a measurement taking place after a certain amount of plastic deformation occurred, ranging from the pop-in as elastic–plastic transition to a full hardness imprint that imposes a certain amount of strain on the material with an accordingly evolved microstructure. However, in this chapter we will also highlight recent micro-mechanical spectroscopy probing mechanical material characteristics in the elastic regime, as well as the natural extension of this towards elastic–plastic fracture experiments.

Nanoindentation is an extremely powerful technique, yet due to its high automation potential it remains seen more as a high throughput measurement, allowing for example fast mapping of material hardness and modulus. This already provides vast amounts of data to be utilized for complementary statistical analysis or machine learning approaches, but chapter 3 further addresses possibilities for additional information or data streams to be gained from *in situ* observation of the nanoindentation-based experiments. This encompasses features such as a current crack length or the strain field near the crack tip, as well as means to blend and bridge this information commonly accessibly only by certain instruments.

Finally, to account for significant advances achieved by the community in recent years, in chapter 4 we will focus on adding different environments to probe not only extreme temperatures, but also examine the response of materials to radiation or electro-chemical modification, as well as testing organic materials and tissues in an environment that closer resembles *in vivo* conditions. This in fact provides the opportunity to converge the tremendous possibilities offered by micro- and nanomechanical testing techniques with the actual operating conditions or environment of the material problem of concern.

Ideally, at the end we hope to have provided some thoughts on how a wide range of materials, from biological structures to novel nanomaterials, can be examined in conditions possibly close to their native or designated extreme environment by using advanced nanoindentation or related micro-/nanomechanical *in situ* or *operando* testing strategies in academic as well as industrial applications.

2. CSM enabled novel experiments

Within the last 10–15 years the field of so-called advanced nanoindentation has expanded tremendously. At the beginning mostly hardness and modulus values analyzed according to the Oliver-Pharr method [1] were in focus of research, and only some further attempts towards addressing the quasi-static pop-in behavior for an experimental evaluation of theoretical strength values [21,22] were made. The commercial implementation of dynamic indentation protocols opened a vast space for further mechanical characterization possibilities beyond simple hardness and modulus. Of course this also demanded a more profound understanding of the general processes [23] and limitations [24,25] that come along with dynamic nanoindentation protocols. This, in the end, significantly benefited the development of advanced nanoindentation methodologies that reliably address higher strain rate deformation [25–27] as well as low strain rate creep experiments [9,28]. Today, these procedures operate much more alike realistic macroscopic deformation conditions.

As detailed in 2015 [9], the slight modification of standard indentation protocols to enable features such as strain-rate jump tests or long term creep experiments allows the reliable determination of thermally activated deformations processes. Especially nanoindentation strain-rate jump tests became a versatile tool to characterize strain-rate sensitivity, activation volume and activation energies, and can be applied under ambient [28–31] as well as non-ambient conditions [32–37].

Depending on the used nanoindentation system, the applied strain rates are limited to a range between approximately 1——10^{-3} s^{-1} during these loading profiles. Applying smaller strain rates leads to a significant increase in measurement time and correspondingly to more pronounced drift effects [9,38], where the latter could be mitigated by dynamic indentation techniques. However, previously used approaches resemble a combination between relaxation and creep experiments. Since in literature the extraction of power-law creep data is frequently critically discussed [39–42], few recent works attempted nanoindentation constant pressure creep approaches. In a mesoscale approach, Matschkal-Amberger et al. [43] used an adapted TMA instrument. More recently, based on the Constant Load Hold (CLH) method described by Durst and Maier [9], Prach et al. [44] and Minnert & Durst [45] came up with a Constant Contact Pressure (CCP) approach. Thereby, the indenter tip is pushed into the material in a strain-rate controlled manner. After reaching a preset force or displacement, the contact pressure is kept constant at a slightly reduced value compared to the previously measured initial hardness. To maintain the indentation stress inside the plastic zone constant, the applied load is increased continuously during the hold segment according to the increasing contact area. Notably, this is in contrast to macroscopic uniaxial creep experiments and a consequence of the expanding plastic zone. Moreover, by applying Berkovich indentation, also the deformation strain is much higher compared to conventional macroscopic creep testing, which is commonly initiated in the elastic regime. Despite some remaining differences to conventional macroscopic creep tests, material specific contact pressures can be preset during the holding segment, and the corresponding creep rates accordingly calculated. During CLH experiments the measured contact pressure was only depending on the holding time, with longer hold relating to lower pressures. The CCP protocol allows determination of nanoindentation creep response even at lower and better controlled contact pressures. Here again the dynamic approach is indispensable, as maintaining the contact area at a constant contact pressure is achieved via monitoring the continuous stiffness signal according to Sneddons equation [46].

A further step towards even higher fidelity data for nanoindentation experiments is possible by carefully considering the choice of indenter geometry. Not only can the used tip be adapted to simulate various *operando* contact situations, using different geometries also supplies more information for material characterization. Pyramidal tips are

relatively simple to fabricate and convenient to calibrate, they imply a fixed representative strain dictated by the respective self-similar geometry. These properties make them ideal for many high-throughput and mapping techniques, but also for advanced methods such as strain-rate jump tests or observation of size effects. Conical, spherical or ball indenter geometries imply varying deformation strains with increasing indentation depth depending on the applied spherical radius. This allows to vary strain with penetration depth, as depicted for two different conical tips on nanocrystalline Ni in Fig. 1. As such, not a fixed strain material characteristic, but the response to increasing plastic deformation can be probed, namely the complete material flow curve as detailed in the next chapter.

2.1. Quasi-static flow curves

Combining advanced CSM based techniques with spherical indentation tips allows the continuous measurement of flow curves from indentation experiments [47,48]. This can even be achieved at constant strain rates if displacement–time profiles are adjusted accordingly [49,50]. Of utmost importance is thereby the definition of the applied strain and equivalent uniaxial stress, which are not directly accessible to indentation measurements [48]. CSM testing can lay the foundation for accessing these values through the continuous determination of elastic modulus and hardness. Previously, flow curves from spherical indentation testing required a multitude of experiments to varying indentation depths [51] or multiple partial-unloading approaches [52]. Furthermore, a continuous assessment of the constraint factor relating the measured hardness to an equivalent stress is essential [49]. This constraint factor was determined as close to three for fully plastic deformation by Tabor [51]. In more detail, it also depends on the ratio of plastic to elastic deformation underneath the indenter, and thereby on the applied strain [51]. The degree of plasticity can either be derived from the ratio of final to maximum indentation depth, or from the ratio of loading to unloading slope [53]. The latter is especially interesting, as it can be assessed in a continuous fashion during indentation testing using the CSM signal [53]. Still, a remaining limitation for pronounced plastic deformation is that calculation of the constraint factor depends on the strain hardening behavior of the investigated material [53]. This requires some a-priori assumption to be made, which can later be adjusted to the actual material response.

For the calculation of the strain inflicted by spherical indentation, the suggestion by Tabor was used for a long time. This assumes the strain ε to be proportional to the ratio of contact diameter d to indenter diameter D [51], as presented in Eq. (1):

$$\varepsilon \propto \frac{d}{D} \tag{1}$$

A more recent recommendation by Kalidindi & Pathak [47] replaces this proportionality with a more physical strain definition. They suggested Eq. (2) [47] to represent indentation strain, which relates the indentation depth h to the contact radius a. This is more similar to a classical strain definition in the sense that h is a measure of the deformation length, which is then related to a being a measure for the specimen size [47]:

$$\varepsilon = \frac{4h}{3\pi a} \tag{2}$$

With this more physical strain definition, a further step towards measurement of flow curves from spherical indentation tests was made. However, the question regarding the relation between hardness and uniaxial stress remained unanswered. Patel & Kalidindi [54] subsequently used finite element simulations to relate indentation and uniaxial stress–strain curves.

A novel strategy toward such relation was put forward by Leitner et al. [49]. They applied the aforementioned continuous constraint factor measurement with the strain definition by Kalidindi & Pathak [47] (Eq. (2)) to accomplish the determination of uniaxial stress–strain curves from spherical indentation experiments [49]. The applied relation of the constraint factor to the loading to unloading stiffness ratio was not linear as suggested by Hay et al. [53]. Instead a more complicated relation, split into four separate regimes, was used [49]. These were adopted from the simulation work of Park & Pharr [55]. The first regime represents purely elastic loading, while the second identifies the situation where plasticity occurs underneath the surface, according to Hertzian contact theory [56], but is still fully constrained by the surrounding elastic material - thus coined pseudo Hertzian [55]. In the third regime the plastic zone reaches the sample surface and constraint is relieved, while the fourth regime represents the fully relieved and plastified state [55]. The result of such a continuous constraint measurement is depicted in Fig. 2. The onset of plasticity can be clearly seen from the suddenly rising constraint factor.

Furthermore, to account for the inherently imperfect spherical indentation tip shape, the determination of the contact radius was not based on the assumption of a perfect sphere [49]. Rather, an evaluation using the Oliver-Pharr method [1] and an area function calibrated on fused quartz were used [49]. This area function (Eq. (3) [49] was derived from the geometrical relationship for a perfect sphere and adapted to contain three fitting parameters for calibration:

$$A_c = B_0 h_c^{B_1} - B_2 h_c^2 \tag{3}$$

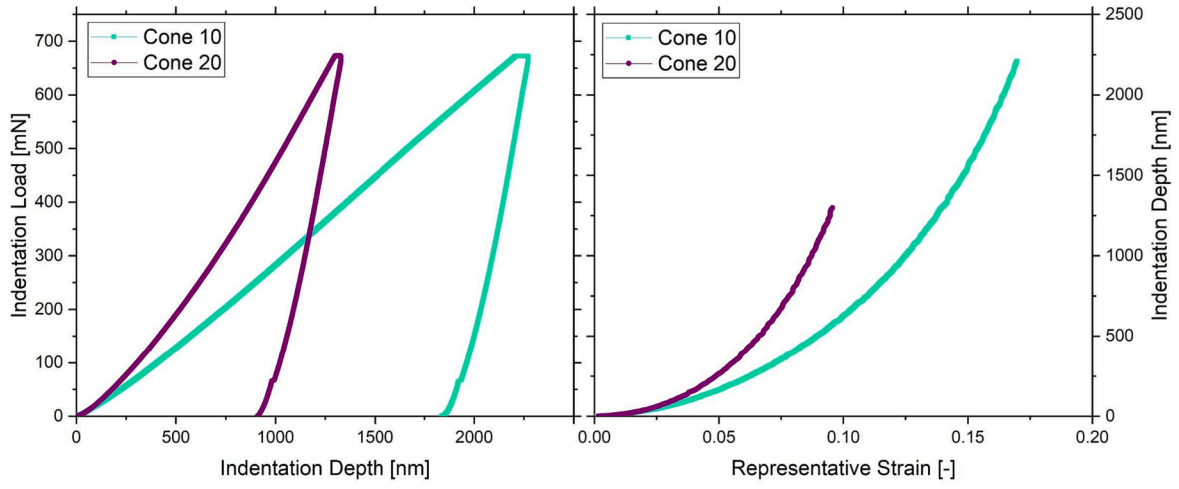

Fig. 1. Load-displacement curves and corresponding indentation depth vs. representative strain curves for two different conical indentation tips applied on nc-Ni.

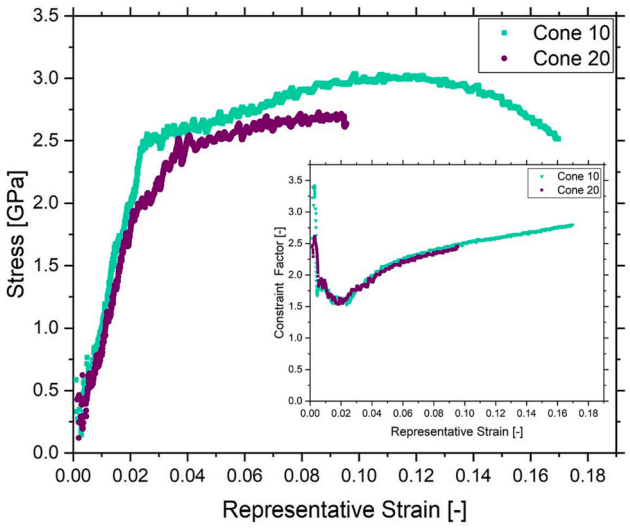

Fig. 2. Spherical stress–strain measurements for nc-Ni applying a 10 μm and a 20 μm conical indentation tip. The inlay shows the depth/strain dependent constraint factor measured continuously during the experiment.

with A_c the contact area, B_i the fitting constants and h_c the Oliver-Pharr contact depth. With these refinements Leitner et al. [49] obtained local stress–strain curves from spherical indentation experiments that compared favorably to ones obtain from uniaxial pillar compression experiments. The applicability of this concept has also been demonstrated for elevated temperature indentation testing of structurally inhomogeneous materials [57].

Furthermore, it showcased the importance of the strain rate, respectively proper strain rate control, during these experiments [49]. For spherical indentation no easily applicable load profile to obtain constant strain rate – such as the $\dot{P}/P$ concept for self-similar indenters [58] – exists. This is rooted in the fact that the strain depends on the indentation depth to contact area ratio and thus on the investigated materials properties. Leitner et al. [49] addressed this problem by regulating the loading rate with a fast PID controlled feedback loop to attain a constant strain rate. An example of constant strain rate flow curves measured with this method is shown in Fig. 2. While such a feedback loop has several benefits, such as its independence of an underlying model and its ability to adapt to changes in the material, it also has some drawbacks. Mainly, these are the fine tuning between a slow-to-respond and an oscillating controller, which currently still requires a tedious trial-and-error optimization and experienced operators. This, to a certain extent, limits the achievable throughput and ease of use of the technique. Accordingly, it would be desirable to perform such tests with simpler, more uniform loading conditions. One conceivable way to move forward would be the application of machine learning to the existing bulk of data in order to predict optimum settings for new materials based on some simple input data, such as a conventional indentation experiment.

Furthermore, issues arise at the very initial point of contact. Not only can the determination of an effective contact point be important [47], CSM can also deliver erroneous values at very small contact depths [13,23,59]. These errors typically result in an overestimation of the contact stiffness. Consequently, the constraint factor is overestimated for very shallow indentations, which can give rise to an apparent curvature of the elastic regime, rather than a straight line.

In conclusion, recent refinements made to spherical indentation testing and the data evaluation thereafter [47,49] allow the reliable measurement of flow curves. Current protocols also ensure the testing at controlled strain rates, which is essential for investigating any strain rate sensitive material. However, there are still some shortcomings of this concept that could benefit from further advancement, such as the rate control requiring tinkering of PID parameters, or the reliability of CSM at very shallow indentation depths.

2.2. CSM unloading for the acquisition of transformation pressures

A comparably recent application is the continuous measurement of stiffness during unloading of indentations [7,8]. Assuming purely elastic unloading of indentation experiments, no additional information from the CSM would be expected, as the slope of the unloading load–displacement curve corresponds to the elastic contact stiffness. However, Merle et al. [7] regarded that the unloading segment can be influenced by non-elastic deformation such as creep. These non-elastic responses are more likely to influence the overall unloading slope rather than the CSM signal sampled within a very short time interval [7]. Therefore, the CSM signal delivers a more reliable measurement of the contact stiffness during unloading [7]. Knowledge of the contact stiffness allows calculation of the contact geometry during unloading, namely the contact depth and, given knowledge of the reduced modulus of the system, the contact area.

Employing this technique, Merle et al. [7] were able to measure the effective indenter shape during unloading introduced by Pharr & Bolshakov [60]. Furthermore, the geometry of the residual imprint could be determined, thereby avoiding the need for subsequent imaging should the Vickers hardness be calculated [7]. Moreover, the unloading stiffness was used to determine the Oliver-Pharr ε factor for the used tip, which yielded very similar results to the typically applied value of $\varepsilon = 0.75$ for Berkovich indenters [7].

Recently, this method was also applied to assess the transformation pressures in silicon [8]. A vast number of investigations previously dealt with the pressure-driven phase transformations occurring during indentation of silicon [61–72]. In addition to instrumented indentation, they were also characterized utilizing complementary information such as Raman spectroscopy [65,69], the change in electric contact resistance acquired *in situ* during indentations using conductive tips [61,67], by TEM [64,72], and by X-ray diffraction (XRD) [62]. Conclusively, distinctive shapes of the unloading branch of the load–displacement curve could be linked to differences in the phase transformation [65]. The attained hardness is limited by the onset of the phase transformation. Thus the transformation pressure can be estimated during loading, but the respective transformation pressures during unloading are not directly accessible via conventional nanoindentation experiments. In the past, contact pressure calculations were based on the assumption of Novikov *et al.* [73], which avoids the need for continuous contact stiffness determination to calculate a contact depth. In that case, it is assumed that the elastic sink-in is proportional to the square of the applied load [66,71]. Schaffar *et al.* [8] recently applied the CSM unloading technique to acquire the actual unloading transformation pressures based on continuous stiffness data. There, the known reduced elastic modulus as acquired dynamically during loading was used jointly with the measured dynamic unloading stiffness to calculate the contact area during unloading. A graphical representation and the most important formulas used for this technique are presented in Fig. 3**a**. Subsequently, in analogy to the hardness calculation during loading, a mean contact pressure is equated from the applied load during unloading, as depicted in Fig. 3**b**. Note that the assumption of a constant reduced modulus during unloading is only satisfied until the onset of the unloading phase transformation. Therefore, this method is suitable for measurement of the onset pressures of transformations, while the pressure changes during transformation will be influenced by the rapid change of the contact situation. The resultant onset pressures of these transformations as well as their dependence on the unloading rate are depicted in Fig. 3**c**.

2.3. Micromechanical spectroscopy

Investigating materials by driven harmonic oscillations dates back as

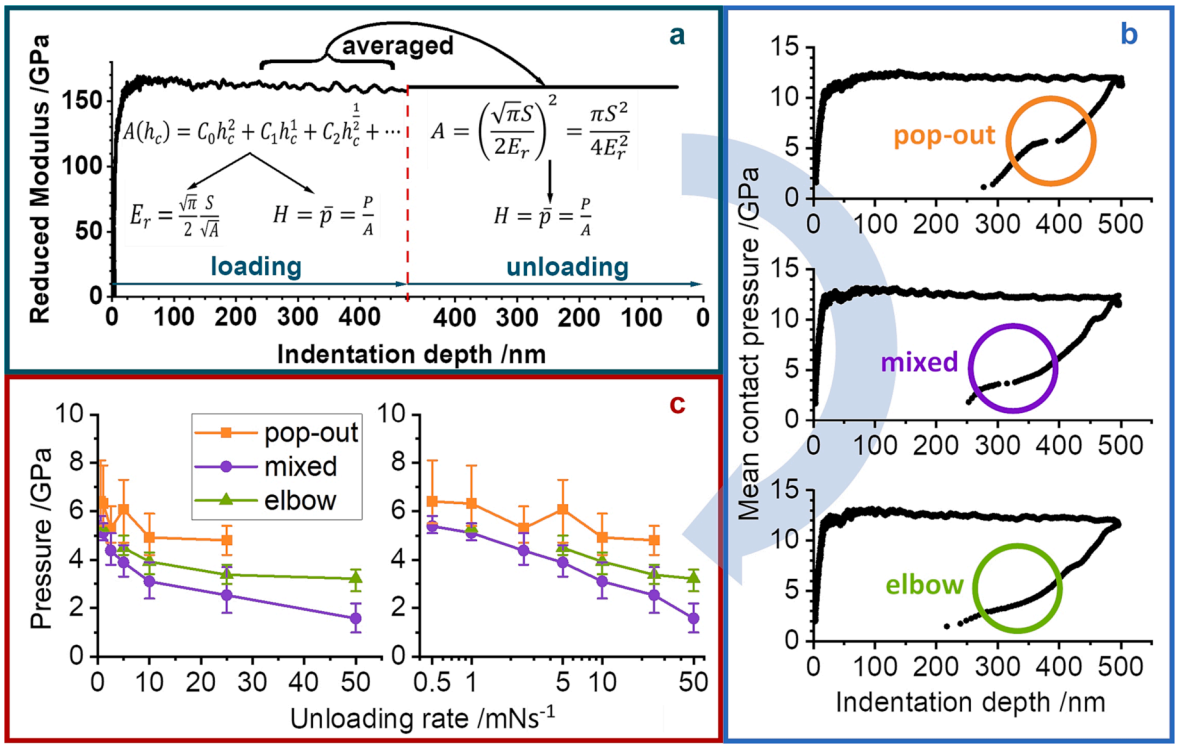

Fig. 3. (a) Schematic of the CSM unload technique used to calculate transformation pressures during unloading. The reduced elastic modulus is averaged during loading and subsequently used as an input parameter in the rearranged Oliver-Pharr formula relating stiffness, reduced modulus, and contact area. (b) Using the calculated contact area, mean contact pressure traces can be calculated for unloading as well as loading. (c) Average onset pressures for each deformation feature measured by this strategy depicted on a linear and logarithmic unloading rate scale, respectively. The subfigures were adapted with permission from [8].

far as 1909, where Poynting [74] twisted piano wires manually back and forth to study quasi-elastic lengthening/shortening as a function of oscillation count. Since then, technology has made quite a leap, enabling automated measurements of oscillating displacements and loads with such a high temporal resolution that even very small phase shifts between these signals can be resolved. While such measurement techniques were referred to differently over the years, from dynamic mechanical analysis (DMA) [75] over internal friction [76] or anelastic relaxation measurements [77] to mechanical spectroscopy [78], the principles have always been the same, namely measuring the dissipative portion of the energy during one oscillation. These differences can then be correlated to various damping processes occurring within the material. Similar to the ambiguity in technique names, also the naming convention for the measured normalized quantity of damping has not been very uniform, but rather dependent on the measurement technique and general focus of the field of research. Resonance based techniques have commonly stuck to the inverse quality factor Q^{-1} description of a single degree of freedom oscillator model, which is the loss in energy ΔW per total oscillation energy within on cycle W. This is oftentimes measured from the resonance peak shape as peak width at half maximum $\Delta\omega_{-3dB}$ (commonly referred to -3dB in signal processing) over resonance frequency ω_0. In initial impact measurements, where the decrease in oscillation amplitude as a function of time is measured, the prevalent nomenclature has been the logarithmic decrement δ as the natural log of one peak amplitude over the following one. With the rise of lock-in amplified systems [79], it became much easier to directly measure the phase shift ϕ between driving signal, *e.g.* load, and trailing signal, *e.g.* displacement. The resulting quantities within mechanical materials science related topics are oftentimes described as loss modulus E'' and storing modulus E', respectively, as shown in equation (4).

$$Q^{-1} = \frac{\Delta W}{2\pi W} \approx \frac{\Delta\omega_{-3dB}}{\omega_0} \approx \delta \approx tan\phi = \frac{E''}{E'} \quad (4)$$

With the rise of CSM-based nanoindentation techniques, such measurements have also found their way into the small scale testing community, theoretically enabling measurements on confined volumes such as thin films, aggregates of few grains, individual boundaries or interfaces. However, the most conveniently obtainable approach in nanoindentation is based on phase shift measurements, as most dynamic measurement systems are inherently based on lock-in amplification.

Inherently higher damping materials such as natural wood [80] and shales [81] have been successfully measured using classical Berkovich indentation, with Q^{-1} values ranging from 0.03 to 0.44, respectively (Fig. 4**a**). To improve the accuracy for such measurements it is vital to remain within the (an)elastic regime of material deformation, as any form of irreversible deformation, such as plasticity or bond breaking, would dissipate considerably more energy than reversible elastic processes. Therefore, the trend for $\tan(\phi)$ measurements using nanoindentation instruments evolved to employing less sharp indentation tips on rather soft materials. Representative results from spherical tips (radius = 3.4 μm) on synthetic polymers (PMMA, PC) [82] range between 0.087 and 0.052, respectively (Fig. 4**a**). The most preferred quasi-ideal nanoindentation setup for such investigations has been introduced by Hay & Herbert [83] using a flat punch indenter, thereby creating a nearly ideally elastic contact. They investigated different common polyethylene (PE) derivatives: linear low density PE (LLDPE), low density PE (LDPE), very low density PE (VLDPE) and high density PE (HDPE) as well as highly plasticized polyvinylchloride (HP-PVC). Changing damping characteristics with frequency depending on the material, with decreasing Q^{-1} for all PE derivates was reported on one hand, while the HP-PVC on the other hand showed increasing Q^{-1} with increasing frequency. Weyand *et al.* [84] further built on this methodology to investigate the changes from energy-elastic to entropy-elastic behavior with respect to the glass transition temperature of various trimethylolpropane glycidylether based cyclic carbonates (TMPGC) and pentaerythritol glycidylether based cyclic carbonates (PGC) with

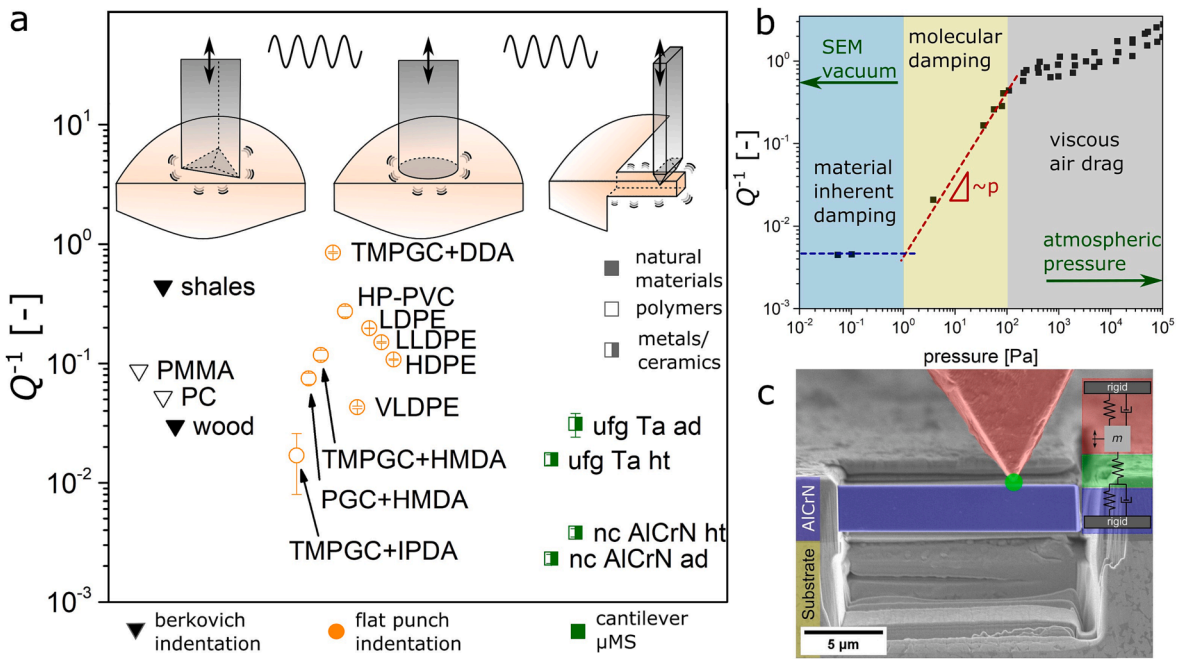

Fig. 4. (a) Comparison of micron scale damping capability measurements using phase shift techniques with Berkovich and flat punch tips on various natural (filled symbols [80,81]) and polymer (open symbols [82–84]) materials. Comparably, micromechanical spectroscopy (µMS) results on cantilever shaped ufg Ta [89] and nc AlCrN [91] (half-filled symbols) resolve Q^{-1} values as low as 0.0023. (b) Q^{-1} results on etched Si cantilevers, reproduced after Blom [90], which depict three distinct pressure regimes involving viscous air damping, molecular damping, and dedicated inherent material damping in high vacuum conditions. (c) Single-degree-of-freedom physical interpretation of the highly localized µMS experiments.

different diamines (hexamethylene diamine: HMDA, isophorone diamine: IPDA, dodecamethylene diamine: DDA). They synthesized these systems from basic components using classical polymer chemistry and showed a promising tuneability range of storage modulus from 359 MPa (TMPGC + IPDA) to 4580 MPa (TMPGC + DDA) and damping capability from $Q^{-1} = 0.017 \pm 0.009$ (TMPGC + IPDA) to $Q^{-1} = 0.85 \pm 0.014$ (TMPGC + DDA), as shown in Fig. 4**a**.

A benefit of these phase shift measurements is their accessibility, as only a flat surface is required. Consequently, they can also be realized under certain environmental conditions, and further allow frequency sensitive measurements. Furthermore, since both E'' and E' are dependent on the same area, phase shift measurements are essentially unaltered by slight tip or surface imperfections as long the contact between them is purely elastic. The sensible lower limit for such phase shifts is limited to roughly $Q^{-1} = 0.01$ ($\phi \approx 0.57^{\circ}$), as even very dedicated high phase resolution systems using specified sub-sampling techniques and very high signal-to-noise ratio input signals are only able to achieve phase errors of $\Delta\phi = 0.13^{\circ}$ [85]. Therefore, the strength of this measurement approach is for higher damping materials, for example polymers or natural materials. Investigating very low attenuation mechanism of metallic materials or ceramics, *e.g.* Snoek-Köster relaxation [86], dislocation kink-pair motions [87] or grain boundary relaxations [88], by common single phase shift measurements in this small scale regime will be very demanding, as these can be as low as $Q^{-1} \approx 10^{-4}$.

To resolve such relaxation phenomena relevant for modern high performance materials using dynamic measurements requires different approaches. Recent advances have been made utilizing a resonance shape change measurement technique using an indentation system in contact with cantilever shaped specimens inside an SEM, termed micromechanical spectroscopy (µMS) [89]. The premise is that the inherent resonance compliance signal of the indentation system is already large in comparison to the signal-to-noise ratio. Thus the change of this resonance shape in contact with the cantilever shaped specimen can be explained using simple physical spring-dashpot models in the framework of a single degree of freedom oscillator system, as schematically shown in Fig. 4**c**. Furthermore, the measurement inside an SEM enables not only the accurate positioning of the probing system with respect to the specimen, but the low vacuum is also very beneficial with respect to reduced environmental damping. Blom [90] conducted resonance measurements on few micron thick, few mm long cantilevers as a function of pressure to test for their utilization as vacuum gauges. A distinct separation into three regimes, with a viscous air damping regime between 100 Pa to atmospheric pressures, a linear regime between 1 Pa and 100 Pa, corresponding to individual air molecule impact damping, and a dedicated purely material inherent damping regime below pressures of 1 Pa was identified, see Fig. 4**b**. This implies that in order to measure any material inherent characteristics, the high vacuum environment within SEMs ($\sim 10^{-3}$ Pa) is crucial, as even a pressure of only a few tens of Pa could potentially conceal such low attenuation mechanisms of interest.

The µMS technique has originally been presented on high-pressure torsion deformed high purity Ta specimens [89] with an ultrafine grain size (ufg) of ~125 nm, revealing a decrease of Q^{-1} from 0.0312 ± 0.0070 in the as-deformed (ad) state to 0.0157 ± 0.0016 after a heat treatment (ht) of 400 °C for 30 min. Using high resolution TEM (HRTEM) and analytical arguments, this change in damping capability was correlated to relaxation phenomena occurring within the highly deformed non-equilibrium grain boundaries.

Recent experiments on a 6 µm thick nanocrystalline (nc) $Al_{0.8}Cr_{0.2}N$ film processed by cathodic arc evaporation [91] revealed for the first time the applicability of this method for very confined volumes, as well as the possibility to measure Q^{-1} as low as 0.0023 ± 0.0002 for the specimens in as-deposited (ad) condition. Furthermore, in this thin film system an increase in Q^{-1} to 0.0038 ± 0.0003 after a 5 min annealing treatment at 1050 °C could be identified. Correlative methods such as HRTEM and X-ray diffraction in conjunction with analytical models confirmed the formation of few nm wide cubic CrN precipitates within the otherwise wurtzite AlCrN structure. The measured change in damping capabilities could be attributed to the formation of new

incoherent boundaries between precipitates and matrix. Hence, μMS is capable of resolving very small Q^{-1} changes and sensitive to minor changes within interfacial structures. This distinct combination makes the approach uniquely suited for measuring previously unobtainable features, such as changes in the microstates of individual grain boundaries [92], using dynamic vibration concepts.

Additionally, the physically sound and established spring-dashpot model description allows for the determination of an absolute elastic modulus within the framework of a generalized beam theory, without the explicit need for the materials Poisson's ratio. For example, results on the AlCrN system [91] demonstrate a distinct increase in modulus from 205 ± 6 GPa to 280 ± 9 GPa upon precipitation formation. This would be very challenging to resolve using standard nanoindentation techniques due to common thin film challenges, such as the high surface roughness and comparatively low film thickness, which challenge elimination of elastic substrate influences.

Notably, the additional fabrication of cantilever shaped specimens is more demanding compared to mirror surface polishing as necessary for nanoindentation experiments. However, the high relative resolution and local nature of these measurements could be utilized to determine slight modulus changes in materials exhibiting structural or chemical gradients, without the influence of the surrounding volume, as only the material inside the cantilever specimen is under significant mechanical load during the experiment.

2.4. Elastic-plastic fracture

With the increasing complexity of micron scaled systems, also necessary investigations with regards to individual features became more and more intricate. Nowadays, not only the fracture properties of complete devices, but rather the individual characteristics of submicrometer multilayer components or individual interfaces are the focus of intense research. Determining the 'weakest' interface in highly heterogeneous systems, *e.g.* transistors or thermal barrier coatings, is an indispensable approach for improving the service lifetime of the whole device. With these premises the simplified assumptions given by linear elastic fracture mechanics are oftentimes not sufficient to capture the governing fracture processes, raising the need for more advanced evaluation schemes and incorporation of elastic–plastic fracture mechanics concepts. The two most widely recognized methods are based on the *J*-integral and the crack tip opening displacement (CTOD) measurements [93–96], respectively. Independent of which method is applied, both consider the whole fracture process including non-linear deformation processes, such as plasticity, phase transformations, or crack bridging, to name a few [97]. Therefore, for any analysis the most important parameter to determine is the actual crack extension during the fracture process.

In analogy to macroscopic methodologies, a translation from a specimens' stiffness to crack extension is also possible in few micron sized cantilever specimens. Initial approaches were based on sequential unloading steps [98], which allowed for only a couple of determined crack extension values, while CSM based testing is uniquely suitable to determine the crack extension quasi-continuously during a single experiment. The first successful experiments on notched 10 × 10 × 40 μm^3 NiAl cantilevers were conducted by Ast *et al.* [10] using an *ex situ* nanoindenter capable of CSM measurements. There the *J*-integral based evaluation revealed a distinctly increased fracture toughness by approximately 50% in comparison to what would result from a purely linear elastic evaluation.

Recent works focused on implementing this quasi-continuous crack length measurement with *in situ* electron microscopy systems to establish correlation between direct imaging and mechanical data, as well as to simplify the positioning of the specimen with regards to the indenter tip [99]. This incorporation has its own challenges, as the application within a vacuum system significantly reduces the system damping, which has a strong influence on the stability of the oscillating load signal. Especially for an extending crack and the comparatively large change in stiffness of the measurement chain, the dynamics of the system need to be carefully tuned to obtain trustworthy results. In particular for situations where the current experimental system stiffness locates in the vicinity of instrument resonance frequencies, slight changes in crack length can lead to over-proportional decrease in stiffness or signal-to-noise ratio, which is nearly impossible to separate from the pure geometric shape change. Depending on the eigenfrequency of the used loading device, working well below that characteristic can impose strings on the attainable data fidelity.

Furthermore, as such micron scaled specimens are fabricated out of a host material they are still connected to, they lack the nearly ideal rigid clamping that is necessary to separate the stiffness of the whole load train from that of the specimen. Therefore, it is crucial to determine the individual stiffness contributions, such as that of the contact between wedge tip and specimen, *e.g.* by additional H-bar experiments [10,100], or the machine (stiff load train) compliance, *e.g.* by cantilever base measurements [99].

After careful calibration of the system it is necessary to translate the determined change in stiffness to actual crack extension. Initial arguments based on a simplified 'reduction of cantilever height' analogy deviated significantly from experimental as well as computational data [98]. Therefore, researchers opted to conduct finite element simulations for each experimental setup to obtain 'stiffness-to-crack length' calibration curves. Such simulations provide the most accurate results for individual cantilever geometries and materials. However, the time consuming nature of 3-dimensional FEM simulations, and the oftentimes unknown homogeneous or undefined heterogeneous elastic properties remain a significant obstacle for generalization of this method. To counteract the necessity for conducting FEM simulations, a simplified two-dimensional Euler-Bernoulli cantilever model has been developed and validated by excessive FEM simulations, which describes the relation between normalized crack length and normalized stiffness as shown in equation (5) [101]:

$$\int_0^{a_n} \frac{a}{W} Y\left(\frac{a}{W}\right)^2 da = \frac{\left(\frac{k_0}{k_n} - 1\right) L^3}{18\pi(1-\nu^2){L_c}^2} \tag{5}$$

whereby a_n is the crack length, corresponding to a stiffness k_n at point n, k_0 is the virtual unnotched cantilevers' stiffness, W is the cantilevers' thickness, L and L_c are the lengths from the tip to the cantilever base and the notch position, respectively, and $Y(a/W)$ is the stress intensity geometry function for cantilever shaped specimens, as given in Eq. (6) [102]:

$$Y\left(\frac{a}{W}\right) = \sqrt{\frac{2W}{\pi a} tan\left(\frac{\pi a}{2W}\right)} \; \frac{0.923 + 0.199\left(1 - sin\left(\frac{\pi a}{2W}\right)\right)^4}{cos\,\frac{\pi a}{2W}} \tag{6}$$

While the initial integral term in above equation cannot be solved analytically, it is straightforward to compute it numerically and tabulate/interpolate it with respect to crack length at arbitrary resolution in a look-up table.

As mentioned, this analytical model was validated by a multitude of two-dimensional FEM simulations for varying crack lengths, notch positions and relative cantilever lengths proving overall good agreement, with a maximum root mean square deviation of 1.6% for very unlikely geometries. The only potentially unknown material parameter within this equation is Poisson's ratio ν, which ranges from 0.2 to 0.35 for common engineering materials. Hence, the 1-ν^2 term enumerates in a range from 0.96 to 0.88, so a deviation by maximum 9%. This leads us to conclude that this solution exhibits only minor local material dependence and can therefore also be safely used for the assessment of heterogeneous systems if such precision is sufficient for the question at hand.

Note that the unnotched cantilever stiffness k_0 in Eq. (5) can be obtained by analytical assumptions (Euler-Bernoulli) or by reverse

calculation based on experimentally measurements of the initial crack length and notched cantilever stiffness, whereby the latter leads to better results and is independent of any further assumptions.

In general, the methodology of quasi-continuous *J*-integral measurements has been validated with respect to macroscopic data of semi-brittle W and NiAl [94] single crystals and shows overall agreement for crack growth initiation, *i.e.* fracture toughness. Furthermore, it has successfully been used, for example, to determine fracture toughness differences with respect to deformation in nanocrystalline W-Cu [103] thin film systems, or for white etching layers [104] commonly encountered in railway systems.

The strongest case for such quasi-continuous measurements, however, is the possibility to quantitatively evaluate the whole fracture process, and not only a single event. Especially in conjunction with *in situ* capabilities, e.g. SEM or TEM imaging, the crack initiation as well as propagation within previously inaccessible features such as individual grain boundaries or multilayer interfaces becomes feasible. For example, in commercially processed TiAl alloys this technique has been used to determine the interface fracture toughness between individual lamellae within the eutectic microstructure [105]. These investigations revealed strong stochasticity with respect to the local microstructure, but also a trend for the γ/α_2 interface as being the weakest interface (~6.5 $MPam^{1/2}$), while γ/γ interfaces exhibited dedicated crack path multiplicity.

Furthermore, specifically positioning the initial notch using FIB enables to determine crack growth behavior very locally, as demonstrated for a Cu-WTi-SiOx-Si system commonly found in the microelectronics industry [106]. There the notches were positioned on both sides as well as within the interior of the only ~300 nm thick WTi diffusion barrier layer to investigate the change from nearly ideal brittle (WTi/SiOx) to pure blunting (WTi/Cu) crack extension behavior.

This example was chosen to provide some details as to the amounts of local fracture information that can be extracted from such highly localized *in situ* fracture experiments. Fig. 5 showcases two continuous J-integral experiments on the mentioned SiOx/WTi/Cu multilayer system, where (a) and (b) depict before and after secondary electron images of a deliberately weakened WTi/Cu interface, as achieved by O-enrichment [107]. (c) and (d) depict the alike information for a SiOx/WTi interface [106], while (e) summarizes the *J*-integral over crack extension data. The red circles in (a) to (d) correspond to the respective initial notch tip positions. Focusing on these, it is evident that the WTi/Cu interface (Fig. 5**a to b**) incorporated considerably more plastic deformation in terms of crack tip blunting before crack propagation occurred. In contrary, the SiOx/WTi (Fig. 5**c to d**) does not reveal any major deformation in the vicinity of the crack tip. This is also represented in the data, where the WTi/Cu interface (red curve) depicts a continuous concave-up shape in the beginning, before at a rather distinct transition point (74 J/m^2) a linear crack extension regime starts. This initial concave-up shape is unphysical and corresponds to dislocation plasticity within the Cu phase. Therefore, the crack growth initiation toughness can be considered as the point at the transition knee to the linear regime. For the SiOx/WTi interface no plastic deformation is evident, and consequently the initial J-integral versus crack extension regime depicts rather sequential rapid crack extension events, which relates to the propagation of the crack tip from the initial FIB notch to the interface. Therefore, the crack growth initiation toughness corresponds to the difference between the last crack extension plateau and the onset of stable crack growth (14 J/m^2).

Furthermore, the continuous nature of the J-integral versus crack extension data allows to determine not only the initiation toughness, but also the resistance upon crack growth. Commonly, this R-curve behavior is described with a normalized tearing modulus, requiring knowledge of the local Young's modulus and yield strength, respectively. While this is not rigorously defined for heterogeneous systems on any length scale, one can still compare the slopes in the crack growth regime to estimate the quantitative difference in crack growth resistance. The present data suggests that it is roughly five times harder for a crack to grow within the WTi/Cu than in the SiOx/WTi interface, which is presumably due to noticeable energy dissipation by plasticity within the former.

3. Additional insights from *in situ* experiments

Nanoindentation can provide statistically significant data of very high precision. Nonetheless, in particular if the result is different to or against expectations, direct observation of the ongoing deformation processes is invaluable [108], and electron microscopes are ideally suited to provide this visual information [109]. As such, it was only natural to design systems that allow for *in situ* nanoindentation experiments to be conducted inside scanning [15] or transmission [17]

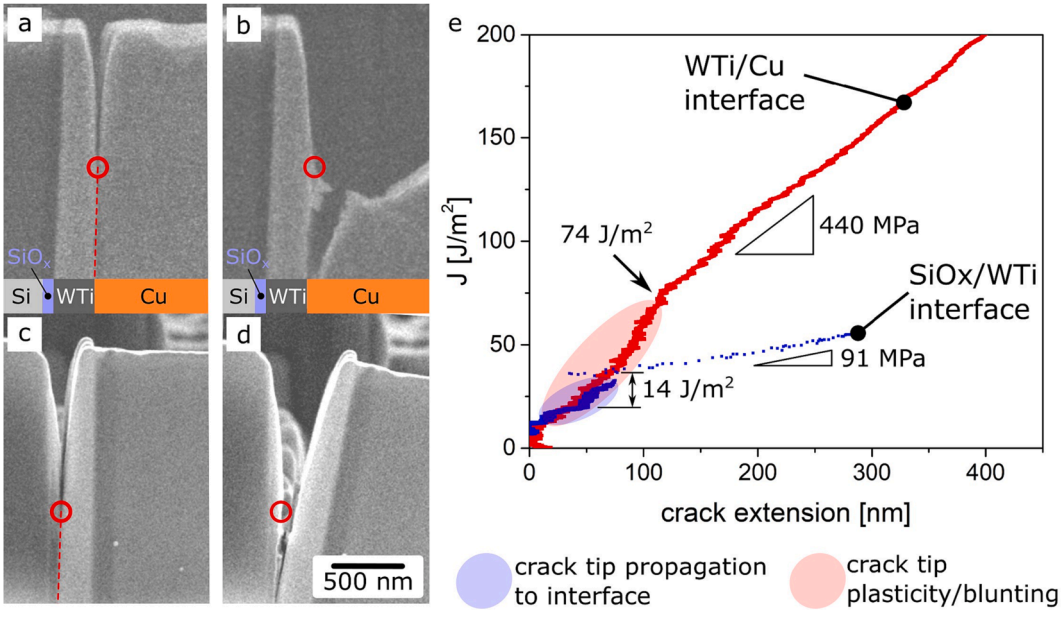

Fig. 5. Interface fracture on a local scale studied by continuous *in situ* fracture experiments. (a, b) WTi/Cu interface before and after fracture. (c, d) SiOx/WTi interface before and after fracture. Red circles and dashed lines indicate initial crack tip and interface position, respectively. (e) Comparison of initiation toughness and crack growth resistance between the two interfaces shown.

electron microscopes. While quasi-*in situ* stepwise static deformation experiments date back quite a while and have been covered by excellent review articles [110], the field of quantitative miniaturized dynamic experiments is rather young. Thus, we will mostly focus on these kinds of experiments.

3.1. Direct crack shape characteristics

While quantitative mechanical data is essential for comparable fracture investigations, the confidence of any measured parameter is based on whether the underlying initial model assumptions, such as a continuously straight crack front or a stable single crack tip, are trustworthy. An example that this is not always a given is depicted in Fig. 6**a**, where an *in situ* observation of a fracture experiment on isotropic IP-DIP resin processed by two-photon lithography [111,112] with a deliberate '*crack stopping hole*', as common in macroscopic engineering approaches, is depicted. The specimen showed a complex behavior involving crack path deflection towards a free surface, re-nucleation of a crack at the bottom of the respective hole, to final crack tip branching. While all these effects are beneficial in dissipating energy and thereby contribute to toughening the material [97], none of these rather complex crack path features could have been resolved without imaging capabilities. This common example is intended to showcase that high fidelity experimental approaches conducted *in situ* are more desirable, since they enable a direct correlation of mechanical crack driving force and microstructural crack path information, especially when the material response is unknown or unpredictable due to local variations in microstructure or inhomogeneities [113–115]. Furthermore, in addition to the direct observation of crack tip deviations as a sanity check for the measurement of crack extension, this data can also be used as input for quantitative fracture mechanical analysis. Schmuck *et al.* [116] developed a semi-automatic algorithm based on image filtering and contour tracking to measure the instantaneous crack tip length of miniaturized cantilever shaped specimens. Notably, this was realized directly from the challenging contrast features of common *in situ* SEM or TEM images absent of any dedicated speckle pattern or markers. It was shown that good overall agreement with stiffness based methods is achieved, given the crack front grows stable and quasi homogeneous over the specimen width. This is expected, for example, for quasi-isotropic materials of nanocrystalline or ultra-fine grained nature, as the average crack front is expected to be straight [117] or only undulating on the order of the microstructural feature dimension. While strongly inhomogeneous crack extension due to varying plane-strain/plane-stress states or microstructural heterogeneities can be challenging and might not always be fully captured on the surface of the specimen, this methodology is still very useful for research groups that do not have access to CSM based experimental setups. Furthermore, *in situ* crack tip tracking enables to collect a much higher density of crack length values in comparison to the often applied sequential unloading method [98], which is beneficial for detailed determination of '*R*-curve' behavior or stable to unstable crack propagation transitions. In general, the correlative *in situ* crack tip tracking from image data can serve as an additional information channel in parallel to CSM based evaluation for validation of the general crack length or current crack tip position in any small scale experiment [105].

Furthermore, in analogy to macroscopic evaluation schemes, the automated measurements of geometric parameters such as crack mouth opening displacement (CMOD), crack tip opening angle (CTOA) and crack tip opening displacement (CTOD), as depicted in Fig. 6**b**, have a direct correlation to energetic fracture parameters, such as the *J*-integral [98]. Just as the crack length, once the crack shape is tracked from the collected image data, these parameters can also be assessed. Therefore, future experiments using *in situ* CSM based techniques to resolve the quasi-continuous crack extension process could be utilized to obtain a more complete description of the fracture characteristics by concurrently employing these two fundamentally different concepts in the same experiment.

3.2. Local deformation fields through computer aided processing

A logical extension of *in situ* imaging is the use of computer aided image processing to obtain detailed information on local surface displacement fields and the subsequently derived strain fields. Such methodologies are commonly referred to as digital image correlation (DIC) and are based on matching of subset windows. Most often, this is realized by normalized cross-correlation of the gray-scale histogram within the subset window from one reference frame to the image of interest. To obtain the highest possible resolution, it is important to utilize as much of the gray-scale range as possible within a small subset window of only a few pixel squared. Thus, it is imperative that the images have possibly high contrast and a stochastic pattern which avoids ambiguity amongst correlation spots. For SEM imaging this is synonymous with a high dwell time per pixel and therefore a long image acquisition duration, up to minutes per image [118], which necessitates a stable mechanical setup, *i.e.* no thermal drift but also no continuous deformation.

Furthermore, for the use of such matching algorithms it is essential that the illumination at a certain position on the specimen remains independent of the relative position within the field of view. This is not always the case, as electron optical aberrations can alter the incoming beam based on the current scan position. While slight overall constant electrostatic/electromagnetic imperfections in the lenses lead to

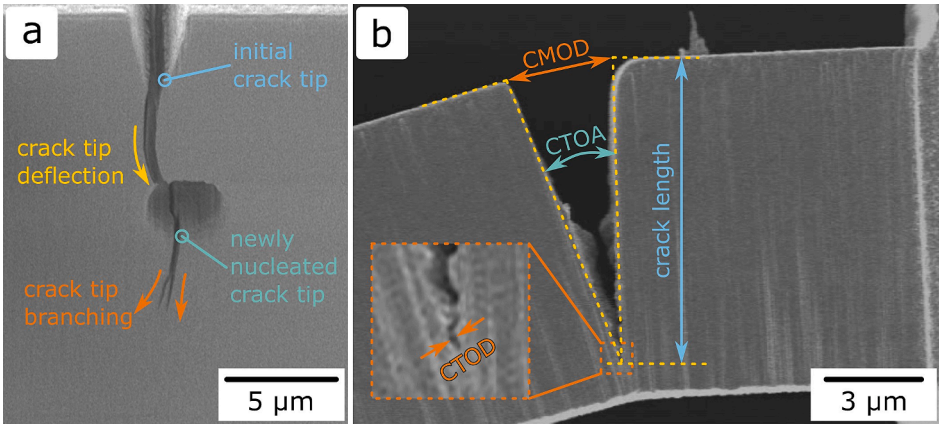

Fig. 6. (a) Crack tip morphology of an IP-DIP cantilever shaped fracture specimen, depicting the change in crack propagation direction due to a deliberate crack stopping hole, followed by nucleation of a new crack tip and subsequent crack tip branching. (b) *In situ* micrograph of a nanocrystalline W specimen showcasing the geometric measurements of crack length, CMOD, CTOA and CTOD, respectively.

stigmatic errors, deviations with respect to the beam path within such lenses (angle, position) cause spherical aberrations. The former can be easily counteracted by the operator, adjusting the respective settings for astigmatism. But the latter is inherently given by the electron lens setup and requires correction within the column using octo-/quadropoles within double/multi lens configurations [119]. The same is true for chromatic aberrations, where deviations of the generated kinematic electron energy (*e.g.* from an unstable power source or imperfection of the cathode) lead to different beam deflections within the column and therefore an additional dependence on the scan position (beam path) [120]. While the hardware correction of these aberrations is utilized to significantly improve overall resolution, the resulting illumination errors can be also counterbalanced using data processing routines [121]. As the electron column inherent aberrations are time-independent, one can map the spatial illumination deviations for a given experimental setup to compensate subsequent DIC measurements and obtain displacement data without additional errors through image formation [121].

Lenthe *et al.* [122] studied the imaging parameters of their SEM setup in detail by implementing an external scan controller unit. They found a strong influence of the scan geometry, where a snake-type scan lead to shifting of every other pixel line due to the 'left-to-right'/'right-to-left' scanning alternation, while shifts in a raster-type scan are continuously and therefore do not add to the overall stochasticity of the image. Furthermore, their results suggested that unwanted pixel shifts are reduced by using lower acceleration voltages, lower magnifications and secondary electron instead of backscatter electron detection. However, the by far most pronounced impact is given by the fact that the electron beam requires time to settle on each pixel individually. So even if the electron output is high enough for detection of high contrast features, if the dwell time of the electron beam is lower than the settling time of the beam scan generation unit, the image will remain with a low signal-to-noise ratio due to undetermined individual pixel shifts. Lenthe *et al.* [122] reported that these pixel shifts follow a sigmoidal curve shape and used their obtained data to fit a correction function for lower dwell times as depicted in Fig. 7**a**, where the same subset window of an etched Ti-6Al-4V sample is shown with pixel dwell times of 1 μs and 10 μs as raw and corrected images, respectively.

The DIC methodology can be utilized by both, large-scale macroscopic *in situ* investigations where only a portion of the sample is of interest, or micron-scale specimens where the whole specimen deformation is captured in one image, as depicted in Fig. 7**b and c**. Micron-scale experiments are commonly processed via FIB milling and have a rather smooth surface finish, which necessitates the application of additional high contrast surface feature, such as dedicated Pt speckle patterns [123,124] for any type of image correlation. Using high resolution post-deformation images (HR-DIC) this technique can be applied to study very erratic deformation characteristics such as twinning [125] and single slip [126], or even the complex strain field in front of crack tips [127]. However, the necessity of slow scan speeds for such high resolution image acquisitions remains and is still challenging for obtaining such strain field during a quasi-continuous deformation experiment. To counteract this, one must work with noisier lower resolution images, dropping the premise for highly accurate gray-scale subset window matching algorithms and change to a more robust feature tracking algorithm. This has been addressed by Alfreider *et al.* [128], where periodic single spot FIB features are used as bases for a plane quadrilateral mesh strain field description (Fig. 7**b**). While this methodology lacks the high-resolution of classical DIC, which is essential for resolving small elastic strains, it is considerably more robust against image noise and distortions introduced through large plastic deformations. Therefore, such a feature tracking type approach can be beneficially employed in conjunction with *in situ* continuous deformation experiments and enables quantifiable strain data over the whole process rather than only at predetermined dedicated stopping times, which is beneficial for unknown or unpredictable deformation characteristics.

Opposite to the strive towards ever smaller volumes to be investigated, another research strategy with DIC is the trend towards larger fields and statistically significant data. Specifically with current hardware developments aiming towards multi-beam SEM configurations, the possibility for acquiring square mm large images while still maintaining nm resolution in reasonable time frames enables to obtain information on multiple hundred thousand individual slip events within one experiment [129]. Additional information can also be gathered using clever mathematical concepts, such as enriching classical shape functions by Heaviside-functions, termed Heaviside DIC (H-DIC) [130]. This methodology in conjunction with electron backscatter diffraction (EBSD) allows to quantify in-plane and out-of-plane shear displacements of individual slip steps, which is oftentimes challenging or even impossible for classical DIC techniques and gives additional insight into local deformation characteristics (see Fig. 7**d**).

All in all, the applied methodology of choice depends on the boundary conditions, such as a precisely determined local loading state (compression, tension, bending) versus a global far field loading, unidirectional continuous deformation versus fatigue investigations, or the

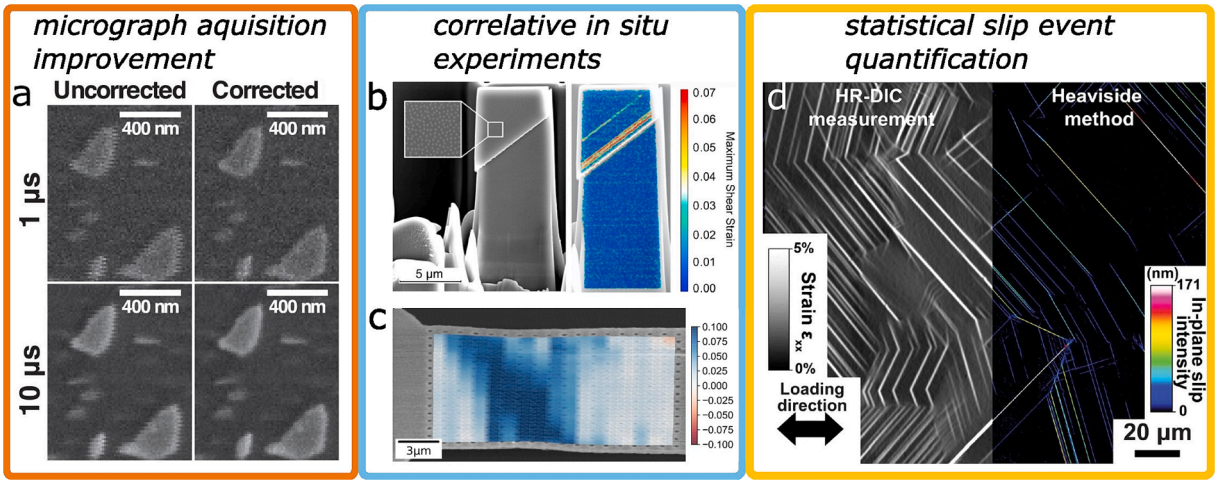

Fig. 7. (a) Detailed image correlation feature depicting the influence of SEM micrograph acquisition time and beam drift correction [122]. (b, c) *In situ* micromechanical experiments using classical grayscale matching [126] (b) and point feature tracking algorithms [128] (c) for digital image correlation. (d) High resolution DIC (HR-DIC) and heaviside DIC (H-DIC) images of a fatigued Ni-based superalloy specimen depicting the quantification of in-plane slip traces [131]. Reproduced with permission.

necessity of applying certain environmental testing conditions, all of which will determine the best suitable technique for a given research question.

3.3. Bridging from scanning to transmission electron microscopy

Investigations on detailed mechanical processes are oftentimes conducted within a dedicated TEM [109], with the common setup of conventional instruments allowing only for very small specimen and holder volumes. Resultant, any scientific equipment for variable *in situ* conditions, such as mechanical loading transducers, thermal heating/cooling devices [132], electrical measuring/charging probes [133] or alternative liquid/gaseous environments [134] necessitate very specific and dedicated, oftentimes one-of-a-kind, solutions. In conventional SEM instruments the comparatively spacious specimen chamber, in conjunction with larger stage movement and easier access to the inside of the device via commercially obtainable feedthroughs is a non-negligible argument for easier correlative *in situ* experiments in such microscopes. It would be much more convenient and easier accessible to a broader community to realize such *operando* testing configurations within the environment of an SEM. Nevertheless, the lack of detailed defect imaging conditions, which are frequently the fundamental objects of interest governing the underlying material behavior, is the oftentimes mentioned drawback for such SEM investigations. However, while it is indeed very convenient to view crystal defects down to atomic details by TEM, they can to an appreciable extent also be imaged using an SEM based on recent technical and methodological advancements.

One way to obtain defect information would be electron channel contrast imaging (ECCI) [135,136], where the backscattered primary electrons channel easier close to surface defects such as dislocations and stacking faults, resulting in a locally higher signal. While this methodology is able to probe bulk-sized specimens at their near surface region, the background noise through scattering and diffraction phenomena in the bulk reduces the contrast quite significantly [137]. This again necessitates long beam dwell times and is therefore not an optimal technique for *in situ* investigations of continuously deforming specimens.

Another approach is following the well-known and studied thin foil processing route for standard TEM specimen preparation to obtain electron transparent foils, but place them in an SEM with a detector mounted beneath the specimen in a transmission configuration. Independent on whether the literature name is 'STEM-in-SEM' [138,139] or 'TSEM' (transmission SEM) [140–142], this technique is essentially equal to the well-known scanning TEM (STEM), where a convergent electron beam focused on the specimen plane is scanned pixel-by-pixel over the region of interest to obtain an image. The main difference is therefore the acceleration voltage, which in most common SEM instruments is only up to 30 kV, while common dedicated TEM machines offer a primary beam with energies up to 300 keV.

Such reduced acceleration voltages do have drawbacks in terms of specimen preparation, as the foil thickness needs to be noticeably smaller than for a 200 kV TEM to obtain the same illumination intensity. Using inelastic mean free paths [143] for single phase Mg and W as low and high scattering examples, one can estimate the maximum foil thickness for at least 5% transmitted intensity as a common rule of thumb [144] to be 129 nm and 61 nm for a 30 kV beam, while a 200 kV beam would allow thicknesses of 493 nm and 228 nm, respectively. While this factor of roughly 3.7 would on one hand allow for thicker specimens to be investigated, it essentially means on the other hand that already thin specimens allow for a noticeably better signal-to-noise ratio in high kV systems. However, low acceleration voltages imply shorter extinction distances and therefore more detail when observing defects such as stacking faults or dislocations. This was detailed by Callahan *et al.* [140], who investigated the same region of interest in a cobalt-base superalloy using various image formation modes (*e.g.* bright field BF, dark field DF, high-angle annular dark field HAADF) on a conventional 200 kV TEM in comparison with a 30 kV TSEM, as depicted in Fig. 8**a and b**. They reported that the effective extinction distance in TSEM images is roughly equal to weak beam dark field imaging in TEM (**g**−3**g**), which is commonly used for very sharp contrast changes at defect features. However, while **g**−3**g** imaging utilizes large excitation errors, *i.e.* weak beams with low intensity to obtain such small extinction distance, TSEM imaging allows for the same with strong beams, which enables shorter beam dwell times and thereby faster image acquisition.

Therefore, TSEM imaging is uniquely suited for quasi-continuous *in situ* experimentation, not only from the perspective of extended equipment space available in an SEM, but also from an image formation point of view. For example, Stinville *et al.* [141] utilized this technique on twinned René 88DT Ni-based superalloy specimens to obtain

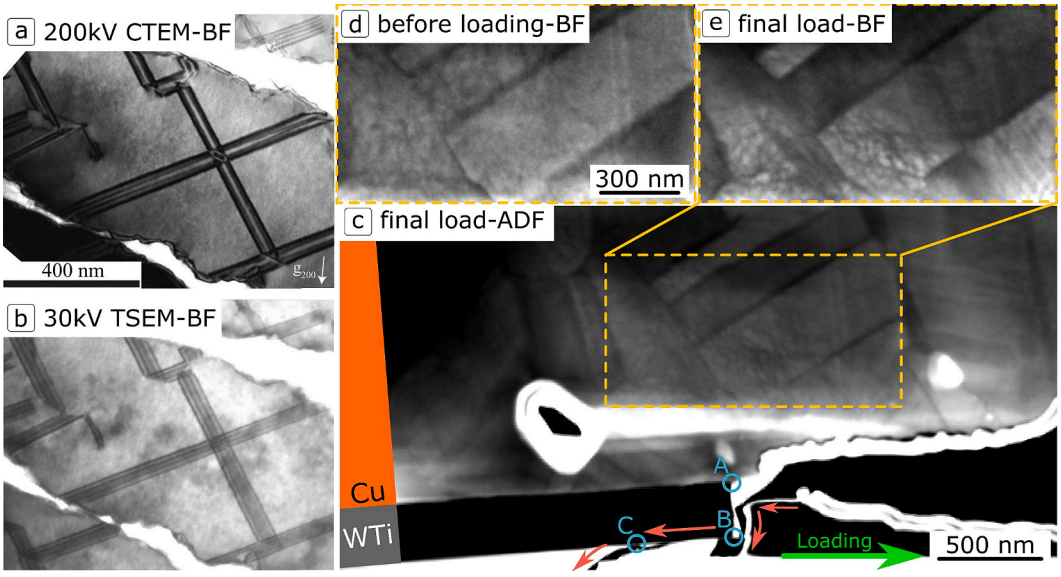

Fig. 8. Comparison of the same field of view in a cobalt based superalloy using (a) 200 kV conventional TEM and (b) 30 kV transmission SEM bright-field imaging [140] (Reproduced with permission). (c–e) Showcase of an *in situ* shear fracture experiment on a Cu-WTi-Si multilayer system (after [142]), where the crack path (A–C) is evidently deviating from the WTi-Cu interface to the Si-WTi interface, as depicted by the annular dark-field micrograph in (c). The local dislocation activity within the Cu phase can be observed best as comparative bright-field insets of the specimen (d) before loading and (e) at the final load.

quantitative load–displacement data in correlation with *in situ* observations of slip band formation, as well as dislocation decorelation/recorelation around γ' precipitates and formation of anti-phase boundaries. Such correlative detailed information would be demanding to acquire from either bulk deformation or *in situ* TEM experiments, respectively.

In another example, Alfreider *et al.* [142] used *in situ* TSEM imaging to investigate interface fracture characteristics of an elastic-plastically deforming Cu-WTi bi-material interface. There, specimens were fabricated on push-to-pull devices with tensile (mode I) and shear loading geometries (mode II), revealing purely ductile crack growth within the Cu phase for mode I loading, while interface crack nucleation and growth was evident for mode II loading. Fig. 8**c** depicts an annular dark field (ADF) micrograph of one such experiment at maximum load to showcase the utility of this experimental setup. The ADF images allow for a detailed investigation of the crack path, since edge effects are considerably reduced in comparison to BF imaging. In Fig. 8**c** it is evident that the crack grew from the initial notch along the WTi-Cu interface (point A) until it deflected straight through the WTi layer, presumably along columnar grain boundaries (point B). From there, the crack continued to grow along the WTi-Si interface until at a certain point the local loading configuration lead to deflection of the crack into the interior of the Si (point C). While the ADF images are beneficial for crack path features, simultaneous BF images enable easier observation of defect features, as depicted in Fig. 8**d and e**, where both correspond to the same region of interest before (d) and after (e) loading. The formation and movement of dislocations within individual Cu grains reveals the high amount of plasticity that is present concomitantly with the crack propagation process.

Taken together, TSEM offers quite promising characteristics for future experimental investigations, with oftentimes easier access for researchers compared to dedicated TEM instruments, more space for *in situ* equipment, *e.g.* mechanical transducers, thermal heaters/coolers or electrical probes, while still allowing for comparatively fast image acquisition. Especially with recent development of new monolithic detectors available for SEMs [145], image acquisition times could be lowered even further. Moreover, these fast observations during testing can be complemented with additional information acquired through previous or post-mortem conventional image formation modes, such as transmission Kikuchi diffraction mapping.

4. Towards extreme environments

4.1. Temperature control: From cryo to melting

To perform application relevant *operando* experiments, oftentimes testing under non-ambient temperatures is required. Especially many production processes and applications of advanced materials take place at high temperatures (HT). Accordingly, small-scale mechanical testing devices are equipped with heating systems to perform experiments under such HT conditions. However, not only the gathering of mechanical data at application temperatures was targeted in recent years. A lot of effort focused on multi-temperature testing approaches to acquire the activation parameters of the plastic deformation mechanism for the investigated material. As shown in Fig. 9, the highest achievable testing temperatures have been continually pushed upwards in recent years [146,147], with the highest reported temperatures now reaching 1100 °C [148]. As an outlier from the general trend, Grosso *et al.* [149] have shown that miniaturized testing can be performed even at temperatures beyond 2000 °C. However, at these extreme temperatures, shape changes of the test specimens due to surface diffusion and plasticity of the punch were reported as problematic [149]. Notably, these experiments were not performed in a conventional nanoindentation setting, but rather *in situ* in the extremely versatile TEM of Sandia Laboratory utilizing local infrared laser heating [149,150].

It must be noted that small scale mechanical testing at exceptionally high temperatures is not a straight forward task, and just because such experiments are possible does not mean they can be regularly performed with the same ease as a conventional nanoindent. On the contrary, a lot of time and effort needs to be spent in ensuring a well-controlled stable experimental setup. However, if certain limitations and pitfalls are carefully considered, such miniaturized local mechanical probing is an extremely powerful technique for mechanical characterization. The 2015 review by Wheeler *et al.* [146] already dealt exhaustively with most of these considerations, thus in the following only a brief résumé is given.

All micromechanical and nanoindentation devices rely on some kind of manipulator or tip to apply forces or displacements to the sample. As

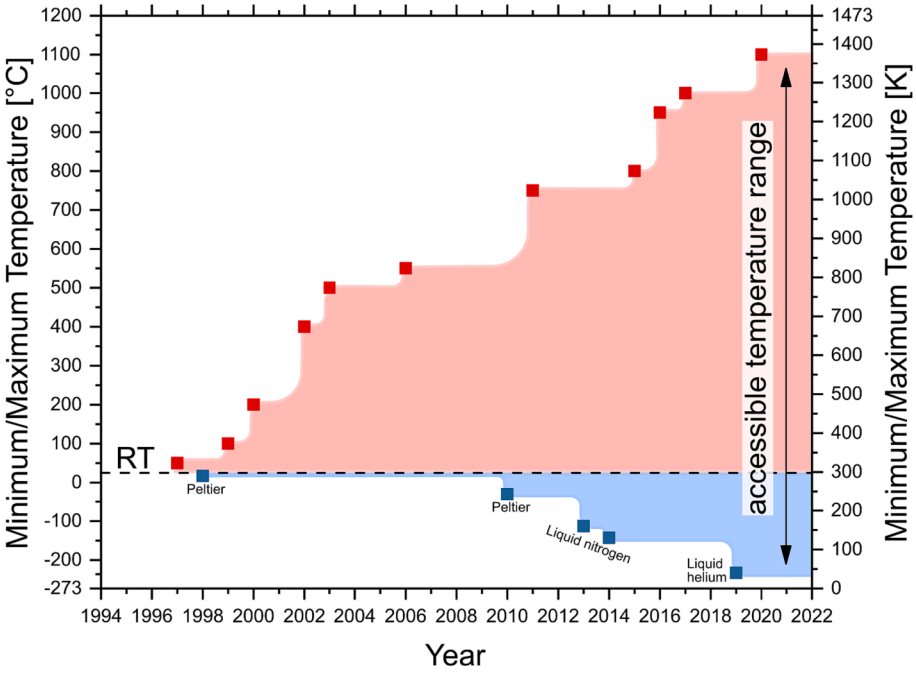

Fig. 9. Evolution of published maximum and minimum indentation temperatures over the last 28 years. Data in part taken from [146,147].

prominently discussed by Wheeler *et al.* [146], it is paramount that this probe and the sample are kept at the same temperature prior to and during contact. This "thermal match" is important, as any heat flux, and therefore a change of local contact temperature, will cause "contact drift" due to thermal expansion [146]. Another form of drift caused by the heating of the device is "frame drift" due to a contact independent heating of the machine components supporting the tip and sample [146]. This form of drift is less actively controllable. Typically, holding times of the machine at the desired measurement temperature are used to allow thermal gradients to settle. Also, additionally to keeping parts at safe operating temperatures, active cooling of indenter components can be used to retain the frame at a more stable temperature and thus reduce this drift component. As drift is a time-related phenomenon, another way to avoid or minimize its influence is to perform the test possibly fast to reduce the contact time. Such a fast HT indentation technique has recently been presented by Tiphene *et al.* [151]. In that "high-temperature scanning indentation" method the fast indentation even allows measurement while changing the experiment temperature [151].

A further important consideration when performing HT tests is the choice of an adequate tip material for the manipulator. Again, an overview of mechanically and chemically suitable combinations of manipulator and sample materials was presented by Wheeler & Michler [152]. However, another topic that has by comparison only been discussed scarcely by the community is the adhesion of the sample material to the manipulator. For example, Barnoush *et al.* [147] pointed toward cheap and quick-to-replace manipulators. This, however, jeopardizes the tip calibration, as in an extreme scenario a single experiment would require a tip that needs to be calibrated before. Such strategy seems not desirable for a high-throughput or high resolution investigation. Another path worth exploring is the application of friction and adhesion-reducing agents to the manipulator. However, such particles need to be applied in a way that does not adversely affect the contact. Preliminary data of the authors suggests that the application of finely dispersed MoS_2 particles can help to avoid the attachment of micropillars, which fail in a brittle manner at HT, to the flat punch manipulator. Therefore, the punch was immersed in isopropanol containing sub-micrometer-sized MoS_2 particles dispersed in it. After drying the particles remained on the tip. The MoS_2 was then evenly distributed on the punch by pushing it against the substrate prior to conducting the first experiments. However, it must be noted that this coating gets consumed during testing and loses its function eventually, thereby again placing limits on the attainable throughput. Also, it should be noted that high contact pressures and long contact times appear to promote the adhesion of sample material [153]. Accordingly, this is typically more problematic during indentation or creep testing compared to other forms of miniaturized mechanical experiments.

As established in the beginning of this chapter, small scale mechanical testing has been extensively applied to the characterization of various stress-, rate-, temperature, crystallography, structure and chemistry dependent deformation mechanisms. For example, testing at varying temperatures in combination with advanced protocols such as strain-rate jump tests enables the quantification of activation energies and activation volumes of the rate-controlling mechanisms of plasticity. The following segment is dedicated to highlighting some examples where such methods were successfully used.

Korte & Clegg [154] applied HT micropillar compression already in 2009 on spinel, where they performed compression experiments at different strain rates to obtain insights into the rate sensitivity and activation volume of dislocation plasticity. Furthermore, they reported a strong shift of the brittle to ductile transition temperature due to the small sample size.

Subsequently, these strain rate variation approaches were further developed through the introduction of strain-rate jump tests to the nanoindentation community by Alkorta *et al.* [155] and Maier *et al.* [156]. Numerous investigations using this technique have subsequently been performed on various materials. A prominent combination of methods was conducted by Wheeler *et al.* [157], where the activation parameters of ultra-fine-grained aluminum were assessed and comparison to bulk compression tests confirmed the applicability of the local strain-rate jump technique to HT nanoindentation [157]. For evaluation of the apparent activation energy, Wheeler *et al.* [157] used the method by Sherby & Armstrong [158]. This requires the input of a creep stress exponent [158], for which Wheeler et al. [157] assumed a value of 5 typical for dislocation creep. Contrarily, in a more recent study on tungsten, Kappacher *et al.* [159] took advantage of the fact that the creep stress exponent is the inverse of the strain rate sensitivity, and therefore directly accessible by strain-rate jump tests. The evaluation of the apparent activation energy can thus be based solely on measurement results, avoiding the need of assumptions regarding the material behavior. With that approach, Kappacher *et al.* [159] showed a reduction in the Peierls potential of tungsten through alloying with rhenium. Recently, Schaffar *et al.* [160] further adapted this approach by considering the change of constraint factor with temperature. Basing the activation energy analysis on an equivalent flow stress, rather than on hardness values, allows to account for the indentation response becoming more plastic with increasing temperature [160]. With this approach changes in the rate controlling dislocation mechanisms in silicon, previously reported for other semiconductors [161–163], were identified [160]. Alternatively, Choi *et al.* [164] and Lee *et al.* [165] avoided the use of the creep stress exponent entirely by adapting the activation energy evaluation of Shoeck [166] to indentation data. Utilizing this approach Choi *et al.* [164] investigated changes in deformation mechanisms in chromium, while Lee *et al.* [165] measured an increase in thermally activated plasticity above 200 °C in CoCrFeMnNi high-entropy alloys and suggested grain boundary diffusion as the underlying mechanism. In another study on cobalt, Kappacher *et al.* [36] also demonstrated the applicability of these strain rate jump techniques to the mechanical description of phase transformations.

These techniques for the evaluation of activation parameters are not exclusively used in indentation testing. Examples of their application to other nanomechanical techniques are the pillar experiments on semiconductors by Chen *et al.* [163,167], where experiments gathered a data set for the plasticity of silicon in small volumes from room temperature to 500 °C [167]. From this data, they addressed the frequently debated transition of perfect "shuffle" to dissociated "glide" dislocations at ca. 300 °C. For a short overview of dislocations on "shuffle" and "glide" planes in silicon, readers may refer to Duesbery & Joos [168]. Recent compression experiments on germanium pillars by the same group of authors [163] suggest a further change of dissociated back to perfect dislocations at even higher homologous temperatures.

To summarize, high temperature small scale mechanical testing is nowadays an established technique. These experiments can gather application-relevant data under *operando* conditions. Furthermore, variable temperature micromechanical experiments are a powerful tool to assess the thermal activation parameters of plasticity, and therefore typical characteristics for the identification of rate-controlling deformation mechanisms.

While impressive results regarding the measurement of activation parameters of plasticity have been achieved, the methods currently applied are frequently time consuming and prone to errors due to drift, tip degradation and adhesion of sample material to the tip. Fast testing approaches, such as the high-temperature scanning indentation technique [151] show a lot of promise, as they allow to avoid time related influences. However, while Tiphene *et al.* [151] demonstrate that their protocol can also be used to acquire thermal activation parameters, fast testing is obviously limited to higher strain rates than usually applied. Furthermore, the chosen load profile induces different strain rates, which depend on the hardness and therefore temperature [151]. Lastly, evaluating strain rate sensitivities from non-constant strain rate segments introduces the necessity to deconvolute strain rate and indentation size effects [169]. Accordingly, still a tradeoff remains regarding the choice of technique, and the related potential sources of error that are

more acceptable for the planned investigation.

In addition to these advancements in nanoindentation at elevated temperatures, *in situ* nanomechanical testing at sub-ambient temperatures is gaining increasing attention, as seen in Fig. 9. Vickers hardness testing at cryogenic temperatures has already been realized in the 1960s [170] by placing the whole testing setup in a bath of liquid nitrogen. Since modern nanoindentation devices are equipped with highly sensitive force and displacement sensors as well as actuators, such a rather crude approach cannot be taken without severe risk of damaging the system. The first account of depth-sensing indentation at sub-ambient temperatures has been published by Syed Asif & Pethica [171] in 1998. They used an indentation setup including Peltier elements and heat sinks on both the indenter and sample side to regulate temperature and protect the sensitive indentation electronics. As mentioned above, temperature matching between sample and indenter tip is crucial for the accurate assessment of properties during indentation at non-ambient temperatures. In theory, the Peltier elements could cool the sample and indenter tip down to about -40 °C. However, the formation of ice from air humidity limited the testing temperatures in their work to above the freezing point. A similar setup was utilized by Chen *et al.* in 2010 [172] to study the mechanical properties of polypropylen below its glass transition temperature, and in 2011 to explore the wear resistance of diamond-like carbon at low temperatures [173]. They adapted the Peltier setup by flooding the test chamber with argon, which prevents the formation of ice and allows for the first published instance of below freezing nanoindentation at minimum temperatures of −30 °C.

It was at this point in time that the limits of Peltier cooling were reached and there was no more circumventing "classical" cooling concepts involving direct cooling via mediums such as liquid nitrogen. Moreover, previously only conventional *ex situ* nanoindentation hardness testing has been performed at low temperatures. Lee *et al.* [174,175] and Lupinacci *et al.* [176] were the first to utilize custom-built cold finger setups in conjunction with liquid nitrogen inside an SEM to perform *in situ* micropillar compression at temperatures down to 160 K and 130 K, respectively. In both setups the evaporated nitrogen flows through the cold finger to cool down a Cu block inside the SEM, from which Cu wires connect to both, the specimen holder and indenter tip holder, respectively. The temperature can be regulated either by controlling the flow of nitrogen gas, or by employing additional heating elements. Aside from the possibility to perform *in situ* experiments, an additional advantage of the SEM chamber is that the vacuum environment prevents the formation of ice as long as it remains closed, and unwanted heating of the system through convection. This kind of low temperature indentation setup has since then seen many applications in metal, ceramic and polymer research [163,177–184] and is considered the state-of-the-art when it comes to sub-ambient nanomechanical testing. So much so, that there are now even commercially available indentation modules utilizing a cold-finger setup, such as the Alemnis LTM-CRYO module. By replacing liquid nitrogen with liquid helium, even lower temperatures can be reached [185–188], with the current world record being held by the lab of Seok-Woo Lee with a minimum temperature of 40 K [185].

Progressing low temperature nanoindentation from *ex situ* to *in situ* allowed for detailed investigation of failure mechanisms, crack propagation and deformation characteristics. Taking a step further, combining such systems with EBSD analysis can be beneficially applied to detect and observe stress-driven grain growth [189], deformation twinning [190] or phase transformations in great detail during mechanical loading at cryogenic temperatures.

The applications of nanomechanical testing at sub-ambient temperatures have been widespread, yet can mostly be associated with studying plasticity and deformation mechanisms at low temperatures [171,174,175,177–181,183,190], investigating phase transformations and glass transitions [163,172,191,192], testing mechanical properties of materials used in space flight or other cryogenic applications [176,182,189], or combinations of these. As such, low temperature nanoindentation provides a valuable means to further enhance our understanding of material plasticity and to mechanically test high-performance cryo-materials in their operating environment. However, it is also worth mentioning that such low temperature experiments open up possibilities for a more direct comparison to ab-initio calculations such as density functional theory, since these are commonly performed at or close to 0 K, thereby facilitating the in concerto operation of experiment and modeling.

Given the recent progress in high and low temperature nanoindentation and related small scale testing techniques, the scientific community has now access to an impressive range of temperatures for mechanical testing at the micro- and nanoscale (see Fig. 9), paving the way for further investigation of mechanical behavior in dependence of temperature, as well as for the more accurate assessment of properties of high-performance materials under operating conditions in extreme environments.

4.2. Irradiation effects

Micro- and nanomechanical testing has become an integral part of nuclear materials engineering in recent years. This is reasoned in part by the drastically reduced necessary sample size, making the handling of radioactive specimen much more straight forward since hot cells are typically not required [147,193]. Needless to say that in times of life time extension and limited surveillance specimens, miniaturized material volumes are great news for nuclear engineers. Another, even more prevalent reason, is the uprising of ion beam irradiation as a surrogate to neutron irradiation in the study of materials responses to (high dose) irradiation damage and resulting radiation effects [194]. Although neutrons are the main source of radiation damage for materials in nuclear environments, their practicality for materials irradiation studies is poor. Irradiated samples get easily activated, the access to neutron irradiation sources (typically reactors) for research is limited and the dose rate is extremely low, resulting in irradiation times from days up to several years for reasonable dose levels [195]. In contrast, ion beam irradiation offers a non-activating, more easily accessible and higher dose rate alternative, taking mere hours to achieve exceedingly high radiation doses that simulate damage from neutron irradiation almost perfectly [194,196]. The most significant drawback of ion irradiation is the charged nature of the radiation particles, leading to rapid energy loss due to interactions with electrons in the target material, and consequently a very shallow penetration depth and a related irradiated zone of several 100 nm up to 100 μm for high-energy ion beam sources [193,195]. Also, one should note that transmutation effects are typically absent in ion irradiation.

It is this rather limited volume of irradiation-affected material that calls for small-scale mechanical testing methods to assess radiation effects on mechanical properties, as an impressive amount of recent research works attest [193,195,197–199]. Conventional nanoindentation hardness testing [200–202], micropillar compression [203,204], microtensile testing [205,206] and microcantilever bending and fracture experiments [207,208] have been utilized to great success *ex situ* and *in situ* to study radiation hardening, irradiation-induced creep, radiation embrittlement or irradiation-induced segregation in a wide host of nuclear-relevant materials, often also at elevated temperatures.

However, the microstructural evolution and defect formation during irradiation can paint a rather complex picture that one cannot hope to capture completely only via mechanical testing. Complementary characterization methods coupled with nanomechanical testing have gained recent attention in the community, allowing for a more profound understanding of radiation-induced defects and their consequences for microstructure evolution and related changes in mechanical properties. Conventional XRD [209] and synchrotron μXRD [210] have been commonly utilized to study defect densities of irradiated materials and complement nanoindentation studies. However, there exist now higher

resolution methods to investigate defect densities and distributions. Positron annihilation spectroscopy (PAS) offers the depth resolution to quantify the defect density distribution in implantation direction, and also allows in some cases for the differentiation between vacancy- and interstitial-type defects [211–213]. Naturally, this spectroscopy technique has seen application in nuclear materials research for characterization of the distribution and amount of radiation-induced defects [212,213], yet studies utilizing PAS in combination with nanoindentation and nanomechanical testing are scarce [214]. Given exceptional improvements in detector and computing technology, 4-dimensional scanning TEM (4D-STEM) is now also a viable tool to study defect evolution in irradiated materials. Using nanobeam electron diffraction, 2D diffraction patterns can be recorded for each pixel of a 2D TEM image, hence the name "4D" STEM [215]. This technique allows for nanometer to atomic spacing in spatial resolution and has already been utilized to investigate vacancy concentration and distribution in ion-beam irradiated materials [216]. Combining these high-resolution defect characterization methods with small-scale mechanical testing in the future has great potential for detailed exploration of the interplay of irradiation induced defects with plasticity, fracture and time-dependent mechanical properties (see Fig. 10**a**).

The methods and works mentioned so far all investigated materials before and after irradiation. However, we can obtain even more information from observing and testing materials during irradiation. After all, the microstructure and introduced defects could cluster, annihilate or relax between irradiation treatment and mechanical testing. Materials exposed to radiation environments, e.g. reactor materials, are however exposed to mechanical and thermal loads while being irradiated, which can have important implications on dynamic defect formation, evolution and clustering and, hence, on mechanical property degradation. *In situ* TEM irradiation facilities, such as I^{3}TEM (In situ Ion Irradiation TEM) at Sandia National Laboratory [150,217] and MIAMI (Microscope and Ion Accelerators for Materials Investigations) at the University of Huddersfield [218], attempt to unravel these influences. By combining ion irradiation beamlines with sample heating options and nanomechanical testing devices within a TEM, microstructure, mechanical properties and defect behavior can be investigated during irradiation at relevant temperatures and mechanical loads (Fig. 10**a**). Research on these devices have focused on microstructural evolution and defect formation so far [150,217,219–224], yet some works have already utilized nanomechanical testing options. For example, it was shown that mechanical loading immediately after irradiation of ufg Au can lead to stress-driven GB migration, which in turn results in healing of radiation-induced defects and an overall radiation tolerant behavior [225]. There have also been some works studying irradiation-induced creep of different materials at ambient and elevated temperatures inside such an *in situ* irradiation TEM facility [150,226,227]. These examples highlight the hidden or at least not fully tapped potential of *in situ* nanomechanical testing under realistic reactor conditions, which will certainly play a significant role in the development of future nuclear fission and fusion reactors as well as the structural materials deployed therein [228].

Apart from these multi-characterization testing techniques, another topic that has gained traction over recent years is the influence of helium on microstructure and properties of nuclear materials. Helium as a noble gas is insoluble in metals and readily forms gas bubbles within them, leading to structural disintegrity and tremendous swelling. Helium has always posed a minor problem for nuclear materials as a transmutation product of alloying elements or in specific reactor models, such as the CANDU reactor [229,230]. However, with the increased interest in nuclear fusion and helium being a product of the most commonly used deuterium–tritium fusion reaction, new enthusiasm has been sparked to investigate the influence of helium on structural candidate materials for fusion reactors. Aside from conventional ion accelerators and beamlines, another option has provided even easier access to helium implantation of materials: the helium ion microscope (HIM) [231,232]. Using such a HIM, helium ions with energies up to 25 keV can be implanted to fusion relevant fluences within minutes to hours in typical areas of $10\times10\ \mu m^2$. As such, a specimen to study He dose effects can be realized within a day requiring only a mm sized polished sample.

Helium-induced swelling can be measured easily using atomic force microscopy (AFM) [233–238]. Given the rather small ion energies, typical penetration depths of the helium ions are only between 100 and 300 nm, making it challenging even for nanoindentation to probe radiation-induced property changes, as it becomes difficult to avoid substrate effects arising from the unimplanted material. In a sense, the community came back to one of the initial motivations to build a nanoindentation device: probing irradiated surfaces [239,240]. However, modern CSM indentation allows for more informative hardness and modulus data with indentation depth and should be considered in favor of single data points from conventional nanoindentation testing (see Fig. 10**b**) [233,235–238]. To extract only the hardness of the irradiated layer, certain plastic zone size models can be applied [198,235,241], allowing for the approximation of radiation-induced property changes even for irradiation layers of below 500 nm depth (see Fig. 10**c**). Using such combined HIM, AFM and indentation approaches, several works reported that helium implantation leads to competing radiation hardening, predominant at lower helium fluences,

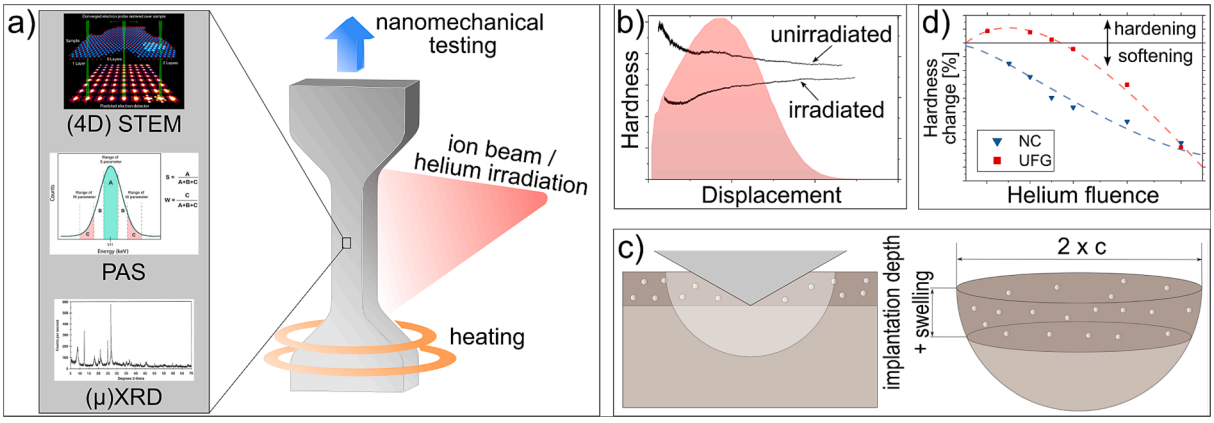

Fig. 10. *In situ* material radiation examination. (a) Schematic of multipurpose characterization of nanomechanical specimen in reactor-like conditions (adapted with permission from [212,215]). (b) CSM indentation reveals hardness evolution with indentation depth of unirradiated and helium-implanted Cu-Fe-Ag. Red shaded area represents dose profile. (c) Plastic zone size model used for extracting hardness of only the irradiated layer. (d) Nanoindentation reveals competing radiation hardening and gas bubble softening mechanisms in ufg Cu-Fe-Ag. (b), (c) and (d) reproduced with permission from [235].

and gas bubble softening, predominant at higher helium fluences, effects in ufg and coarse grained materials [233,235,236,238,242,243] (Fig. 10**d**). For nanocrystalline metals, the softening mechanism is more pronounced [235,236], while in all cases elastic modulus decreases and swelling increases continuously with increasing helium fluence.

The investigation of radiation-induced mechanical property changes using nanomechanical testing techniques continues to receive a lot of attention. The focus shifts from lone post-irradiation mechanical testing to coupling indentation-based methods with high resolution characterization tools. This serves to study microstructure and defect evolution under mechanical loads, not only after but also during irradiation and exposure to reactor-like environments. Moreover, the influence of helium implantation on swelling and mechanical properties has emerged as exciting research topic, given the concrete application case in nuclear fusion. In the future, combining these capabilities with TEM analytics, we might be able to establish links between interface microstates and irradiation defect sink efficiency, opening completely new avenues for interface design of low alloyed materials deployed in radiative environments, be it a reactor or a deep space probe.

4.3. *Electro-chemical nanoindentation*

In the previous chapters, the experimental possibilities and challenges for *in situ* and *operando* conditions with respect to application temperatures or irradiation were regarded. Another important area of *operando* investigations concerns the area of electro-chemical nanoindenation, vital for example to test biological structures in their native environment or to further deepen our understanding of hydrogen-material interactions [244,245]. Firstly applied *operando* by Barnoush & Vehoff [246] in 2006 and subsequently, this experimental approach recently gained increasing attention due to the global energy challenges. The basic idea arose from liquid cell nanoindentation, were the indentation experiments are performed within a liquid medium. However, in this case also a more or less controlled electrochemical potential is applied. With this "front-side" charging approach, where the electrolyte is in direct contact with the investigated material, several aspects for battery [247] and hydrogen-material interaction were successfully investigated. Besides basic nanoindentation testing for hardness and modulus measurements [248], also further pop-in load analyses [249] were conducted to shed more light onto hydrogen-caused changes in the local deformation behavior. Nanoindentation probes the plastic deformation in a multiaxial compression mode and is therefore limited in assessing damage or failure. Thus, further micromechanical testing techniques such as pillar compression [250] or micro bending experiments [251,252] were applied to directly examine hydrogen embrittlement during electro-chemical charging in small volumes.

Notably, these electro-chemical charging setups installed within nanoindentation systems sometimes suffer from machine stiffness issues due to the necessity for long tip shafts, lifting tables, etc. To address these challenges, Ebner *et al.* [253] introduced a modified stiffened sandwich-like setup, which allows reliable and reproducible experiments to higher loads, and correspondingly higher displacements. This is essential in order to probe larger microstructurally representative plastically deformed volumes and avoid unintended indentation size effects due to shallow imprints. Combining this stiffer setup with the implementation of nanoindentation strain-rate jump tests, it was possible to directly measure changes in strain-rate sensitivity, and thus activation volume, during hydrogen charging. An example is shown in Fig. 11 for a Ni based alloy by a rigorous comparison of elastic and plastic parameters in air, under electrolyte, in hydrogen charged condition, and after outgassing of H. Such a controlled strategy is essential to eliminate potential unwanted influences, for example due to chemical attack of the surface by the electrolyte. This verified quantitative information was enhanced by correlative microscopy approaches using confocal laser scanning microscopy (Fig. 11). A detailed analysis of the pile-up formation and plastically deformed zone provided first hints that under the influence of hydrogen the deformation occurs more localized, leading to smaller plastically deformed zones and higher pile up formations.

Notably, during front side charging some materials suffer corrosion influences from the electrolyte, which impedes surface sensitive experiments or the reliable analysis thereof. Consider, for example, a pop-in analysis, whereby the surface is potentially roughened or deformed due to chemical attack or stress built up during the electro-chemical charging. Clearly, an unbiased analysis can become a challenging endeavor. In recent years, this stimulated further discussions on alternative charging procedures in literature. While for mesoscale tensile testing different contamination free approaches are described in literature [134,255,256], Duarte *et al.* [257] recently conducted a comparison between the conventional front side charging approach and a newly developed backside charging cell. There the electrolyte is stored underneath the surface, while the micromechanical experiments are performed on the surface without electrolyte influence. This approach is

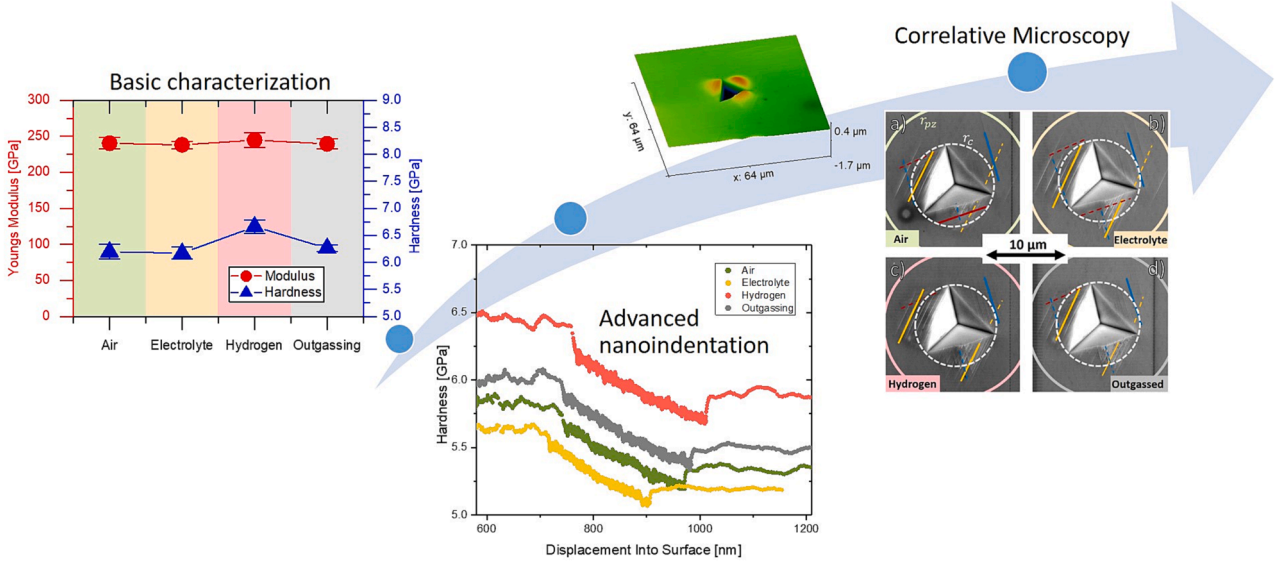

Fig. 11. *In situ* electrochemical nanoindentation: Applying advanced nanoindentation methods such as strain-rate jump tests under non-ambient conditions together with correlative microstructural characterization methods allows to shed light into advanced deformation processes such as hydrogen material interactions. (adapted with permission from [253,254].)

beneficial in avoiding the corrosion issues. However, longer diffusion times and related concentration gradients depending of the diffusion characteristics of the examined material [255], as well as possible setup stiffness issues due to employing a rather thin material membrane to reduce charging times in low diffusivity materials, must be taken into account when applying this backside charging method.

4.4. Biological materials

Given the hierarchical nature of many biological materials, mechanical testing spanning multiple length scales is key to understanding the mechanical property amplification arising from the hierarchical arrangement of typically rather brittle material constituents, such as organic polymers and ceramics [97,258–262]. This is reflected in many research works ranging from the tensile testing of individual collagen fibrils [263], to fracture testing of whole human femurs [264–266] and even whale baleen [267]. In a multi-scale consideration, micro- and nanomechanical testing techniques hereby provide the possibility to probe a length scale that is considered quite important in the ultrastructure of biomaterials. Crack deflection, crack arrest and crack bifurcation at compliant layers [258,264,268,269], pullout of collagen, cellulose or keratine fiber [258,265,266] or cross-linking of proteins and other organic polymers [258,270–272] are just a few examples for mechanisms at the micro- to nanoscale that give rise to the attractive combinations of strength, stiffness and fracture toughness of materials such as bone [97,264–266], teeth [273–276], antler [258], sea shells [97,258,277], and others. Mechanical testing at such length scales is not only crucial for the understanding of property amplification concepts and the possible adaption of said concepts to synthetic biomimetic materials [260,261,278], but can also have a large impact on biomedical research, as e.g. the influence of certain diseases on mechanical behavior of bone or teeth can be revealed [279–281].

While nanoindentation is increasing in usage for mechanical assessment of biological materials [282–288], nanomechanical testing of more complex geometries has not attained a lot of attention yet, be it *ex situ* or *in situ*. This is a consequence of a multitude of challenges that arise with mechanical testing of organics-containing materials. Aside from dynamic issues regarding the viscoelastic nature of such materials and tissues [289,290], as well as typically poor statistics given the time consuming sample preparation and influence of age and disease on mechanical properties, by far the most challenging problem is that the majority of biological materials behave mechanically very differently in hydrated and dehydrated state [258,289,291]. As the hydrated state of course resembles the conditions found within living organisms, testing of biomaterials in dry conditions can be seen as rather pointless, yet is still a fairly common practice as a large body of research works [292–295] shows. Naturally, the prerequisite of testing biological materials in a hydrated state poses a major challenge for nanomechanical testing devices. A quick but unsound workaround would be to immerse the specimen in a salt based solution with physiological pH for multiple hours and then examine the mechanical properties quickly and with frequent rehydration in between dry indentation cycles. However, one can only be certain of measuring correct results by either performing the testing with the sample immersed in liquid throughout the whole experiment, or by continuously hydrating the samples. This is realized, for example, by performing small-scale mechanical testing in liquid cell AFM- or nanoindentation devices [282,289,291], or by meticulously controlling the humidity inside an indentation chamber [296–298]. However, the lack of *in situ* capabilities with these instruments leads to the necessity of realizing nanomechanical testing of biological materials within environmental SEMs (ESEMs), where humidity can be regulated in low vacuum modes [299] and specimen can be observed during testing (see Fig. 12**a**).

The micromachining of miniaturized specimen geometries using a FIB inside a combined FIB/SEM workstation is also challenging. Although Jimenez-Palomar *et al.* [300] reported no change in (micro) mechanical properties of bone samples after exposure to an SEM vacuum for two hours, one should take care that biological specimen do not dehydrate too much during FIB processing and perform regular rehydration steps. However, one cannot be certain if irreversible damage occurs to biological tissue during dehydration in an SEM vacuum [301]. Here, mesoscale machining tools that do not need an electron microscope vacuum to operate, such as femtosecond laser workstations [302,303], provide a helpful workaround, albeit only for coarse and larger structures on the mesoscale (>20 μm).

As mentioned above, an exciting application of small-scale testing is unraveling the secrets of the hierarchical structure and ensuing mechanical property amplification of biomaterials. It has therefore found plenty of use in research regarding bone mechanics. Besides a plethora of nanoindentation studies [282,292,293,304], also other nanomechanical test geometries have recently been utilized to great effect. Micropillar compression [291,294,305,306], microbeam bending [289,307] and microtensile testing [308] have been performed on single bone lamellae to study the effect of collagen orientation and hydration on mechanical properties and deformation characteristics. These studies revealed that on the lamellar level bone exhibits a much higher strength and better ductility than on the macroscale, and it is theorized that the quasi-brittle nature of bone stems from cracks running in between lamellae [294,306]. Moreover, a huge effect of mineralized collagen fibril orientation on strength has been observed, with the strength of pillars containing fibrils with parallel orientation being almost three times higher than those with perpendicular arrangement [305]. The effect of hydration was also studied with hydrated bone specimens, showing a strength of only 60% compared to dehydrated samples [291] and modulus values of up to five times smaller [289]. These exemplary studies highlight the potential that micro- and nanomechanical testing techniques have for the exploration of highly hierarchical structural composite biomaterials, such as bone. In future, fracture and fatigue testing at these length scales should provide valuable information, but also come with a plethora of experimental challenges.

Sometimes the application of micro- and nanomechanical testing on biological materials is inevitable, given their small physical size. This is for example the case for many gastropod teeth. These teeth are usually ceramic composites and tend to be almost completely free of organics,

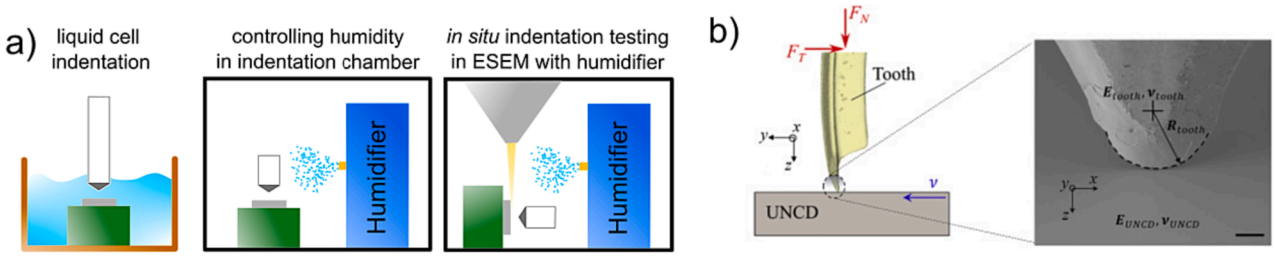

Fig. 12. (a) Different experimental setups for nanomechanical testing of biological materials in hydrated condition. (b) *In situ* wear testing of sea urchin teeth with the tooth mounted as indenter tip.
(Reproduced with permission from [313]).

making dry testing feasible. It is interesting to note that some of these teeth, such as limpet (*Patella vulgata*) and chiton (*Cryptochiton stelleri*) teeth exhibit extraordinary high strength and hardness, respectively [274–276]. These findings could only be achieved via small-scale testing methods, given that these teeth have a typical length of around or below 500 μm. Barber *et al.* [274] utilized *in situ* nanomechanical tensile tests within an AFM to unveil a strength between 4 and 7 GPa and an elastic modulus of 120 GPa of the limpet tooth, making it the strongest material in nature. Recently, a rotational response of ceramic nanorod bundles during *in situ* TEM tensile loading and, as a consequence, nanoscale localized auxeticity has been documented in the leading part of these teeth [275]. This auxeticity is believed to be the main reason for their extreme strength and expected to also increase wear resistance. The same work reports slightly lower strength values of 3 to 4 GPa and more reasonable modulus values of about 38 GPa utilizing *in situ* micropillar compression tests. Interesting enough, the auxetic response of the limpet tooth microstructure seems to cause microdamage formation within the material when indented with a sharp tip (*i.e.* high indentation strain), as revealed by Berkovich nanoindentation and micromechanical FEM studies [309]. This leads to the rather peculiar phenomenon of measuring lower hardness values in nanoindentation than strength values in pillar compression in the leading part of limpet tooth, and highlights once more the importance of performing complementary testing techniques when aiming to fully characterize such complex materials.

Micro- and nanomechanical testing, especially nanoindentation, has become a popular tool for the mechanical characterization of gastropod and other miniaturized teeth [276,295,310–312]. However, one work that utilizes different nanomechanical testing and deserves highlighting is by Espinosa *et al.* [313,314]. Apart from nanoindentation and micropillar compression testing, they identified that the most important mechanical property of sea urchin and chiton teeth is wear resistance, as they feed from rocky substrates and sometimes even bore holes into rocks to hide from predators. Rather than performing conventional nanoindentation wear studies, they mounted individual teeth in place of the indenter tip and performed tribological wear testing on an extremely hard ultra-nanocrystalline diamond substrate (Fig. 12**b**). Using this creative approach, they could unravel the micromechanics behind the self-sharpening nature of sea urchin and chiton teeth.

Taken together, the application of small-scale mechanical testing to biological material has huge potential given the hierarchical structure and small physical size of important mechanical features. However, established testing routines still need to be developed, especially to deal with issues arising from having to test specimen in hydrated condition. In particular, the local fracture and fatigue testing of bone and other biomaterials would be very interesting, not only for the materials science, but also the biomechanics and medical research communities. Here reliable *in situ* crack tracking methods have to be applied, as the observation within the vacuum environment of conventional SEMs leads to dehydration of the specimen, and unloading stiffness approaches have been proven to not be reliable for biomaterials such as bone [290]. *In situ* nanomechanical testing in an ESEM seems to be a promising option to provide a path towards ensuring this goal and should be pursued more in the future.

Aside from testing of biological tissue, it should be noted that nanomechanical testing has also found its way into pharmaceutical applications, such as drug delivery, in recent years. Strength, ductility, hardness, fracture toughness, and adhesion properties of drugs, such as pharmaceutical single crystals and molecular crystals, play an especially important role in their manufacturing processes. These can include mechanically challenging procedures, such as milling, mixing, granulation, and compression, but also processes in non-standard environments, such as crystallization and storage or the application in a physiological environment inside the human body. Given the rather small size and difficult environmental conditions, nanomechanical testing in humidity-controlled conditions and at elevated and low temperatures, as described in this review, has gained traction in the past few years. Majumder *et al.* [315] summarized the advancements in this field in a recent review, to which the interested reader is referred.

5. Conclusion

Recent developments and achievements in nanoindentation instrumentation as well as micro- and nanomechanical tests building on these tools now enable valuable novel avenues of research. However, there is still plenty of room at the bottom [316], and below we attempt to highlight our personal opinion on significant possibilities as well as potentially missing features:

- Realistic testing conditions from room temperature to extreme environments

  Predicting the mechanical performance of a material employed under extreme conditions from limited data at ambient conditions can be done. However, recent developments allow to conduct the characterization at well-controlled conditions close to the in use scenario, for example in terms of temperature, strain rate, and environment, to name a few. This certainly provides on the one hand an opportunity for studying more extreme material conditions, but on the other hand also the possibility to broaden the field of applications, since based on successful developments within the small scale community, these capabilities are now commercially available for a more general use.

- Heterogenous materials - Bridging length scales from macro to nano

  Not only can experiments be conducted at increasingly extreme conditions, the concurrent development efforts also allow to conduct them in a scale-bridging manner from nano to micro. What remains an unavoidable persistent question is the link from local microscopic scales probed in nanoindentation or miniaturized testing to bulk behavior. Obviously, these techniques can conveniently examine individual mechanisms, such as a specific grain boundary, or probe bulk properties of nanostructured materials. However, linking to macroscopic properties in strongly heterogeneous materials, as resultant e.g. from additive manufacturing, remains challenging and would benefit from stronger links to three-dimensional material modeling, *meso*-scale material testing, or intensified local flow curve mapping of such materials.

- High quality miniaturization of demanding non-static material testing approaches

  While some time ago nanoindentation was regarded as an exceptional technique, as it can locally measure hardness and modulus, nowadays much more demanding properties such as strain rate sensitivity or local flow curves can be mapped over representative material volumes. At the same time, miniaturized mechanical experiments provide access to dynamic material properties spanning from creep to fracture. While the techniques are available, the experimental protocols and analysis routines are not as well established as for classical nanoindentation results, which could present a barrier or potential pitfalls to the interested non-experts. Open data sharing of testing and analysis protocols by the community could be a valuable source to spread knowledge and avoid misinterpretation.

- Detailed complementary mechanistic observations during *operando* experiments

While mechanically probing individual grains or interfaces can be accomplished today, even under rather harsh environments, establishing the link to atomistic details or individual dislocation processes remains a challenge. This is rooted in the much more demanding and space limited environment of the TEM compared to an SEM or platform nanoindenter. Further pushing TSEM approaches, potentially even merging them with environmental microscopy, might be an auspicious path to close this knowledge gap on defect dynamics under extreme environments.

- Great opportunities for data driven materials design approaches

It is imperative to realize that modern instrumentation and related experiments not only deliver a few data points on material hardness and modulus, they rather provide complete mappings of elastic, plastic and transient material properties with a resolution challenging optical microscopy. Adding *in situ* experimentation to this, the data pool changes from a two dimensional mapping of property versus time information to sparser experiments, but these now also include two dimensional time resolved image data on top of the mechanical characteristics. While there is currently not too much use of this kind of information for data driven materials exploration, it could be a rewarding effort to combine such different data streams, one of high-throughput, the other of high fidelity, both probably produced in different labs using various instruments, into a multi-fidelity machine learning model to support more resource efficient and sustainable materials design.

- High potential for inter- and transdisciplinary research

With the rising availability of such CSM capable instruments and the advances in testing methodology, there is a growing field of potential applications not accessible previously. This ranges from deep space exploration to fusion-based energy, from corrosive attack to hydrogen storage and conversion, from precious heritage objects via natural materials to biological structures and medical challenges, to name just a few. Materials science as a community certainly possess the capabilities to examine the mechanical properties of such unconventional or extraordinary materials or objects. The non-materials science expert studying the respective problem might, however, be challenged by the required instrumentation or not even aware of the possibilities existing. In that aspect, some network activities such as the ongoing MecaNano COST action (CA 21121) could be valuable platforms to spread micro- and nanomechanics to a wider community.

In conclusion, despite all the significant advances achieved in recent years, there still seems to be a vibrant future ahead. Realizing that it took a time span of about twenty years from when the first nanoindentation results were conducted until CSM techniques became broadly available to the scientific community, also serving as the enabling feature for the content of this work, one might curiously wonder how much longer it takes for the next evolutionary leap in nanomechanics to occur, and what currently unheard possibilities it will enable.

Declaration of Competing Interest

The authors declare that they have no known competing financial interests or personal relationships that could have appeared to influence the work reported in this paper.

Data availability

Data will be made available on request.

Acknowledgments

Funding by the European Research Council (ERC) under grant number 771146 (TOUGHIT) is greatly acknowledged.

References

[1] W.C. Oliver, G.M. Pharr, An improved technique for determining hardness and elastic modulus using load and displacement sensing indentation experiments, J. Mater. Res. 7 (1992) 1564–1583, https://doi.org/10.1557/JMR.1992.1564.
[2] H. Nili, K. Kalantar-zadeh, M. Bhaskaran, S. Sriram, In situ nanoindentation: probing nanoscale multifunctionality, Prog. Mater. Sci. 58 (2013) 1–29, https://doi.org/10.1016/j.pmatsci.2012.08.001.
[3] J.M. Wheeler, B. Gan, R. Spolenak, Combinatorial investigation of the Ni–Ta system via correlated high-speed nanoindentation and EDX mapping, Small Methods. 6 (2022) 2101084, https://doi.org/10.1002/smtd.202101084.
[4] J.B. Pethica, W.C. Oliver, Mechanical properties of nanometre volumes of material: use of the elastic response of small area indentations, MRS Proc. 130 (1988) 13, https://doi.org/10.1557/PROC-130-13.
[5] J. Hay, P. Agee, E. Herbert, Continuous stiffness measurement during instrumented indentation testing, Exp. Tech. 34 (2010) 86–94, https://doi.org/10.1111/j.1747-1567.2010.00618.x.
[6] W.C. Oliver, G.M. Pharr, Measurement of hardness and elastic modulus by instrumented indentation: advances in understanding and refinements to methodology, J. Mater. Res. 19 (2004) 3–20, https://doi.org/10.1557/jmr.2004.19.1.3.
[7] B. Merle, V. Maier, M. Göken, K. Durst, Experimental determination of the effective indenter shape and ε -factor for nanoindentation by continuously measuring the unloading stiffness, J. Mater. Res. 27 (2012) 214–221, https://doi.org/10.1557/jmr.2011.245.
[8] G.J.K. Schaffar, J. Kappacher, D. Tscharnuter, V. Maier-Kiener, The phase transformation of silicon assessed by an unloading contact pressure approach, JOM 74 (2022) 2220–2230, https://doi.org/10.1007/s11837-022-05290-4.
[9] K. Durst, V. Maier, Dynamic nanoindentation testing for studying thermally activated processes from single to nanocrystalline metals, Curr. Opin. Solid State Mater. Sci. 19 (2015) 340–353, https://doi.org/10.1016/j.cossms.2015.02.001.
[10] J. Ast, B. Merle, K. Durst, M. Göken, Fracture toughness evaluation of NiAl single crystals by microcantilevers - a new continuous J-integral method, J. Mater. Res. 31 (2016) 3786–3794, https://doi.org/10.1557/jmr.2016.393.
[11] G.M. Pharr, E.G. Herbert, Y. Gao, The indentation size effect: a critical examination of experimental observations and mechanistic interpretations, Annu. Rev. Mater. Res. 40 (2010) 271–292, https://doi.org/10.1146/annurev-matsci-070909-104456.
[12] K. Durst, B. Backes, M. Göken, Indentation size effect in metallic materials: correcting for the size of the plastic zone, Scr. Mater. 52 (2005) 1093–1097, https://doi.org/10.1016/j.scriptamat.2005.02.009.
[13] K. Durst, O. Franke, A. Böhner, M. Göken, Indentation size effect in Ni–Fe solid solutions, Acta Mater. 55 (2007) 6825–6833, https://doi.org/10.1016/j.actamat.2007.08.044.
[14] W.D. Nix, H. Gao, Indentation size effects in crystalline materials: a law for strain gradient plasticity, J. Mech. Phys. Solids. 46 (1998) 411–425, https://doi.org/10.1016/s0022-5096(97)00086-0.
[15] B. Moser, J.F. Löffler, J. Michler, Discrete deformation in amorphous metals: an in situ SEM indentation study, Philos. Mag. 86 (2006) 5715–5728, https://doi.org/10.1080/14786430600627301.
[16] D. Kiener, C. Motz, T. Schöberl, M. Jenko, G. Dehm, Determination of mechanical properties of copper at the micron scale, Adv. Eng. Mater. 8 (2006) 1119–1125, https://doi.org/10.1002/adem.200600129.
[17] A.M. Minor, S.A. Syed Asif, Z. Shan, E.A. Stach, E. Cyrankowski, T.J. Wyrobek, O. L. Warren, A new view of the onset of plasticity during the nanoindentation of aluminium, Nat. Mater. 5 (2006) 697–702, https://doi.org/10.1038/nmat1714.
[18] Z.W. Shan, R.K. Mishra, S.A. Syed Asif, O.L. Warren, A.M. Minor, Mechanical annealing and source-limited deformation in submicrometre-diameter Ni crystals, Nat. Mater. 7 (2008) 115–119, https://doi.org/10.1038/nmat2085.
[19] D. Kiener, W. Grosinger, G. Dehm, R. Pippan, A further step towards an understanding of size-dependent crystal plasticity: in situ tension experiments of miniaturized single-crystal copper samples, Acta Mater. 56 (2008) 580–592, https://doi.org/10.1016/j.actamat.2007.10.015.
[20] P.D. Ispánovity, D. Ugi, G. Péterffy, M. Knapek, S. Kalácska, D. Tüzes, Z. Dankházi, K. Máthis, F. Chmelík, I. Groma, Dislocation avalanches are like earthquakes on the micron scale, Nat. Commun. 13 (2022) 1975, https://doi.org/10.1038/s41467-022-29044-7.
[21] M. Göken, R. Sakidja, W.D. Nix, J.H. Perepezko, Microstructural mechanical properties and yield point effects in Mo alloys, Mater. Sci. Eng. A. 319–321 (2001) 902–908, https://doi.org/10.1016/S0921-5093(01)01086-3.
[22] M. Göken, M. Kempf, Pop-ins in nanoindentations – the initial yield point, Int. J. Mater. Res. 92 (2001) 1061–1067, https://doi.org/10.3139/ijmr-2001-0193.
[23] G.M. Pharr, J.H. Strader, W.C. Oliver, Critical issues in making small-depth mechanical property measurements by nanoindentation with continuous stiffness measurement, J. Mater. Res. 24 (2009) 653–666, https://doi.org/10.1557/JMR.2009.0096.
[24] B. Merle, V. Maier-Kiener, G.M. Pharr, Influence of modulus-to-hardness ratio and harmonic parameters on continuous stiffness measurement during

nanoindentation, Acta Mater. 134 (2017) 167–176, https://doi.org/10.1016/j.actamat.2017.05.036.
[25] B. Merle, W.H. Higgins, G.M. Pharr, Critical issues in conducting constant strain rate nanoindentation tests at higher strain rates, J. Mater. Res. 34 (2019) 3495–3503, https://doi.org/10.1557/jmr.2019.292.
[26] B. Merle, W.H. Higgins, G.M. Pharr, Extending the range of constant strain rate nanoindentation testing, J. Mater. Res. 35 (2020) 343–352, https://doi.org/10.1557/jmr.2019.408.
[27] P. Sudharshan Phani, B.L. Hackett, C.C. Walker, W.C. Oliver, G.M. Pharr, High strain rate nanoindentation testing: recent advancements, challenges and opportunities, Curr. Opin. Solid State Mater. Sci. 27 (2023), 101054, https://doi.org/10.1016/j.cossms.2022.101054.
[28] V. Maier-Kiener, K. Durst, Advanced nanoindentation testing for studying strain-rate sensitivity and activation volume, Jom. 69 (2017) 2246–2255, https://doi.org/10.1007/s11837-017-2536-y.
[29] K.M. Schmalbach, N.A. Mara, Algorithms for nanoindentation strain rate jump testing and analysis, Exp. Mech. 62 (2022) 885–888, https://doi.org/10.1007/s11340-022-00833-x.
[30] V. Maier-Kiener, X. An, L. Li, Z. Zhang, R. Pippan, K. Durst, Influence of solid solution strengthening on the local mechanical properties of single crystal and ultrafine-grained binary Cu–Al X solid solutions, J. Mater. Res. 32 (2017) 4583–4591, https://doi.org/10.1557/jmr.2017.320.
[31] H. Ovri, E.T. Lilleodden, New insights into plastic instability in precipitation strengthened Al–Li alloys, Acta Mater. 89 (2015) 88–97, https://doi.org/10.1016/j.actamat.2015.01.065.
[32] L. Krämer, V. Maier-Kiener, Y. Champion, B. Sarac, R. Pippan, Activation volume and energy of bulk metallic glasses determined by nanoindentation, Mater. Des. 155 (2018) 116–124, https://doi.org/10.1016/j.matdes.2018.05.051.
[33] V. Maier-Kiener, B. Schuh, E.P. George, H. Clemens, A. Hohenwarter, Insights into the deformation behavior of the CrMnFeCoNi high-entropy alloy revealed by elevated temperature nanoindentation, J. Mater. Res. 32 (2017) 2658–2667, https://doi.org/10.1557/jmr.2017.260.
[34] O. Renk, V. Maier-Kiener, C. Motz, J. Eckert, D. Kiener, R. Pippan, How the interface type manipulates the thermomechanical response of nanostructured metals: a case study on nickel, Materialia. 15 (2021), 101020, https://doi.org/10.1016/j.mtla.2021.101020.
[35] G.H. Balbus, J. Kappacher, D.J. Sprouster, F. Wang, J. Shin, Y.M. Eggeler, T. J. Rupert, J.R. Trelewicz, D. Kiener, V. Maier-Kiener, D.S. Gianola, Disordered interfaces enable high temperature thermal stability and strength in a nanocrystalline aluminum alloy, Acta Mater. 215 (2021), 116973, https://doi.org/10.1016/j.actamat.2021.116973.
[36] J. Kappacher, M. Tkadletz, H. Clemens, V. Maier-Kiener, High temperature nanoindentation as a tool to investigate plasticity upon phase transformations demonstrated on Cobalt, Materialia. 16 (2021), 101084, https://doi.org/10.1016/j.mtla.2021.101084.
[37] J. Kappacher, O. Renk, D. Kiener, H. Clemens, V. Maier-Kiener, How grain boundary characteristics influence plasticity close to and above the critical temperature of ultra-fine grained bcc Ta2.5W, Acta Mater. 216 (2021) 117110. doi:10.1016/j.actamat.2021.117110.
[38] V. Maier, B. Merle, M. Göken, K. Durst, An improved long-term nanoindentation creep testing approach for studying the local deformation processes in nanocrystalline metals at room and elevated temperatures, J. Mater. Res. 28 (2013) 1177–1188, https://doi.org/10.1557/jmr.2013.39.
[39] P.S. Phani, W.C. Oliver, G.M. Pharr, Influences of elasticity on the measurement of power law creep parameters by nanoindentation, J. Mech. Phys. Solids. 154 (2021), 104527, https://doi.org/10.1016/j.jmps.2021.104527.
[40] P. Sudharshan Phani, W.C. Oliver, G.M. Pharr, On the Measurement of Power Law Creep Parameters from Instrumented Indentation, JOM 69 (2017) 2229–2236, https://doi.org/10.1007/s11837-017-2535-z.
[41] P. Baral, G. Kermouche, G. Guillonneau, G. Tiphene, J.-M. Bergheau, W.C. Oliver, J.-L. Loubet, Indentation creep vs. indentation relaxation: a matter of strain rate definition? Mater. Sci. Eng. A. 781 (2020), 139246 https://doi.org/10.1016/j.msea.2020.139246.
[42] P. Baral, G. Guillonneau, G. Kermouche, J.-M. Bergheau, J.-L. Loubet, Theoretical and experimental analysis of indentation relaxation test, J. Mater. Res. 32 (2017) 2286–2296, https://doi.org/10.1557/jmr.2017.203.
[43] D. Matschkal-Amberger, M. Kolb, S. Neumeier, S. Gao, A. Hartmaier, K. Durst, M. Göken, New flat-punch indentation creep testing approach for characterizing the local creep properties at high temperatures, Mater. Des. 183 (2019), 108090, https://doi.org/10.1016/j.matdes.2019.108090.
[44] O. Prach, C. Minnert, K.E. Johanns, K. Durst, A new nanoindentation creep technique using constant contact pressure, J. Mater. Res. 34 (2019) 2492–2500, https://doi.org/10.1557/jmr.2019.188.
[45] C. Minnert, K. Durst, Nanoindentation creep testing: advantages and limitations of the constant contact pressure method, J. Mater. Res. 37 (2022) 567–579, https://doi.org/10.1557/s43578-021-00445-6.
[46] I.N. Sneddon, The relation between load and penetration in the axisymmetric boussinesq problem for a punch of arbitrary profile, Int. J. Eng. Sci. 3 (1965) 47–57.
[47] S.R. Kalidindi, S. Pathak, Determination of the effective zero-point and the extraction of spherical nanoindentation stress–strain curves, Acta Mater. 56 (2008) 3523–3532, https://doi.org/10.1016/j.actamat.2008.03.036.
[48] S. Pathak, S.R. Kalidindi, Spherical nanoindentation stress–strain curves, Mater. Sci. Eng. R Reports. 91 (2015) 1–36, https://doi.org/10.1016/j.mser.2015.02.001.
[49] A. Leitner, V. Maier-Kiener, D. Kiener, Essential refinements of spherical nanoindentation protocols for the reliable determination of mechanical flow curves, Mater. Des. 146 (2018) 69–80, https://doi.org/10.1016/j.matdes.2018.03.003.
[50] A. Ruiz-Moreno, P. Hähner, F. Fumagalli, V. Haiblikova, M. Conte, N. Randall, Stress−strain curves and derived mechanical parameters of P91 steel from spherical nanoindentation at a range of temperatures, Mater. Des. 194 (2020), 108950, https://doi.org/10.1016/j.matdes.2020.108950.
[51] D. Tabor, The Hardness of Metals, Clarendon Press, Oxford, 1951.
[52] J.S. Field, M.V. Swain, A simple predictive model for spherical indentation, J. Mater. Res. 8 (1993) 297–306, https://doi.org/10.1557/JMR.1993.0297.
[53] J.L. Hay, W.C. Olive, A. Bolshakov, G.M. Pharr, Using the ratio of loading slope and elastic stiffness to predict pile-up and constraint factor during indentation, MRS Proc. 522 (1998) 101, https://doi.org/10.1557/PROC-522-101.
[54] D.K. Patel, S.R. Kalidindi, Correlation of spherical nanoindentation stress-strain curves to simple compression stress-strain curves for elastic-plastic isotropic materials using finite element models, Acta Mater. 112 (2016) 295–302, https://doi.org/10.1016/j.actamat.2016.04.034.
[55] Y.G. Park, G.M. Pharr, Nanoindentation with spherical indenters: finite element studies of deformation in the elastic–plastic transition regime, Thin Solid Films. 447–448 (2003) 246–250, https://doi.org/10.1016/S0040-6090Ž03.01102-7.
[56] H. Hertz, Ueber die Berührung fester elastischer Körper, Crelle's J. 1882 (1882) 156–171, https://doi.org/10.1515/crll.1882.92.156.
[57] A. Leitner, V. Maier-Kiener, D. Kiener, High temperature flow behavior of ultra-strong nanoporous au assessed by spherical nanoindentation, Nanomaterials. 8 (2018) 366, https://doi.org/10.3390/nano8060366.
[58] M.J. Mayo, W.D. Nix, A micro-indentation study of superplasticity in Pb, Sn, and Sn-38 wt% Pb, Acta Metall. 36 (1988) 2183–2192, https://doi.org/10.1016/0001-6160(88)90319-7.
[59] M.J. Cordill, M.S. Lund, J. Parker, C. Leighton, A.K. Nair, D. Farkas, N.R. Moody, W.W. Gerberich, The Nano-Jackhammer effect in probing near-surface mechanical properties, Int. J. Plast. 25 (2009) 2045–2058, https://doi.org/10.1016/j.ijplas.2008.12.015.
[60] G.M. Pharr, A. Bolshakov, Understanding nanoindentation unloading curves, J. Mater. Res. 17 (2002) 2660–2671, https://doi.org/10.1557/JMR.2002.0386.
[61] D.R. Clarke, M.C. Kroll, P.D. Kirchner, R.F. Cook, B.J. Hockey, Amorphization and conductivity of silicon and germanium induced by indentation, Phys. Rev. Lett. 60 (1988) 2156–2159, https://doi.org/10.1103/PhysRevLett.60.2156.
[62] J. Crain, G.J. Ackland, J.R. Maclean, R.O. Piltz, P.D. Hatton, G.S. Pawley, Reversible pressure-induced structural transitions between metastable phases of silicon, Phys. Rev. B. 50 (1994) 13043–13046, https://doi.org/10.1103/PhysRevB.50.13043.
[63] S. Wong, B. Haberl, J.S. Williams, J.E. Bradby, Phase transformation as the single-mode mechanical deformation of silicon, Appl. Phys. Lett. 106 (2015), 252103, https://doi.org/10.1063/1.4923205.
[64] V.G. Eremenko, V.I. Nikitenko, Electron microscope investigation of the microplastic deformation mechanisms of silicon by indentation, Phys. Status Solidi. 14 (1972) 317–330, https://doi.org/10.1002/pssa.2210140139.
[65] V. Domnich, Y. Gogotsi, S. Dub, Effect of phase transformations on the shape of the unloading curve in the nanoindentation of silicon, Appl. Phys. Lett. 76 (2000) 2214–2216, https://doi.org/10.1063/1.126300.
[66] V. Domnich, Y. Gogotsi, Phase transformations in silicon under contact loading, Rev. Adv. Mater. Sci. 3 (2002) 1–36.
[67] J.E. Bradby, J.S. Williams, M.V. Swain, In situ electrical characterization of phase transformations in Si during indentation, Phys. Rev. B. 67 (2003), 085205, https://doi.org/10.1103/PhysRevB.67.085205.
[68] T. Juliano, V. Domnich, Y. Gogotsi, Examining pressure-induced phase transformations in silicon by spherical indentation and Raman spectroscopy: a statistical study, J. Mater. Res. 19 (2004) 3099–3108, https://doi.org/10.1557/JMR.2004.0403.
[69] J. Jang, M.J. Lance, S. Wen, T.Y. Tsui, G.M. Pharr, Indentation-induced phase transformations in silicon: influences of load, rate and indenter angle on the transformation behavior, Acta Mater. 53 (2005) 1759–1770, https://doi.org/10.1016/j.actamat.2004.12.025.
[70] S. Wong, B. Haberl, J.S. Williams, J.E. Bradby, The influence of hold time on the onset of plastic deformation in silicon, J. Appl. Phys. 118 (2015), 245904, https://doi.org/10.1063/1.4938480.
[71] T. Juliano, Y. Gogotsi, V. Domnich, Effect of indentation unloading conditions on phase transformation induced events in silicon, J. Mater. Res. 18 (2003) 1192–1201, https://doi.org/10.1557/JMR.2003.0164.
[72] M.S.R.N. Kiran, T.T. Tran, L.A. Smillie, B. Haberl, D. Subianto, J.S. Williams, J. E. Bradby, Temperature-dependent mechanical deformation of silicon at the nanoscale: phase transformation versus defect propagation, J. Appl. Phys. 117 (2015), 205901, https://doi.org/10.1063/1.4921534.
[73] N.V. Novikov, S.N. Dub, Y.V. Milman, I.V. Gridneva, S.I. Chugunova, Study of the semiconductor-metal phase transformation in silicon by nanoindentation, J. Superhard Mater. 18 (1996).
[74] J.H. Poynting, On pressure perpendicular to the shear planes in finite pure shears, and on the lengthening of loaded wires when twisted, Proc. R. Soc. London. Ser. A, Contain. Pap. a Math. Phys. Character. 82 (1909) 546–559, https://doi.org/10.1098/rspa.1909.0059.
[75] K.P. Menard, N.R. Menard, Dynamic Mechanical Analysis, CRC Press, 2020 doi:10.1201/9780429190308.
[76] M.S. Blanter, I.S. Golovin, H. Neuhäuser, H.-R. Sinning, Internal Friction in Metallic Materials, Springer, Berlin, Heidelberg, 2007 doi:10.1007/978-3-540-68758-0.

[77] A.S. Nowick, B.S. Berry, J.L. Katz, Anelastic relaxation in crystalline solids, J. Appl. Mech. 42 (1975) 750–751, https://doi.org/10.1115/1.3423694.

[78] A. Eisenberg, B.C. Eu, Mechanical spectroscopy: an introductory review, Annu. Rev. Mater. Sci. 6 (1976) 335–359, https://doi.org/10.1146/annurev.ms.06.080176.002003.

[79] S.A.S. Asif, K.J. Wahl, R.J. Colton, Nanoindentation and contact stiffness measurement using force modulation with a capacitive load-displacement transducer, Rev. Sci. Instrum. 70 (1999) 2408–2413, https://doi.org/10.1063/1.1149769.

[80] T. Zhang, S.L. Bai, Y.F. Zhang, B. Thibaut, Viscoelastic properties of wood materials characterized by nanoindentation experiments, Wood Sci. Technol. 46 (2012) 1003–1016, https://doi.org/10.1007/s00226-011-0458-3.

[81] K. Liu, M. Ostadhassan, B. Bubach, R. Dietrich, V. Rasouli, Nano-dynamic mechanical analysis (nano-DMA) of creep behavior of shales: Bakken case study, J. Mater. Sci. 53 (2018) 4417–4432, https://doi.org/10.1007/s10853-017-1821-z.

[82] G. Huang, B. Wang, H. Lu, Measurements of viscoelastic functions of polymers in the frequency-domain using nanoindentation, Mech. Time-Dependent Mater. 8 (2004) 345–364, https://doi.org/10.1007/s11043-004-0440-7.

[83] J. Hay, E. Herbert, Measuring the complex modulus of polymers by instrumented indentation testing, Exp. Tech. 37 (2013) 55–61, https://doi.org/10.1111/j.1747-1567.2011.00732.x.

[84] S. Weyand, H. Blattmann, V. Schimpf, R. Mülhaupt, R. Schwaiger, Structure-property-glass transition relationships in non-isocyanate polyurethanes investigated by dynamic nanoindentation, Mater. Res. Express. 3 (2016), 075019, https://doi.org/10.1088/2053-1591/3/7/075019.

[85] J.M. Algueta-Miguel, J.J. Beato-López, A.J. López-Martín, Analog lock-in amplifier design using subsampling for accuracy enhancement in GMI sensor applications, Sensors. 23 (2022) 57, https://doi.org/10.3390/s23010057.

[86] L.B. Magalas, Snoek-Köster Relaxation. New Insights - New Paradigms, Le J. Phys. IV. 06 (1996) C8-163-C8-172. doi:10.1051/jp4:1996834.

[87] T. Arai, S. Okuda, Relaxation spectrum analysis of the bordoni peak in Cu by nonlinear least-squares fitting, Phys. Status Solidi. 122 (1990) 535–544, https://doi.org/10.1002/pssa.2211220213.

[88] M. Sun, W. Jiang, X. Liu, T. Chen, X. Wang, Q. Fang, A comparative study on the grain boundary internal friction peak of pure iron, Mater. Lett. 305 (2021), 130814, https://doi.org/10.1016/j.matlet.2021.130814.

[89] M. Alfreider, I. Issa, O. Renk, D. Kiener, Probing defect relaxation in ultra-fine grained Ta using micromechanical spectroscopy, Acta Mater. 185 (2020) 309–319, https://doi.org/10.1016/j.actamat.2019.12.011.

[90] F.R. Blom, Dependence of the quality factor of micromachined silicon beam resonators on pressure and geometry, J. Vac. Sci. Technol. B Microelectron. Nanom. Struct. 10 (1992) 19, https://doi.org/10.1116/1.586300.

[91] M. Alfreider, M. Meindlhumer, T. Ziegelwanger, R. Daniel, J. Keckes, D. Kiener, Revealing dynamic-mechanical properties of precipitates in a nanostructured thin film using micromechanical spectroscopy, MRS Bull. (2023), https://doi.org/10.1557/s43577-023-00549-w.

[92] T. Meiners, T. Frolov, R.E. Rudd, G. Dehm, C.H. Liebscher, Observations of grain-boundary phase transformations in an elemental metal, Nature. 579 (2020) 375–378, https://doi.org/10.1038/s41586-020-2082-6.

[93] T.L. Anderson, Fracture Mechanics: Fundamentals and Applications, fourth ed., Taylor & Francis Group, Boca Raton, 2017.

[94] J. Ast, M. Ghidelli, K. Durst, M. Göken, M. Sebastiani, A.M. Korsunsky, A review of experimental approaches to fracture toughness evaluation at the micro-scale, Mater. Des. 173 (2019), 107762, https://doi.org/10.1016/j.matdes.2019.107762.

[95] R. Pippan, S. Wurster, D. Kiener, Fracture mechanics of micro samples: fundamental considerations, Mater. Des. 159 (2018) 252–267, https://doi.org/10.1016/J.MATDES.2018.09.004.

[96] D. Kiener, S.M. Han, 100 years after Griffith: From brittle bulk fracture to failure in 2D materials, MRS Bull. 47 (2022) 792–799, https://doi.org/10.1557/s43577-022-00379-2.

[97] R.O. Ritchie, The conflicts between strength and toughness, Nat. Mater. 10 (2011) 817–822, https://doi.org/10.1038/nmat3115.

[98] S. Wurster, C. Motz, R. Pippan, Characterization of the fracture toughness of micro-sized tungsten single crystal notched specimens, Philos. Mag. 92 (2012) 1803–1825, https://doi.org/10.1080/14786435.2012.658449.

[99] M. Alfreider, D. Kozic, O. Kolednik, D. Kiener, In-situ elastic-plastic fracture mechanics on the microscale by means of continuous dynamical testing, Mater. Des. 148 (2018) 177–187, https://doi.org/10.1016/j.matdes.2018.03.051.

[100] S. Gabel, B. Merle, B. Merle, Small-scale high-cycle fatigue testing by dynamic microcantilever bending, MRS Commun. 10 (2020) 332–337, https://doi.org/10.1557/mrc.2020.31.

[101] M. Alfreider, S. Kolitsch, S. Wurster, D. Kiener, An analytical solution for the correct determination of crack lengths via cantilever stiffness, Mater. Des. 194 (2020), 108914, https://doi.org/10.1016/j.matdes.2020.108914.

[102] A. Riedl, R. Daniel, M. Stefenelli, T. Schöberl, O. Kolednik, C. Mitterer, J. Keckes, A novel approach for determining fracture toughness of hard coatings on the micrometer scale, Scr. Mater. 67 (2012) 708–711, https://doi.org/10.1016/j.scriptamat.2012.06.034.

[103] M. Burtscher, M. Alfreider, C. Kainz, K. Schmuck, D. Kiener, In-situ micromechanical analysis of a nano-crystalline W-Cu, Mater. Des. 220 (2022), 110848, https://doi.org/10.1016/j.matdes.2022.110848.

[104] M. Freisinger, L. Zauner, R. Hahn, H. Riedl, P.H. Mayrhofer, In-situ micro-cantilever bending studies of a white etching layer thermally induced on rail wheels, Mater. Sci. Eng. A. 869 (2023), 144805, https://doi.org/10.1016/j.msea.2023.144805.

[105] M. Burtscher, M. Alfreider, K. Schmuck, H. Clemens, S. Mayer, D. Kiener, In situ fracture observations of distinct interface types within a fully lamellar intermetallic TiAl alloy, J. Mater. Res. (2020), https://doi.org/10.1557/jmr.2020.306.

[106] M. Alfreider, J. Zechner, D. Kiener, Addressing fracture properties of individual constituents within a Cu-WTi-SiOx-Si multilayer, JOM. 72 (2020) 4551–4558, https://doi.org/10.1007/s11837-020-04444-6.

[107] M. Alfreider, R. Bodlos, L. Romaner, D. Kiener, The influence of chemistry on the interface toughness in a WTi-Cu system, Acta Mater. 230 (2022), 117813, https://doi.org/10.1016/j.actamat.2022.117813.

[108] K.J. Hemker, W.D. Nix, Seeing is believing, Nat. Mater. 7 (2008) 97–98, https://doi.org/10.1038/nmat2103.

[109] G. Dehm, J.M. Howe, J. Zweck, In-Situ Electron Microscopy: Application in Physics, Chemistry and Materials Science, Wiley-VCH Verlag & Co KGaA, Weinheim, 2012 doi:10.1002/9783527652167.fmatter.

[110] M. Legros, D.S. Gianola, C. Motz, Quantitative in situ mechanical testing in electron microscopes, MRS Bull. 35 (2010) 354–360, https://doi.org/10.1557/mrs2010.567.

[111] A. Jelinek, S. Zak, M. Alfreider, D. Kiener, High-throughput micromechanical testing enabled by optimized direct laser writing, Adv. Eng. Mater. 25 (2023), https://doi.org/10.1002/adem.202200288.

[112] N. Rohbeck, R. Ramachandramoorthy, D. Casari, P. Schürch, T.E.J. Edwards, L. Schilinsky, L. Philippe, J. Schwiedrzik, J. Michler, Effect of high strain rates and temperature on the micromechanical properties of 3D-printed polymer structures made by two-photon lithography, Mater. Des. 195 (2020), 108977, https://doi.org/10.1016/j.matdes.2020.108977.

[113] B.L. Boyce, S.L.B. Kramer, H.E. Fang, T.E. Cordova, M.K. Neilsen, K. Dion, A. K. Kaczmarowski, E. Karasz, L. Xue, A.J. Gross, A. Ghahremaninezhad, K. Ravi-Chandar, S.-P. Lin, S.-W. Chi, J.S. Chen, E. Yreux, M. Rüter, D. Qian, Z. Zhou, S. Bhamare, D.T. O'Connor, S. Tang, K.I. Elkhodary, J. Zhao, J.D. Hochhalter, A. R. Cerrone, A.R. Ingraffea, P.A. Wawrzynek, B.J. Carter, J.M. Emery, M. G. Veilleux, P. Yang, Y. Gan, X. Zhang, Z. Chen, E. Madenci, B. Kilic, T. Zhang, E. Fang, P. Liu, J. Lua, K. Nahshon, M. Miraglia, J. Cruce, R. DeFrese, E.T. Moyer, S. Brinckmann, L. Quinkert, K. Pack, M. Luo, T. Wierzbicki, The Sandia Fracture Challenge: blind round robin predictions of ductile tearing, Int. J. Fract. 186 (2014) 5–68, https://doi.org/10.1007/s10704-013-9904-6.

[114] B.L. Boyce, S.L.B. Kramer, T.R. Bosiljevac, E. Corona, J.A. Moore, K. Elkhodary, C. H.M. Simha, B.W. Williams, A.R. Cerrone, A. Nonn, J.D. Hochhalter, G. F. Bomarito, J.E. Warner, B.J. Carter, D.H. Warner, A.R. Ingraffea, T. Zhang, X. Fang, J. Lua, V. Chiaruttini, M. Mazière, S. Feld-Payet, V.A. Yastrebov, J. Besson, J.-L. Chaboche, J. Lian, Y. Di, B. Wu, D. Novokshanov, N. Vajragupta, P. Kucharczyk, V. Brinnel, B. Döbereiner, S. Münstermann, M.K. Neilsen, K. Dion, K.N. Karlson, J.W. Foulk, A.A. Brown, M.G. Veilleux, J.L. Bignell, S.E. Sanborn, C. A. Jones, P.D. Mattie, K. Pack, T. Wierzbicki, S.-W. Chi, S.-P. Lin, A. Mahdavi, J. Predan, J. Zadravec, A.J. Gross, K. Ravi-Chandar, L. Xue, The second Sandia Fracture Challenge: predictions of ductile failure under quasi-static and moderate-rate dynamic loading, Int. J. Fract. 198 (2016) 5–100, https://doi.org/10.1007/s10704-016-0089-7.

[115] S.L.B. Kramer, A. Jones, A. Mostafa, B. Ravaji, T. Tancogne-Dejean, C.C. Roth, M. G. Bandpay, K. Pack, J.T. Foster, M. Behzadinasab, J.C. Sobotka, J.M. McFarland, J. Stein, A.D. Spear, P. Newell, M.W. Czabaj, B. Williams, H. Simha, M. Gesing, L. N. Gilkey, C.A. Jones, R. Dingreville, S.E. Sanborn, J.L. Bignell, A.R. Cerrone, V. Keim, A. Nonn, S. Cooreman, P. Thibaux, N. Ames, D.O. Connor, M. Parno, B. Davis, J. Tucker, B. Coudrillier, K.N. Karlson, J.T. Ostien, J.W. Foulk, C. I. Hammetter, S. Grange, J.M. Emery, J.A. Brown, J.E. Bishop, K.L. Johnson, K. R. Ford, S. Brinckmann, M.K. Neilsen, J. Jackiewicz, K. Ravi-Chandar, T. Ivanoff, B.C. Salzbrenner, B.L. Boyce, The third Sandia fracture challenge: predictions of ductile fracture in additively manufactured metal, Int. J. Fract. 218 (2019) 5–61, https://doi.org/10.1007/s10704-019-00361-1.

[116] K. Schmuck, M. Alfreider, D. Kiener, Crack length estimations for small scale fracture experiments via image processing techniques, J. Mater. Res. 37 (2022) 2848–2861, https://doi.org/10.1557/s43578-022-00681-4.

[117] A.K. Saxena, S. Brinckmann, B. Völker, G. Dehm, C. Kirchlechner, Experimental conditions affecting the measured fracture toughness at the microscale: notch geometry and crack extension measurement, Mater. Des. 191 (2020), 108582, https://doi.org/10.1016/j.matdes.2020.108582.

[118] A.D. Kammers, S. Daly, Digital image correlation under scanning electron microscopy: methodology and validation, Exp. Mech. 53 (2013) 1743–1761, https://doi.org/10.1007/s11340-013-9782-x.

[119] H.H. Rose, Historical aspects of aberration correction, J. Electron Microsc. (Tokyo) 58 (2009) 77–85, https://doi.org/10.1093/jmicro/dfp012.

[120] D.C. Joy, The aberration corrected SEM, AIP Conf. Proc. 788 (2005) 535–542, https://doi.org/10.1063/1.2063015.

[121] S. Maraghechi, J.P.M. Hoefnagels, R.H.J. Peerlings, O. Rokoš, M.G.D. Geers, Correction of scanning electron microscope imaging artifacts in a novel digital image correlation framework, Exp. Mech. (2019) 489–516, https://doi.org/10.1007/s11340-018-00469-w.

[122] W.C. Lenthe, J.C. Stinville, M.P. Echlin, Z. Chen, S. Daly, T.M. Pollock, Advanced detector signal acquisition and electron beam scanning for high resolution SEM imaging, Ultramicroscopy. 195 (2018) 93–100, https://doi.org/10.1016/j.ultramic.2018.08.025.

[123] F. Di Gioacchino, W.J. Clegg, Mapping deformation in small-scale testing, Acta Mater. 78 (2014) 103–113, https://doi.org/10.1016/j.actamat.2014.06.033.

[124] F. Di Gioacchino, J. Quinta da Fonseca, Plastic strain mapping with sub-micron resolution using digital image correlation, Exp. Mech. 53 (2013) 743–754, https://doi.org/10.1007/s11340-012-9685-2.
[125] T.E.J. Edwards, F. Di Gioacchino, R. Muñoz-Moreno, W.J. Clegg, Deformation of lamellar TiAl alloys by longitudinal twinning, Scr. Mater. 118 (2016) 46–50, https://doi.org/10.1016/j.scriptamat.2016.03.004.
[126] J.T. Pürstl, H.O. Jones, T.E.J. Edwards, R.P. Thompson, F. Di Gioacchino, N. G. Jones, W.J. Clegg, On the extraction of yield stresses from micro-compression experiments, Mater. Sci. Eng. A. 800 (2021), 140323, https://doi.org/10.1016/j.msea.2020.140323.
[127] T.E.J. Edwards, X. Maeder, J. Ast, L. Berger, J. Michler, Mapping pure plastic strains against locally applied stress: revealing toughening plasticity, Sci. Adv. 8 (2022), https://doi.org/10.1126/sciadv.abo5735.
[128] M. Alfreider, M. Meindlhumer, V. Maier-Kiener, A. Hohenwarter, D. Kiener, Extracting information from noisy data: strain mapping during dynamic in situ SEM experiments, J. Mater. Res. 36 (2021) 2291–2304, https://doi.org/10.1557/s43578-020-00041-0.
[129] R.L. Black, T. Garbowski, C. Bean, A.L. Eberle, S. Nickell, D. Texier, V. Valle, J. C. Stinville, High-throughput high-resolution digital image correlation measurements by multi-beam SEM imaging, Exp. Mech. (2023), https://doi.org/10.1007/s11340-023-00961-y.
[130] F. Bourdin, J.C. Stinville, M.P. Echlin, P.G. Callahan, W.C. Lenthe, C.J. Torbet, D. Texier, F. Bridier, J. Cormier, P. Villechaise, T.M. Pollock, V. Valle, Measurements of plastic localization by heaviside-digital image correlation, Acta Mater. 157 (2018) 307–325, https://doi.org/10.1016/j.actamat.2018.07.013.
[131] J.C. Stinville, M.A. Charpagne, A. Cervellon, S. Hemery, F. Wang, P.G. Callahan, V. Valle, T.M. Pollock, On the origins of fatigue strength in crystalline metallic materials, Science (80-.) 377 (2022) 1065–1071, https://doi.org/10.1126/science.abn0392.
[132] R. Fritz, D. Kiener, Development and application of a heated in-situ SEM micro-testing device, Measurement. 110 (2017) 356–366, https://doi.org/10.1016/j.measurement.2017.07.012.
[133] H. Bishara, S. Lee, T. Brink, M. Ghidelli, G. Dehm, Understanding grain boundary electrical resistivity in Cu: the effect of boundary structure, ACS Nano. 15 (2021) 16607–16615, https://doi.org/10.1021/acsnano.1c06367.
[134] A. Massone, A. Manhard, W. Jacob, A. Drexler, W. Ecker, A. Hohenwarter, S. Wurster, D. Kiener, An SEM compatible plasma cell for in situ studies of hydrogen-material interaction, Rev. Sci. Instrum. 91 (2020), 043705, https://doi.org/10.1063/1.5142043.
[135] S. Zaefferer, N.-N. Elhami, Theory and application of electron channelling contrast imaging under controlled diffraction conditions, Acta Mater. 75 (2014) 20–50, https://doi.org/10.1016/j.actamat.2014.04.018.
[136] M. Koyama, S.M. Taheri-Mousavi, H. Yan, J. Kim, B.C. Cameron, S.S. Moeini-Ardakani, J. Li, C.C. Tasan, Origin of micrometer-scale dislocation motion during hydrogen desorption, Sci. Adv. 6 (2020), https://doi.org/10.1126/sciadv.aaz1187.
[137] D.S. Gianola, T. Ben Britton, S. Zaefferer, New techniques for imaging and identifying defects in electron microscopy, MRS Bull. 44 (2019) 450–458, https://doi.org/10.1557/mrs.2019.125.
[138] C.A. García-Negrete, M.C. Jiménez de Haro, J. Blasco, M. Soto, A. Fernández, STEM-in-SEM high resolution imaging of gold nanoparticles and bivalve tissues in bioaccumulation experiments, Analyst. 140 (2015) 3082–3089, https://doi.org/10.1039/C4AN01643B.
[139] B.W. Caplins, J.D. Holm, R.M. White, R.R. Keller, Orientation mapping of graphene using 4D STEM-in-SEM, Ultramicroscopy. 219 (2020), 113137, https://doi.org/10.1016/j.ultramic.2020.113137.
[140] P.G. Callahan, J.-C. Stinville, E.R. Yao, M.P. Echlin, M.S. Titus, M. De Graef, D. S. Gianola, T.M. Pollock, Transmission scanning electron microscopy: defect observations and image simulations, Ultramicroscopy. 186 (2018) 49–61, https://doi.org/10.1016/j.ultramic.2017.11.004.
[141] J.C. Stinville, E.R. Yao, P.G. Callahan, J. Shin, F. Wang, M.P. Echlin, T.M. Pollock, D.S. Gianola, Dislocation dynamics in a nickel-based superalloy via in-situ transmission scanning electron microscopy, Acta Mater. 168 (2019) 152–166, https://doi.org/10.1016/j.actamat.2018.12.061.
[142] M. Alfreider, G. Balbus, F. Wang, J. Zechner, D.S. Gianola, D. Kiener, Interface mediated deformation and fracture of an elastic–plastic bimaterial system resolved by in situ transmission scanning electron microscopy, Mater. Des. 223 (2022), 111136, https://doi.org/10.1016/j.matdes.2022.111136.
[143] H. Shinotsuka, S. Tanuma, C.J. Powell, D.R. Penn, Calculations of electron inelastic mean free paths. X. Data for 41 elemental solids over the 50 eV to 200 keV range with the relativistic full Penn algorithm, Surf. Interface Anal. 47 (2015) 1132, https://doi.org/10.1002/sia.5861.
[144] D.B. Williams, C.B. Carter, Transmission Electron Microscopy, Springer, US, Boston, MA, 1996 doi:10.1007/978-1-4757-2519-3.
[145] F. Wang, M.P. Echlin, A.A. Taylor, J. Shin, B. Bammes, B.D.A. Levin, M. De Graef, T.M. Pollock, D.S. Gianola, Electron backscattered diffraction using a new monolithic direct detector: high resolution and fast acquisition, Ultramicroscopy. 220 (2021), 113160, https://doi.org/10.1016/j.ultramic.2020.113160.
[146] J.M. Wheeler, D.E.J. Armstrong, W. Heinz, R. Schwaiger, High temperature nanoindentation: the state of the art and future challenges, Curr. Opin. Solid State Mater. Sci. 19 (2015) 354–366, https://doi.org/10.1016/j.cossms.2015.02.002.
[147] A. Barnoush, P. Hosemann, J. Molina-Aldareguia, J.M. Wheeler, In situ small-scale mechanical testing under extreme environments, MRS Bull. 44 (2019) 471–477, https://doi.org/10.1557/mrs.2019.126.
[148] C. Minnert, W.C. Oliver, K. Durst, New ultra-high temperature nanoindentation system for operating at up to 1100 °C, Mater. Des. 192 (2020), 108727, https://doi.org/10.1016/j.matdes.2020.108727.
[149] R.L. Grosso, E.N.S. Muccillo, D.N.F. Muche, G.S. Jawaharram, C.M. Barr, A. M. Monterrosa, R.H.R. Castro, K. Hattar, S.J. Dillon, In situ transmission electron microscopy for ultrahigh temperature mechanical testing of ZrO2, Nano Lett. 20 (2020) 1041–1046, https://doi.org/10.1021/acs.nanolett.9b04205.
[150] R.J. Parrish, D.C. Bufford, D.M. Frazer, C.A. Taylor, J. Gutierrez-Kolar, D. L. Buller, B.L. Boyce, K. Hattar, Exploring coupled extreme environments via in-situ transmission electron microscopy, Micros. Today. 29 (2021) 28–34, https://doi.org/10.1017/s1551929520001595.
[151] G. Tiphéne, P. Baral, S. Comby-Dassonneville, G. Guillonneau, G. Kermouche, J.-M. Bergheau, W. Oliver, J.-L. Loubet, High-Temperature Scanning Indentation: a new method to investigate in situ metallurgical evolution along temperature ramps, J. Mater. Res. 36 (2021) 2383–2396, https://doi.org/10.1557/s43578-021-00107-7.
[152] J.M. Wheeler, J. Michler, Invited article: indenter materials for high temperature nanoindentation, Rev. Sci. Instrum. 84 (2013), 101301, https://doi.org/10.1063/1.4824710.
[153] V. Maier, A. Leitner, R. Pippan, D. Kiener, Thermally activated deformation behavior of ufg-au: environmental issues during long-term and high-temperature nanoindentation testing, JOM. 67 (2015) 2934–2944, https://doi.org/10.1007/s11837-015-1638-7.
[154] S. Korte, W.J. Clegg, Micropillar compression of ceramics at elevated temperatures, Scr. Mater. 60 (2009) 807–810, https://doi.org/10.1016/j.scriptamat.2009.01.029.
[155] J. Alkorta, J.M. Martínez-Esnaola, J. Gil Sevillano, Critical examination of strain-rate sensitivity measurement by nanoindentation methods: application to severely deformed niobium, Acta Mater. 56 (2008) 884–893, https://doi.org/10.1016/j.actamat.2007.10.039.
[156] V. Maier, K. Durst, J. Mueller, B. Backes, H.W. Höppel, M. Göken, Nanoindentation strain-rate jump tests for determining the local strain-rate sensitivity in nanocrystalline Ni and ultrafine-grained Al, J. Mater. Res. 26 (2011) 1421–1430, https://doi.org/10.1557/jmr.2011.156.
[157] J.M. Wheeler, V. Maier, K. Durst, M. Göken, J. Michler, Activation parameters for deformation of ultrafine-grained aluminium as determined by indentation strain rate jumps at elevated temperature, Mater. Sci. Eng. A. 585 (2013) 108–113, https://doi.org/10.1016/j.msea.2013.07.033.
[158] O.D. Sherby, P.E. Armstrong, Prediction of activation energies for creep and self-diffusion from hot hardness data, Metall. Mater. Trans. B. 2 (1971) 3479–3484, https://doi.org/10.1007/BF02811630.
[159] J. Kappacher, A. Leitner, D. Kiener, H. Clemens, V. Maier-Kiener, Thermally activated deformation mechanisms and solid solution softening in W-Re alloys investigated via high temperature nanoindentation, Mater. Des. 189 (2020), 108499, https://doi.org/10.1016/j.matdes.2020.108499.
[160] G.J.K. Schaffar, D. Tscharnuter, V. Maier-Kiener, Exploring the high-temperature deformation behavior of monocrystalline silicon – an advanced nanoindentation study, Mater. Des. 233 (2023), 112198, https://doi.org/10.1016/j.matdes.2023.112198.
[161] B. Kedjar, L. Thilly, J.L. Demenet, J. Rabier, Plasticity of indium antimonide between −176 and 400 °C under hydrostatic pressure. Part I: Macroscopic aspects of the deformation, Acta Mater. 58 (2010) 1418–1425, https://doi.org/10.1016/J.ACTAMAT.2009.10.050.
[162] B. Kedjar, L. Thilly, J.L. Demenet, J. Rabier, Plasticity of indium antimonide between −176 °C and 400 °C under hydrostatic pressure. Part II: Microscopic aspects of the deformation, Acta Mater. 58 (2010) 1426–1440, https://doi.org/10.1016/J.ACTAMAT.2009.10.052.
[163] M. Chen, A.S. Sologubenko, J.M. Wheeler, Exploring defect behavior and size effects in micron-scale germanium from cryogenic to elevated temperatures, Matter. 6 (2023) 1903–1927, https://doi.org/10.1016/j.matt.2023.03.025.
[164] I.-C. Choi, C. Brandl, R. Schwaiger, Thermally activated dislocation plasticity in body-centered cubic chromium studied by high-temperature nanoindentation, Acta Mater. 140 (2017) 107–115, https://doi.org/10.1016/j.actamat.2017.08.026.
[165] D.-H. Lee, I.-C. Choi, G. Yang, Z. Lu, M. Kawasaki, U. Ramamurty, R. Schwaiger, J. Jang, Activation energy for plastic flow in nanocrystalline CoCrFeMnNi high-entropy alloy: a high temperature nanoindentation study, Scr. Mater. 156 (2018) 129–133, https://doi.org/10.1016/j.scriptamat.2018.07.014.
[166] G. Schoeck, The activation energy of dislocation movement, Phys. Status Solidi. 8 (1965) 499–507, https://doi.org/10.1002/pssb.19650080209.
[167] M. Chen, J. Wehrs, A.S. Sologubenko, J. Rabier, J. Michler, J.M. Wheeler, Size-dependent plasticity and activation parameters of lithographically-produced silicon micropillars, Mater. Des. 189 (2020), 108506, https://doi.org/10.1016/j.matdes.2020.108506.
[168] M.S. Duesbery, Dislocation motion in silicon: the shuffle-glide controversy, Philos. Mag. Lett. 74 (1996) 253–258, https://doi.org/10.1080/095008396180191.
[169] V. Maier, C. Schunk, M. Göken, K. Durst, Microstructure-dependent deformation behaviour of bcc-metals – indentation size effect and strain rate sensitivity, Philos. Mag. 95 (2015) 1766–1779, https://doi.org/10.1080/14786435.2014.982741.
[170] D.M. Marsh, Plastic flow in glass, Proc. R. Soc. London. Ser. A. Math. Phys. Sci. 279 (1964) 420–435, https://doi.org/10.1098/rspa.1964.0114.
[171] S.A. Syed Asif, J.B. Pethica, Nano-scale indentation creep testing at non-ambient temperature, J. Adhes. 67 (1998) 153–165, https://doi.org/10.1080/00218469808011105.

[172] J. Chen, G.A. Bell, H. Dong, J.F. Smith, B.D. Beake, A study of low temperature mechanical properties and creep behaviour of polypropylene using a new sub-ambient temperature nanoindentation test platform, J. Phys. D. Appl. Phys. 43 (2010), 425404, https://doi.org/10.1088/0022-3727/43/42/425404.
[173] J. Chen, G.A. Bell, B.D. Beake, H. Dong, Nano-mechanical and tribological properties of a multilayered DLC coating under sub-ambient temperatures, Int. J. Eng. Syst. Model. Simul. 2 (2011) 199, https://doi.org/10.1504/IJESMS.2010.038138.
[174] S.-W. Lee, L. Meza, J.R. Greer, Cryogenic nanoindentation size effect in [0 0 1]-oriented face-centered cubic and body-centered cubic single crystals, Appl. Phys. Lett. 103 (2013), 101906, https://doi.org/10.1063/1.4820585.
[175] S.-W. Lee, Y. Cheng, I. Ryu, J.R. Greer, Cold-temperature deformation of nano-sized tungsten and niobium as revealed by in-situ nano-mechanical experiments, Sci. China Technol. Sci. 57 (2014) 652–662, https://doi.org/10.1007/s11431-014-5502-8.
[176] A. Lupinacci, J. Kacher, A. Eilenberg, A.A. Shapiro, P. Hosemann, A.M. Minor, Cryogenic in situ microcompression testing of Sn, Acta Mater. 78 (2014) 56–64, https://doi.org/10.1016/j.actamat.2014.06.026.
[177] S.-W. Lee, M. Jafary-Zadeh, D.Z. Chen, Y.-W. Zhang, J.R. Greer, Size effect suppresses brittle failure in hollow Cu 60 Zr 40 metallic glass nanolattices deformed at cryogenic temperatures, Nano Lett. 15 (2015) 5673–5681, https://doi.org/10.1021/acs.nanolett.5b01034.
[178] W. Zhang, X. Zhang, B.W. Edwards, L. Zhong, H. Gao, M.J. Malaska, R. Hodyss, J. R. Greer, Deformation characteristics of solid-state benzene as a step towards understanding planetary geology, Nat. Commun. 13 (2022) 7949, https://doi.org/10.1038/s41467-022-35647-x.
[179] J. Ast, J.J. Schwiedrzik, J. Wehrs, D. Frey, M.N. Polyakov, J. Michler, X. Maeder, The brittle-ductile transition of tungsten single crystals at the micro-scale, Mater. Des. 152 (2018) 168–180, https://doi.org/10.1016/j.matdes.2018.04.009.
[180] K. Thomas, G. Mohanty, J. Wehrs, A.A. Taylor, S. Pathak, D. Casari, J. Schwiedrzik, N. Mara, R. Spolenak, J. Michler, Elevated and cryogenic temperature micropillar compression of magnesium–niobium multilayer films, J. Mater. Sci. 54 (2019) 10884–10901, https://doi.org/10.1007/s10853-019-03422-x.
[181] J. Schwiedrzik, R. Ramachandramoorthy, T.E.J. Edwards, P. Schürch, D. Casari, M.J. Duarte, G. Mohanty, G. Dehm, X. Maeder, L. Philippe, J.-M. Breguet, J. Michler, Dynamic cryo-mechanical properties of additively manufactured nanocrystalline nickel 3D microarchitectures, Mater. Des. 220 (2022), 110836, https://doi.org/10.1016/j.matdes.2022.110836.
[182] A. Lupinacci, J. Kacher, A.A. Shapiro, P. Hosemann, A.M. Minor, Cryogenic in-situ clamped beam testing of Sn96, J. Mater. Res. 36 (2021) 1751–1761, https://doi.org/10.1557/s43578-021-00157-x.
[183] R.N. Widmer, A. Groetsch, G. Kermouche, A. Diaz, G. Pillonel, M. Jain, R. Ramachandramoorthy, L. Pethö, J. Schwiedrzik, J. Michler, Temperature–dependent dynamic plasticity of micro-scale fused silica, Mater. Des. 215 (2022), 110503, https://doi.org/10.1016/j.matdes.2022.110503.
[184] R. Dubosq, E. Woods, B. Gault, J.P. Best, Electron microscope loading and in situ nanoindentation of water ice at cryogenic temperatures, PLoS One. 18 (2023) e0281703.
[185] G. Song, V. Borisov, W.R. Meier, M. Xu, K.J. Dusoe, J.T. Sypek, R. Valentí, P. C. Canfield, S.-W. Lee, Ultrahigh elastically compressible and strain-engineerable intermetallic compounds under uniaxial mechanical loading, APL Mater. 7 (2019), 061104, https://doi.org/10.1063/1.5087279.
[186] G. Song, N.K. Aragon, I. Ryu, S.-W. Lee, Low-temperature failure mechanism of [001] niobium micropillars under uniaxial tension, J. Mater. Res. (2020) 1–12, https://doi.org/10.1557/jmr.2020.252.
[187] J.T. Sypek, S. Vijayan, I. Bakst, S. Xiao, M.J. Kramer, P.C. Canfield, M. Aindow, C. R. Weinberger, S.-W. Lee, Uniaxial compression of [001]-oriented CaFe2As2 single crystals:the effects of microstructure and temperature on superelasticity Part I: Experimental observations, Acta Mater. 203 (2021), 116464, https://doi.org/10.1016/j.actamat.2020.11.006.
[188] A.M. Giwa, Z.H. Aitken, P.K. Liaw, Y.-W. Zhang, J.R. Greer, Effect of temperature on small-scale deformation of individual face-centered-cubic and body-centered-cubic phases of an Al0.7CoCrFeNi high-entropy alloy, Mater. Des. 191 (2020), 108611, https://doi.org/10.1016/j.matdes.2020.108611.
[189] D. Frazer, J.L. Bair, E.R. Homer, P. Hosemann, Cryogenic stress-driven grain growth observed via microcompression with in situ electron backscatter diffraction, JOM. 72 (2020) 2051–2056, https://doi.org/10.1007/s11837-020-04075-x.
[190] N.M. della Ventura, C. Tian, A. Sharma, T.E.J. Edwards, J.J. Schwiedrzik, R.E. Logé, J. Michler, X. Maeder, Temperature dependent critical stress for {10-12} twinning in magnesium micropillars at cryogenic temperatures, Scr. Mater. 226 (2023) 115195. doi:10.1016/j.scriptamat.2022.115195.
[191] L.Q. Huston, M.S.R.N. Kiran, L.A. Smillie, J.S. Williams, J.E. Bradby, Cold nanoindentation of germanium, Appl. Phys. Lett. 111 (2017), 021901, https://doi.org/10.1063/1.4993163.
[192] S. Wang, H. Liu, L. Xu, X. Du, D. Zhao, B. Zhu, M. Yu, H. Zhao, Investigations of phase transformation in monocrystalline silicon at low temperatures via nanoindentation, Sci. Rep. 7 (2017) 8682, https://doi.org/10.1038/s41598-017-09411-x.
[193] P. Hosemann, C. Shin, D. Kiener, Small scale mechanical testing of irradiated materials, J. Mater. Res. 30 (2015) 1231–1245, https://doi.org/10.1557/jmr.2015.26.
[194] G.S. Was, J.T. Busby, T. Allen, E.A. Kenik, A. Jensson, S.M. Bruemmer, J. Gan, A. D. Edwards, P.M. Scott, P.L. Andreson, Emulation of neutron irradiation effects with protons: validation of principle, J. Nucl. Mater. 300 (2002) 198–216, https://doi.org/10.1016/S0022-3115(01)00751-6.
[195] D. Kiener, A.M. Minor, O. Anderoglu, Y. Wang, S.A. Maloy, P. Hosemann, Application of small-scale testing for investigation of ion-beam-irradiated materials, J. Mater. Res. 27 (2012) 2724–2736, https://doi.org/10.1557/jmr.2012.303.
[196] G.S. Was, Z. Jiao, E. Getto, K. Sun, A.M. Monterrosa, S.A. Maloy, O. Anderoglu, B. H. Sencer, M. Hackett, Emulation of reactor irradiation damage using ion beams, Scr. Mater. 88 (2014) 33–36, https://doi.org/10.1016/j.scriptamat.2014.06.003.
[197] D. Kiener, P. Hosemann, S.A. Maloy, A.M. Minor, In situ nanocompression testing of irradiated copper, Nat. Mater. 10 (2011) 608–613, https://doi.org/10.1038/nmat3055.
[198] P. Hosemann, D. Kiener, Y. Wang, S.A. Maloy, Issues to consider using nano indentation on shallow ion beam irradiated materials, J. Nucl. Mater. 425 (2012) 136–139, https://doi.org/10.1016/j.jnucmat.2011.11.070.
[199] P. Hosemann, Small-scale mechanical testing on nuclear materials: bridging the experimental length-scale gap, Scr. Mater. 143 (2018) 161–168, https://doi.org/10.1016/j.scriptamat.2017.04.026.
[200] J.S. Weaver, S. Pathak, A. Reichardt, H.T. Vo, S.A. Maloy, P. Hosemann, N. A. Mara, Spherical nanoindentation of proton irradiated 304 stainless steel: a comparison of small scale mechanical test techniques for measuring irradiation hardening, J. Nucl. Mater. 493 (2017) 368–379, https://doi.org/10.1016/j.jnucmat.2017.06.031.
[201] D.L. Krumwiede, T. Yamamoto, T.A. Saleh, S.A. Maloy, G.R. Odette, P. Hosemann, Direct comparison of nanoindentation and tensile test results on reactor-irradiated materials, J. Nucl. Mater. 504 (2018) 135–143, https://doi.org/10.1016/j.jnucmat.2018.03.021.
[202] M. Wurmshuber, D. Frazer, A. Bachmaier, Y. Wang, P. Hosemann, D. Kiener, Impact of interfaces on the radiation response and underlying defect recovery mechanisms in nanostructured Cu-Fe-Ag, Mater. Des. 160 (2018) 1148–1157, https://doi.org/10.1016/j.matdes.2018.11.007.
[203] R. Schoell, D. Frazer, C. Zheng, P. Hosemann, D. Kaoumi, In situ micropillar compression tests of 304 stainless steels after ion irradiation and helium implantation, JOM. 72 (2020) 2778–2785, https://doi.org/10.1007/s11837-020-04127-2.
[204] J.G. Gigax, H. Vo, Q. McCulloch, M. Chancey, Y. Wang, S.A. Maloy, N. Li, P. Hosemann, Micropillar compression response of femtosecond laser-cut single crystal Cu and proton irradiated Cu, Scr. Mater. 170 (2019) 145–149, https://doi.org/10.1016/j.scriptamat.2019.05.004.
[205] H.T. Vo, A. Reichardt, D. Frazer, N. Bailey, P. Chou, P. Hosemann, In situ micro-tensile testing on proton beam-irradiated stainless steel, J. Nucl. Mater. 493 (2017) 336–342, https://doi.org/10.1016/j.jnucmat.2017.06.026.
[206] H.T. Vo, O. Anderoglu, P. Hosemann, S.A. Maloy, The effects of microstructures and radiation damage on the deformation behavior of a HT-9 alloy using microtensile testing, Mater. Charact. 174 (2021), 110972, https://doi.org/10.1016/j.matchar.2021.110972.
[207] D.E.J. Armstrong, C.D. Hardie, J. Gibson, A.J. Bushby, P.D. Edmondson, S. G. Roberts, Small-scale characterisation of irradiated nuclear materials: Part II nanoindentation and micro-cantilever testing of ion irradiated nuclear materials, J. Nucl. Mater. 462 (2015) 374–381, https://doi.org/10.1016/j.jnucmat.2015.01.053.
[208] A.J. Leide, R.I. Todd, D.E.J. Armstrong, Effect of ion irradiation on nanoindentation fracture and deformation in silicon carbide, JOM. 73 (2021) 1617–1628, https://doi.org/10.1007/s11837-021-04636-8.
[209] A. Prasitthipayong, D. Frazer, A. Kareer, M.D. Abad, A. Garner, B. Joni, T. Ungar, G. Ribarik, M. Preuss, L. Balogh, S.J. Tumey, A.M. Minor, P. Hosemann, Micro mechanical testing of candidate structural alloys for Gen-IV nuclear reactors, Nucl. Mater. Energy. 16 (2018) 34–45, https://doi.org/10.1016/j.nme.2018.05.018.
[210] A. Lupinacci, K. Chen, Y. Li, M. Kunz, Z. Jiao, G.S. Was, M.D. Abad, A.M. Minor, P. Hosemann, Characterization of ion beam irradiated 304 stainless steel utilizing nanoindentation and Laue microdiffraction, J. Nucl. Mater. 458 (2014) 70–76, https://doi.org/10.1016/j.jnucmat.2014.11.050.
[211] R.N. West, Positron Studies of Lattice Defects in Metals, in: 1979: pp. 89–144. doi: 10.1007/978-3-642-81316-0_3.
[212] F.A. Selim, Positron annihilation spectroscopy of defects in nuclear and irradiated materials - a review, Mater. Charact. 174 (2021), 110952, https://doi.org/10.1016/j.matchar.2021.110952.
[213] W. Zhang, Y. Xiong, J. Wu, W. Cheng, C. Du, S. Jin, B. Sun, T. Shen, Comparison of helium ion irradiation resistance between nanocrystalline and coarse grained 304 austenitic stainless steel, Nucl. Fusion. 62 (2022), 126034, https://doi.org/10.1088/1741-4326/ac9321.
[214] T. Zhang, H. Schut, Z. Li, H. Wang, Z. Zhang, M. He, Positron annihilation and nano-indentation analysis of irradiation effects on the microstructure and hardening of A508–3 steels used in Chinese HTGR, J. Nucl. Sci. Technol. 55 (2018) 418–423, https://doi.org/10.1080/00223131.2017.1403385.
[215] C. Ophus, Four-dimensional scanning transmission electron microscopy (4D-STEM): from scanning nanodiffraction to ptychography and beyond, Microsc. Microanal. 25 (2019) 563–582, https://doi.org/10.1017/S1431927619000497.
[216] S.H. Mills, S.E. Zeltmann, P. Ercius, A.A. Kohnert, B.P. Uberuaga, A.M. Minor, Nanoscale mapping of point defect concentrations with 4D-STEM, Acta Mater. 246 (2023), 118721, https://doi.org/10.1016/j.actamat.2023.118721.
[217] K. Hattar, D.C. Bufford, D.L. Buller, Concurrent in situ ion irradiation transmission electron microscope, Nucl. Instruments Methods Phys. Res. Sect. B Beam Interact. with Mater. Atoms. 338 (2014) 56–65, https://doi.org/10.1016/j.nimb.2014.08.002.

[218] G. Greaves, A.H. Mir, R.W. Harrison, M.A. Tunes, S.E. Donnelly, J.A. Hinks, New microscope and ion accelerators for materials investigations (MIAMI-2) system at the university of huddersfield, Nucl. Instruments Methods Phys. Res. Sect. A Accel. Spectrometers, Detect. Assoc. Equip. 931 (2019) 37–43, https://doi.org/10.1016/j.nima.2019.03.074.
[219] C.M. Barr, O. El-Atwani, D. Kaoumi, K. Hattar, Interplay between grain boundaries and radiation damage, JOM. 71 (2019) 1233–1244, https://doi.org/10.1007/s11837-019-03386-y.
[220] C.A. Taylor, J.D. Sugar, D.B. Robinson, N.C. Bartelt, R.B. Sills, K. Hattar, Using in situ TEM helium implantation and annealing to study cavity nucleation and growth, JOM. 72 (2020) 2032–2041, https://doi.org/10.1007/s11837-020-04117-4.
[221] J.E. Nathaniel, O. El-Atwani, S. Huang, J. Marian, A.C. Leff, J.K. Baldwin, K. Hattar, M.L. Taheri, Implications of Microstructure in Helium-Implanted Nanocrystalline Metals, Materials (Basel). 15 (2022) 4092, https://doi.org/10.3390/ma15124092.
[222] O. El-Atwani, K. Hattar, J.A. Hinks, G. Greaves, S.S. Harilal, A. Hassanein, Helium bubble formation in ultrafine and nanocrystalline tungsten under different extreme conditions, J. Nucl. Mater. 458 (2015) 216–223, https://doi.org/10.1016/j.jnucmat.2014.12.095.
[223] O. El-Atwani, J.E. Nathaniel, A.C. Leff, B. Muntifering, J.K. Baldwin, K. Hattar, M. L. Taheri, The role of grain size in He bubble formation: Implications for swelling resistance, J. Nucl. Mater. 484 (2017) 236–244, https://doi.org/10.1016/j.jnucmat.2016.12.003.
[224] O. El-Atwani, J.E. Nathaniel, A.C. Leff, K. Hattar, M.L. Taheri, Direct observation of sink-dependent defect evolution in nanocrystalline iron under irradiation, Sci. Rep. 7 (2017) 1–12, https://doi.org/10.1038/s41598-017-01744-.
[225] S. Stangebye, K. Ding, Y. Zhang, E. Lang, K. Hattar, T. Zhu, J. Kacher, O. Pierron, Direct observation of grain-boundary-migration-assisted radiation damage healing in ultrafine grained gold under mechanical stress, Nano Lett. 23 (2023) 3282–3290, https://doi.org/10.1021/acs.nanolett.3c00180.
[226] S.J. Dillon, D.C. Bufford, G.S. Jawaharram, X. Liu, C. Lear, K. Hattar, R. S. Averback, Irradiation-induced creep in metallic nanolaminates characterized by In situ TEM pillar nanocompression, J. Nucl. Mater. 490 (2017) 59–65, https://doi.org/10.1016/j.jnucmat.2017.04.008.
[227] G.S. Jawaharram, P.M. Price, C.M. Barr, K. Hattar, R.S. Averback, S.J. Dillon, High temperature irradiation induced creep in Ag nanopillars measured via in situ transmission electron microscopy, Scr. Mater. 148 (2018) 1–4, https://doi.org/10.1016/j.scriptamat.2018.01.007.
[228] M.L. Taheri, W. Carter, B.P. Uberuaga, On the frontiers of coupled extreme environments, MRS Bull. 47 (2022) 1104–1112, https://doi.org/10.1557/s43577-022-00442-y.
[229] C.D. Judge, V. Bhakhri, Z. Jiao, R.J. Klassen, G. Was, G.A. Botton, M. Griffiths, The effects of proton irradiation on the microstructural and mechanical property evolution of inconel X-750 with high concentrations of helium, J. Nucl. Mater. 492 (2017) 213–226, https://doi.org/10.1016/j.jnucmat.2017.04.045.
[230] C. Howard, C.D. Judge, P. Hosemann, Applying a new push-to-pull micro-tensile testing technique to evaluate the mechanical properties of high dose Inconel X-750, Mater. Sci. Eng. A. 748 (2019) 396–406, https://doi.org/10.1016/j.msea.2019.01.113.
[231] G. Hlawacek, V. Veligura, R. van Gastel, B. Poelsema, Helium ion microscopy, J. Vac. Sci. Technol. B, Nanotechnol. Microelectron. Mater. Process. Meas. Phenom. 32 (2014) 020801. doi:10.1116/1.4863676.
[232] F.I. Allen, A review of defect engineering, ion implantation, and nanofabrication using the helium ion microscope, Beilstein J. Nanotechnol. 12 (2021) 633–664, https://doi.org/10.3762/bjnano.12.52.
[233] Y. Yang, D. Frazer, M. Balooch, P. Hosemann, Irradiation damage investigation of helium implanted polycrystalline copper, J. Nucl. Mater. 512 (2018) 137–143, https://doi.org/10.1016/j.jnucmat.2018.09.022.
[234] F.I. Allen, P. Hosemann, M. Balooch, Key mechanistic features of swelling and blistering of helium-ion-irradiated tungsten, Scr. Mater. 178 (2020) 256–260, https://doi.org/10.1016/j.scriptamat.2019.11.039.
[235] M. Wurmshuber, D. Frazer, M. Balooch, I. Issa, A. Bachmaier, P. Hosemann, D. Kiener, The effect of grain size on bubble formation and evolution in helium-irradiated Cu-Fe-Ag, Mater. Charact. 171 (2021), 110822, https://doi.org/10.1016/j.matchar.2020.110822.
[236] M. Wurmshuber, M. Balooch, X. Huang, P. Hosemann, D. Kiener, Helium-induced swelling and mechanical property degradation in ultrafine-grained W and W-Cu nanocomposites for fusion applications, Scr. Mater. 213 (2022), 114641, https://doi.org/10.1016/j.scriptamat.2022.114641.
[237] M. Wurmshuber, S. Doppermann, S. Wurster, S. Jakob, M. Balooch, M. Alfreider, K. Schmuck, R. Bodlos, L. Romaner, P. Hosemann, H. Clemens, V. Maier-kiener, D. Kiener, Enhancing mechanical properties of ultrafine-grained tungsten for fusion applications, Int. J. Refract. Met. Hard Mater. 111 (2023), 106125, https://doi.org/10.1016/j.ijrmhm.2023.106125.
[238] M. Balooch, F.I. Allen, M.P. Popovic, P. Hosemann, Mechanical and structural transformations of tungsten implanted with helium ions, J. Nucl. Mater. 559 (2022), 153436, https://doi.org/10.1016/j.jnucmat.2021.153436.
[239] S.J. Zinkle, W.C. Oliver, Mechanical property measurements on ion-irradiated copper and Cu-Zr, J. Nucl. Mater. 141–143 (1986) 548–552, https://doi.org/10.1016/S0022-3115(86)80100-3.
[240] W.C. Oliver, J.C. McCallum, B.C. Chakoumakos, L.A. Boatner, Hardness and elastic modulus of zircon as a function of heavy-particle irradiation dose, Radiat. Eff. Defects Solids. 132 (1994) 131–141, https://doi.org/10.1080/10420159408224303.
[241] A. Kareer, A. Prasitthipayong, D. Krumwiede, D.M. Collins, P. Hosemann, S. G. Roberts, An analytical method to extract irradiation hardening from nanoindentation hardness-depth curves, J. Nucl. Mater. 498 (2018) 274–281, https://doi.org/10.1016/j.jnucmat.2017.10.049.
[242] W.S. Cunningham, J.M. Gentile, O. El-atwani, C.N. Taylor, M. Efe, S.A. Maloy, J. R. Trelewicz, Softening due to grain boundary cavity formation and its competition with hardening in helium implanted nanocrystalline tungsten, Sci. Rep. 8 (2018) 1–10, https://doi.org/10.1038/s41598-018-20990-1.
[243] W. Cunningham, Y. Zhang, S.L. Thomas, O. El-Atwani, Y. Wang, J.R. Trelewicz, Grain boundary softening from stress assisted helium cavity coalescence in ultrafine-grained tungsten, Acta Mater. 252 (2023), 118948, https://doi.org/10.1016/j.actamat.2023.118948.
[244] Y. Katz, N. Tymiak, W.W. Gerberich, Nanomechanical probes as new approaches to hydrogen/deformation interaction studies, Eng. Fract. Mech. 68 (2001) 619–646, https://doi.org/10.1016/S0013-7944(00)00119-3.
[245] A. Barnoush, H. Vehoff, Recent developments in the study of hydrogen embrittlement: hydrogen effect on dislocation nucleation, Acta Mater. 58 (2010) 5274–5285, https://doi.org/10.1016/j.actamat.2010.05.057.
[246] A. Barnoush, H. Vehoff, Electrochemical nanoindentation: a new approach to probe hydrogen/deformation interaction, Scr. Mater. 55 (2006) 195–198, https://doi.org/10.1016/j.scriptamat.2006.03.041.
[247] E. Epler, V.V. Roddatis, C.A. Volkert, Measuring mechanical properties during the electrochemical lithiation of silicon, Energy Technol. 4 (2016) 1575–1581, https://doi.org/10.1002/ente.201600175.
[248] N. Kheradmand, R. Johnsen, J.S. Olsen, A. Barnoush, Effect of hydrogen on the hardness of different phases in super duplex stainless steel, Int. J. Hydrogen Energy. 41 (2016) 704–712, https://doi.org/10.1016/j.ijhydene.2015.10.106.
[249] A. Barnoush, N. Kheradmand, T. Hajilou, Correlation between the hydrogen chemical potential and pop-in load during in situ electrochemical nanoindentation, Scr. Mater. 108 (2015) 76–79, https://doi.org/10.1016/j.scriptamat.2015.06.021.
[250] A. Barnoush, J. Dake, N. Kheradmand, H. Vehoff, Examination of hydrogen embrittlement in FeAl by means of in situ electrochemical micropillar compression and nanoindentation techniques, Intermetallics. 18 (2010) 1385–1389, https://doi.org/10.1016/j.intermet.2010.01.001.
[251] Y. Deng, T. Hajilou, D. Wan, N. Kheradmand, A. Barnoush, In-situ micro-cantilever bending test in environmental scanning electron microscope: real time observation of hydrogen enhanced cracking, Scr. Mater. 127 (2017) 19–23, https://doi.org/10.1016/j.scriptamat.2016.08.026.
[252] Y. Deng, A. Barnoush, Hydrogen embrittlement revealed via novel in situ fracture experiments using notched micro-cantilever specimens, Acta Mater. 142 (2018) 236–247, https://doi.org/10.1016/j.actamat.2017.09.057.
[253] A.S. Ebner, S. Brinckmann, E. Plesiutschnig, H. Clemens, R. Pippan, V. Maier-Kiener, A modified electrochemical nanoindentation setup for probing hydrogen-material interaction demonstrated on a nickel-based alloy, JOM 72 (2020) 2020–2029, https://doi.org/10.1007/s11837-020-04104-9.
[254] A.S. Ebner, E. Plesiutschnig, H. Clemens, R. Pippan, V. Maier-Kiener, Rate-depending plastic deformation behaviour in a nickel-base alloy under hydrogen influence, Int. J. Hydrogen Energy. 46 (2021) 38132–38143, https://doi.org/10.1016/j.ijhydene.2021.09.030.
[255] A. Massone, D. Kiener, Prospects of enhancing the understanding of material-hydrogen interaction by novel in-situ and in-operando methods, Int. J. Hydrogen Energy. 47 (2022) 10097–10111, https://doi.org/10.1016/j.ijhydene.2022.01.089.
[256] J. Kim, C.C. Tasan, Microstructural and micro-mechanical characterization during hydrogen charging: an in situ scanning electron microscopy study, Int. J. Hydrogen Energy. 44 (2019) 6333–6343, https://doi.org/10.1016/j.ijhydene.2018.10.128.
[257] M.J. Duarte, X. Fang, J. Rao, W. Krieger, S. Brinckmann, G. Dehm, In situ nanoindentation during electrochemical hydrogen charging: a comparison between front-side and a novel back-side charging approach, J. Mater. Sci. 56 (2021) 8732–8744, https://doi.org/10.1007/s10853-020-05749-2.
[258] M.A. Meyers, P. Chen, A.Y. Lin, Y. Seki, Biological materials : structure and mechanical properties, Prog. Mater. Sci. 53 (2008) 1–206, https://doi.org/10.1016/j.pmatsci.2007.05.002.
[259] M.A. Meyers, J. McKittrick, P.-Y. Chen, Structural biological materials: critical mechanics-materials connections, Science (80-.) 339 (2013) 773–779, https://doi.org/10.1126/science.1220854.
[260] U.G.K. Wegst, H. Bai, E. Saiz, A.P. Tomsia, R.O. Ritchie, Bioinspired structural materials, Nat. Mater. 14 (2015) 23–36, https://doi.org/10.1038/nmat4089.
[261] J.W. Pro, F. Barthelat, The fracture mechanics of biological and bioinspired materials (2019) 46–52, https://doi.org/10.1557/mrs.2018.324.
[262] C. Ortiz, M.C. Boyce, Bioinspired structural materials, Science (80-.) 319 (2008) 1053–1054, https://doi.org/10.1126/science.1154295.
[263] O.G. Andriotis, M. Nalbach, P.J. Thurner, Mechanics of isolated individual collagen fibrils, Acta Biomater. (2022), https://doi.org/10.1016/j.actbio.2022.12.008.
[264] R.K. Nalla, J.H. Kinney, R.O. Ritchie, Mechanistic fracture criteria for the failure of human cortical bone, Nat. Mater. 2 (2003) 164–168, https://doi.org/10.1038/nmat832.
[265] M.E. Launey, M.J. Buehler, R.O. Ritchie, On the mechanistic origins of toughness in bone, Annu. Rev. Mater. Res. 40 (2010) 25–53, https://doi.org/10.1146/annurev-matsci-070909-104427.
[266] M.E. Launey, R.O. Ritchie, On the fracture toughness of advanced materials, Adv. Mater. 21 (2009) 2103–2110, https://doi.org/10.1002/adma.200803322.

[267] B. Wang, T.N. Sullivan, A. Pissarenko, A. Zaheri, H.D. Espinosa, M.A. Meyers, Lessons from the ocean: whale baleen fracture resistance, Adv. Mater. 31 (2019) 1–6, https://doi.org/10.1002/adma.201804574.
[268] O. Kolednik, J. Predan, F.D. Fischer, P. Fratzl, Bioinspired design criteria for damage-resistant materials with periodically varying microstructure, Adv. Funct. Mater. 21 (2011) 3634–3641, https://doi.org/10.1002/adfm.201100443.
[269] P. Fratzl, R. Weinkamer, Nature's hierarchical materials, Prog. Mater. Sci. 52 (2007) 1263–1334, https://doi.org/10.1016/j.pmatsci.2007.06.001.
[270] P.J. Thurner, S. Lam, J.C. Weaver, D.E. Morse, P.K. Hansma, Localization of phosphorylated serine, osteopontin, and bone sialoprotein on bone fracture surfaces, J. Adhes. 85 (2009) 526–545, https://doi.org/10.1080/00218460902996424.
[271] S. Bailey, G.E. Sroga, B. Hoac, O.L. Katsamenis, Z. Wang, N. Bouropoulos, M. D. McKee, E.S. Sørensen, P.J. Thurner, D. Vashishth, The role of extracellular matrix phosphorylation on energy dissipation in bone, Elife. 9 (2020) 1–19, https://doi.org/10.7554/eLife.58184.
[272] G.E. Sroga, D. Vashishth, Phosphorylation of extracellular bone matrix proteins and its contribution to bone fragility, J. Bone Miner. Res. 33 (2018) 2214–2229, https://doi.org/10.1002/jbmr.3552.
[273] J. Wilmers, S. Bargmann, Nature's design solutions in dental enamel: Uniting high strength and extreme damage resistance, Acta Biomater. (2020), https://doi.org/10.1016/j.actbio.2020.02.019.
[274] A.H. Barber, D. Lu, N.M. Pugno, Extreme strength observed in limpet teeth, J. R. Soc. Interface. 12 (2015) 20141326, https://doi.org/10.1098/rsif.2014.1326.
[275] S.H. Oh, J.-K. Kim, Y. Liu, M. Wurmshuber, X.-L. Peng, J. Seo, J. Jeong, Z. Wang, J. Wilmers, C. Soyarslan, J. Kim, B. Kittiwirayanon, J. Jeong, H.-J. Kim, Y.H. Huh, D. Kiener, S. Bargmann, H. Gao, Limpet teeth microstructure unites auxeticity with extreme strength and high stiffness, Sci. Adv. 8 (2022) eadd4644, https://doi.org/10.1126/sciadv.add4644.
[276] J.C. Weaver, Q. Wang, A. Miserez, A. Tantuccio, R. Stromberg, K.N. Bozhilov, P. Maxwell, R. Nay, S.T. Heier, E. Dimasi, D. Kisailus, Analysis of an ultra hard magnetic biomineral in chiton radular teeth Recent analyses of the ultrastructural and mechanical properties of, Mater. Today. 13 (2010) 42–52, https://doi.org/10.1016/S1369-7021(10)70016-X.
[277] S.E. Naleway, M.M. Porter, J. McKittrick, M.A. Meyers, Structural design elements in biological materials: application to bioinspiration, Adv. Mater. 27 (2015) 5455–5476, https://doi.org/10.1002/adma.201502403.
[278] F. Barthelat, Biomimetics for next generation materials, Philos. Trans. R. Soc. A Math. Phys. Eng. Sci. 365 (2007) 2907–2919, https://doi.org/10.1098/rsta.2007.0006.
[279] T. Jenkins, L.V. Coutts, S. D'Angelo, D.G. Dunlop, R.O.C. Oreffo, C. Cooper, N. C. Harvey, P.J. Thurner, Site-dependent reference point microindentation complements clinical measures for improved fracture risk assessment at the human femoral neck, J. Bone Miner. Res. 31 (2016) 196–203, https://doi.org/10.1002/jbmr.2605.
[280] F. Rauch, F.H. Glorieux, Osteogenesis Imperfecta, Lancet. 363 (2004) 831–842, https://doi.org/10.1016/B978-012088562-6/50051-0.
[281] C.J. Collins, M. Kozyrev, M. Frank, O.G. Andriotis, R.A. Byrne, H.P. Kiener, M. L. Pretterklieber, P.J. Thurner, The impact of age, mineralization, and collagen orientation on the mechanics of individual osteons from human femurs, Materialia. 9 (2020), https://doi.org/10.1016/j.mtla.2019.100573.
[282] P.J. Thurner, Atomic force microscopy and indentation force measurement of bone, Wiley Interdiscip. Rev. Nanomed. Nanobiotechnol. 1 (2009) 624–649, https://doi.org/10.1002/wnan.56.
[283] N. Rodriguez-Florez, M.L. Oyen, S.J. Shefelbine, Insight into differences in nanoindentation properties of bone, J. Mech. Behav. Biomed. Mater. 18 (2013) 90–99, https://doi.org/10.1016/j.jmbbm.2012.11.005.
[284] O. Franke, K. Durst, V. Maier, M. Göken, T. Birkholz, H. Schneider, F. Hennig, K. Gelse, Mechanical properties of hyaline and repair cartilage studied by nanoindentation, Acta Biomater. 3 (2007) 873–881, https://doi.org/10.1016/j.actbio.2007.04.005.
[285] H.S. Gupta, S. Schratter, W. Tesch, P. Roschger, A. Berzlanovich, T. Schoeberl, K. Klaushofer, P. Fratzl, Two different correlations between nanoindentation modulus and mineral content in the bone–cartilage interface, J. Struct. Biol. 149 (2005) 138–148, https://doi.org/10.1016/j.jsb.2004.10.010.
[286] O. Franke, M. Göken, A.M. Hodge, The nanoindentation of soft tissue: current and developing approaches, JOM. 60 (2008) 49–53, https://doi.org/10.1007/s11837-008-0071-6.
[287] B. Brandt, C. Zollfrank, O. Franke, J. Fromm, M. Göken, K. Durst, Micromechanics and ultrastructure of pyrolysed softwood cell walls, Acta Biomater. 6 (2010) 4345–4351, https://doi.org/10.1016/j.actbio.2010.05.026.
[288] B. Brandt, U. Lohbauer, M. Göken, K. Durst, The influence of particle size on the mechanical properties of dental glass ionomer cements, Adv. Eng. Mater. 12 (2010) B684, https://doi.org/10.1002/adem.201080067.
[289] V. Nedelkovski, O.G. Andriotis, K. Wieland, C. Gasser, A. Steiger-Thirsfeld, J. Bernardi, B. Lendl, M.L. Pretterklieber, P.J. Thurner, Microbeam bending of hydrated human cortical bone lamellae from the central region of the body of femur shows viscoelastic behaviour, J. Mech. Behav. Biomed. Mater. 125 (2022), 104815, https://doi.org/10.1016/j.jmbbm.2021.104815.
[290] D. Dapaah, T. Willett, A critical evaluation of cortical bone fracture toughness testing methods, J. Mech. Behav. Biomed. Mater. 134 (2022), 105419, https://doi.org/10.1016/j.jmbbm.2022.105419.
[291] J. Schwiedrzik, A. Taylor, D. Casari, U. Wolfram, P. Zysset, J. Michler, Nanoscale deformation mechanisms and yield properties of hydrated bone extracellular matrix, Acta Biomater. 60 (2017) 302–314, https://doi.org/10.1016/j.actbio.2017.07.030.
[292] I. Hadjab, D. Farlay, P. Crozier, T. Douillard, G. Boivin, J. Chevalier, S. Meille, H. Follet, Intrinsic properties of osteomalacia bone evaluated by nanoindentation and FTIRM analysis, J. Biomech. 117 (2021), 110247, https://doi.org/10.1016/j.jbiomech.2021.110247.
[293] T. Montalbano, G. Feng, Nanoindentation characterization of the cement lines in ovine and bovine femurs, J. Mater. Res. 26 (2011) 1036–1041, https://doi.org/10.1557/jmr.2011.46.
[294] J. Schwiedrzik, R. Raghavan, A. Bürki, V. Lenader, U. Wolfram, J. Michler, P. Zysset, In situ micropillar compression reveals superior strength and ductility but an absence of damage in lamellar bone, Nat. Mater. 13 (2014) 740–747, https://doi.org/10.1038/nmat3959.
[295] H.C. Lichtenegger, T. Schöberl, M.H. Bartl, H. Waite, G.D. Stucky, High abrasion resistance with sparse mineralization: copper biomineral in worm jaws, Science (80-.). 298 (2002) 389–392. doi:10.1126/science.1075433.
[296] I. Zlotnikov, E. Zolotoyabko, P. Fratzl, Nano-scale modulus mapping of biological composite materials: theory and practice, Prog. Mater. Sci. 87 (2017) 292–320, https://doi.org/10.1016/j.pmatsci.2017.03.002.
[297] R. Lemanis, K. Tadayon, E. Reich, G. Joshi, R. Johannes Best, K. Stevens, I. Zlotnikov, Wet shells and dry tales: the evolutionary 'Just-So' stories behind the structure–function of biominerals, J. R. Soc. Interface. 19 (2022), https://doi.org/10.1098/rsif.2022.0336.
[298] E. Rossi, J. Bauer, M. Sebastiani, Humidity-dependent flaw sensitivity in the crack propagation resistance of 3D-printed nano-ceramics, Scr. Mater. 194 (2021), 113684, https://doi.org/10.1016/j.scriptamat.2020.113684.
[299] K.I. Dragnevski, A brief overview of in-situ mechanical testing in the environmental scanning electron microscope, Micro Nanosyst. 4 (2012) 92–96, https://doi.org/10.2174/1876402911204020092.
[300] I. Jimenez-palomar, A. Shipov, R. Shahar, A.H. Barber, Influence of SEM vacuum on bone micromechanics using in situ AFM, J. Mech. Behav. Biomed. Mater. 5 (2012) 149–155, https://doi.org/10.1016/j.jmbbm.2011.08.018.
[301] M. Shin, M. Zhang, A. vom Scheidt, M.H. Pelletier, W.R. Walsh, P.J. Martens, J. J. Kruzic, B. Busse, B. Gludovatz, Impact of test environment on the fracture resistance of cortical bone, J. Mech. Behav. Biomed. Mater. 129 (2022), https://doi.org/10.1016/j.jmbbm.2022.105155.
[302] S. Jakob, M.J. Pfeifenberger, A. Hohenwarter, R. Pippan, Femtosecond laser machining for characterization of local mechanical properties of biomaterials: a case study on wood, Sci. Technol. Adv. Mater. 18 (2017) 574–583, https://doi.org/10.1080/14686996.2017.1360751.
[303] A. Dong, J. Duckering, J. Peterson, S. Lam, D. Routledge, P. Hosemann, Femtosecond laser machining of micromechanical tensile test specimens, JOM. 73 (2021) 4231–4239, https://doi.org/10.1007/s11837-021-04971-w.
[304] H.S. Gupta, U. Stachewicz, W. Wagermaier, P. Roschger, H.D. Wagner, P. Fratzl, Mechanical modulation at the lamellar level in osteonal bone, J. Mater. Res. 21 (2006) 1913–1921, https://doi.org/10.1557/jmr.2006.0234.
[305] T. Kochetkova, C. Peruzzi, O. Braun, J. Overbeck, A.K. Maurya, A. Neels, M. Calame, J. Michler, P. Zysset, J. Schwiedrzik, Combining polarized Raman spectroscopy and micropillar compression to study microscale structure-property relationships in mineralized tissues, Acta Biomater. 119 (2021) 390–404, https://doi.org/10.1016/j.actbio.2020.10.034.
[306] K.W. Luczynski, A. Steiger-Thirsfeld, J. Bernardi, J. Eberhardsteiner, C. Hellmich, Extracellular bone matrix exhibits hardening elastoplasticity and more than double cortical strength: evidence from homogeneous compression of non-tapered single micron-sized pillars welded to a rigid substrate, J. Mech. Behav. Biomed. Mater. 52 (2015) 51–62, https://doi.org/10.1016/j.jmbbm.2015.03.001.
[307] I. Jimenez-Palomar, A. Shipov, R. Shahar, A.H. Barber, Mechanical behavior of osteoporotic bone at sub-lamellar length scales, Front. Mater. 2 (2015), https://doi.org/10.3389/fmats.2015.00009.
[308] D. Casari, J. Michler, P. Zysset, J. Schwiedrzik, Microtensile properties and failure mechanisms of cortical bone at the lamellar level, Acta Biomater. 120 (2021) 135–145, https://doi.org/10.1016/j.actbio.2020.04.030.
[309] M. Wurmshuber, J. Wilmers, J. Kim, S.H. Oh, S. Bargmann, D. Kiener, Lower hardness than strength: the auxetic composite microstructure of limpet tooth, Acta Biomater. (2023), https://doi.org/10.1016/j.actbio.2023.04.035.
[310] S.N. Gorb, W. Krings, Mechanical property gradients of taenioglossan radular teeth are associated with specific function and ecological niche in Paludomidae (Gastropoda: Mollusca), Acta Biomater. 134 (2021) 513–530, https://doi.org/10.1016/j.actbio.2021.07.057.
[311] W. Krings, M.T. Neiber, A. Kovalev, S.N. Gorb, M. Glaubrecht, Trophic specialisation reflected by radular tooth material properties in an "ancient" Lake Tanganyikan gastropod species flock, BMC Ecol. Evol. 21 (2021) 35, https://doi.org/10.1186/s12862-021-01754-4.
[312] W. Krings, J.-O. Brütt, S.N. Gorb, Ontogeny of the elemental composition and the biomechanics of radular teeth in the chiton Lepidochitona cinerea, Front. Zool. 19 (2022) 19, https://doi.org/10.1186/s12983-022-00465-w.
[313] H.D. Espinosa, A. Zaheri, H. Nguyen, D. Restrepo, M. Daly, M. Frank, J. McKittrick, In situ wear study reveals role of microstructure on self-sharpening mechanism in sea urchin teeth, Matter. 1 (2019) 1246–1261, https://doi.org/10.1016/j.matt.2019.08.015.
[314] N. Alderete, A. Zaheri, H.D. Espinosa, A novel in situ experiment to investigate wear mechanisms in biomaterials, Exp. Mech. 59 (2019) 659–667, https://doi.org/10.1007/s11340-019-00532-0.
[315] S. Majumder, C.C. Sun, N.A. Mara, Nanomechanical testing in drug delivery: theory, applications, and emerging trends, Adv. Drug Deliv. Rev. 183 (2022), 114167, https://doi.org/10.1016/J.ADDR.2022.114167.
[316] R.P. Feynman, There's Plenty of room at the bottom, Eng. Sci. 23 (1960) 22–36.